University of Zurich[UZH]

Spatial and temporal changes in soil water and groundwater chemistry in the Studibach catchment

GEO 511 Master's Thesis

Author
Anita Bruppacher
16-717-852

Supervised by
Dr. Ilja van Meerveld
Anna Leuteritz

Faculty representative
Dr. Ilja van Meerveld

28.08.2022
Department of Geography, University of Zurich

Contents

List of Figures

List of Tables

List of Equations

Glossary

B	Boron (in µg/l)
C-Q	Concentration-discharge relationship
Ca	Calcium (in mg/l)
Co	Cobalt (in µg/l)
CTI	Computed Topographic Index
Cu	Copper (in µg/l)
$\delta^{2}H$	Deuterium (in ‰)
$\delta^{13}C$	Delta-13-C (in %)
$\delta^{15}N$	Delta-15-N (in %)
$\delta^{18}O$	Delta-18-O (in ‰)
DOC	Dissolved Organic Carbon
Fe	Iron (in mg/l)
GMWL	Global Meteoric Water Line
GW	Groundwater
IQR	InterQuartile Range
K	Potassium (in µg/l)
L12.5	Lysimeter buried at 12.5 cm soil depth
L20	Lysimeter buried at 20 cm soil depth
L30	Lysimeter buried at 30 cm soil depth
LMWL	Local Meteoric Water Line
LOI	Loss on ignition
max	Maximum
Mg	Magnesium (in mg/l)
min	Minimum
Mn	Manganese (in µg/l)
Na	Sodium (in µg/l)
NO_3	Nitrate (in µg/l)
Pb	Lead (in µg/l)
pH	Potential of hydrogen, an inverse measure of the logarithm of the hydrogen ion concentration
PO_4	Phosphate (in µg/l)
SD	Standard Deviation
SO_4	Sulphate (in mg/l)
TC	Total carbon content (in %)
TN	Total nitrogen content (in %)
TWI	Topographic Wetness Index
VSMOW	Vienna Standard Mean Ocean Water
XRF	X-Ray Fluorescence
Zn	Zinc (in µg/l)

Abstract

Stream chemistry depends strongly on the flow pathways to the stream and the chemistry of the inflowing water. Changes in stream chemistry during rainfall events are assumed to reflect variations in solute concentrations with depth below the surface because shallower flow pathways become more important during rainfall events. Many studies have looked at the relative contribution of soil water and groundwater to streamflow but the spatial and temporal variability in their chemical composition is rarely assessed.

This thesis addresses the lack of knowledge on the spatial and temporal variability in the stable isotope composition and solute concentrations in soil- and groundwater in pre-alpine headwater catchments. Samples were taken before and after four rainfall events in autumn of 2021 at seven different sites at four depths: 12.5, 20 and 30 cm below the surface and from the groundwater. In addition, samples were taken from precipitation and stream water. The samples were analysed for their isotopic composition and anion and cation concentrations.

The results of the sampling showed that the spatial variability of the dissolved substances was large and for almost all elements larger than the temporal variability. There was no consistent change in mean concentration from before, to after the four rainfall events in the soil or the groundwater and changes over time were very small. The correlations between the mean concentration and the topographic wetness index or the slope was weak. Only the correlation between the mean solute concentration and the groundwater level was slightly better (R^2: 0.01-0.66). The change in concentration with depth below the soil surface depended on the source of the solute. For some solutes, the concentrations stayed relatively constant (e.g. lead), for others it decreased (e.g. deuterium, potassium) or increased (nitrate, calcium).

Stream chemistry reacted strongly during all sampled rainfall events. Stormflow always had slightly to significantly higher concentrations than precipitation or baseflow, which indicated that new source areas of soil water and groundwater with different solute concentrations contributed to the stormflow. The concentration changes in the soil- and groundwater with depth was reflected in stream chemistry for the majority of the solutes. Only for Mg was there an unexpected change in the stream water, as it went down with an increased water level, while the concentrations in the soil were higher near the surface. This indicates that in addition to shallower flow paths contributing to streamflow during events, other areas must start to contribute as well.

The results of this thesis broaden the understanding on the intricate changes in concentration in the soil-, ground- and stream water in headwater catchments. The thesis proves that a better understanding of hydrochemistry in the soil is useful for hydrological studies of headwater catchments and that making assumptions on the spatial variations in concentration solely on stream chemistry is difficult and can cause many uncertainties. The large spatial variation in solute concentrations and changes in hydrological connectivity also affect stream chemistry. Sampling of soil water and groundwater at several locations in the catchment is therefore needed to assess the spatial variability in solute chemistry.

Graphical Abstact

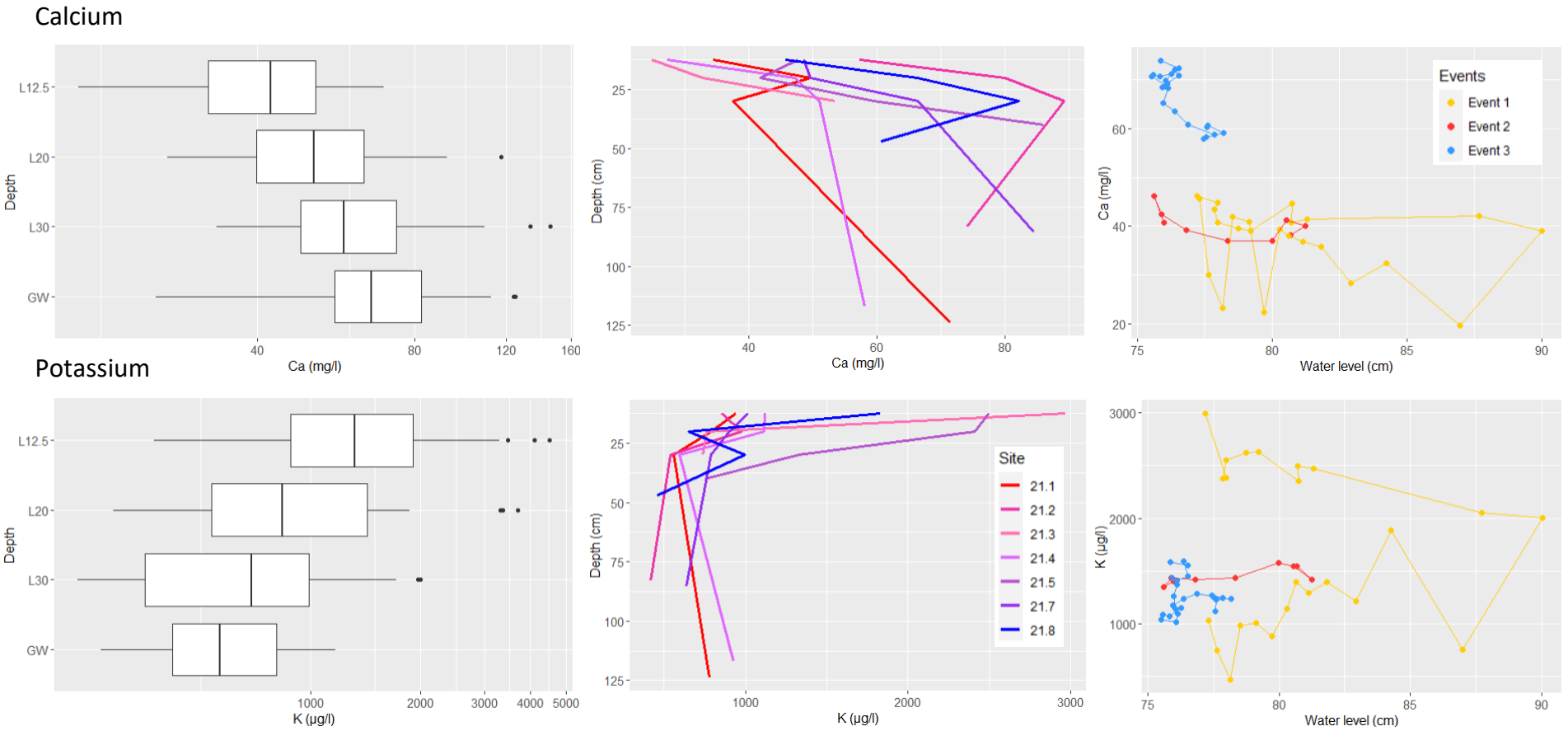

Calcium (in mg/l; top) and potassium concentrations (in µg/l; bottom) that change with soil depth (left) and spatially (middle; lines color-coded based on TWI) can cause changes in stream chemistry during rainfall events (right). For all the solutes see Appendix: Figure 9.1.

1 Introduction

Headwater catchments are key components of the landscape. Their streams make up 70-80% of the total channel length of the world's river networks (Wohl, 2017). Runoff generation depends on external hydroclimatic forcing and internal catchment structures at the surface as well as subsurface (Li et al., 2021). Water chemistry in headwater catchments is strongly influenced by upland flow paths and the chemistry of inflowing water. Headwater catchments are the first absorption point of organic matter and the first barrier to potential water pollution (Wohl, 2017).

Soil water and groundwater are important sources of streamflow, especially in headwater catchments. The concentrations of dissolved substances and the isotopic composition of stream water can change in response to a rainfall event because the relative importance of these flow pathways for streamflow changes (Figure 2.1; Kiewiet et al., 2019; Rinderer et al., 2014; Seibert et al., 2009). For some solutes, the concentrations stay relatively constant (chemostatic behaviour), for others it decreases (dilution behaviour) or increases (mobilization behaviour). The changes in chemistry depend on the source areas for the streamflow as well as reactions during the transport process (Kiewiet et al., 2020; Knapp et al., 2020). Often the composition of soil water varies with the depth below the surface (Seibert et al., 2009; Zhi & Li, 2020). Changes in the water level and the relative contribution of soil- and groundwater to streamflow during rainfall events cause significant changes in stream chemistry (Knapp et al., 2020; Seibert et al., 2009). For example, the nitrate concentrations tend to increase with increasing discharge because the concentration of nitrate in soil water near the surface is higher than deeper in the soil, while the calcium concentrations decrease because the concentration near the surface is lower (Knapp et al., 2020; Stewart et al., 2022). Based on these changes in stream chemistry, inferences are often made about the scarcely studied soil- and groundwater chemistry below the surface (Stewart et al., 2022). Several studies have hypothesized that the solute concentration of subsurface flow regimes and groundwater are related (Kiewiet et al., 2019).

Water chemistry is influenced by numerous factors, such as landscape structure (vegetation, topography, topology), air temperature, the amount of precipitation, and the residence time (Li et al., 2021; Stewart et al., 2022; Zuecco et al., 2019). The stable isotope composition of precipitation can be influenced by the effects of temperature, season, elevation, latitude, continentality and the amount of precipitation (Mook & Geyh, 2000a). Because soil and groundwater contribute to streamflow, the ion concentrations in the stream can provide an indication of differences in weathering conditions, contact times with rocks, or atmospheric influences (Kaushal et al., 2018; Kiewiet et al., 2020).

While it is known that concentrations of dissolved substances change with depth below the soil surface, it is not clear if this change varies across the landscape. For most small catchments, the spatial variability of soil water and groundwater is rarely measured at more than three points (Penna & van Meerveld, 2019) and can therefore not be reliably compared to the composition of stream water. Furthermore, solute concentrations are generally linked to discharge but frequent stream water sampling is cost- and labour-intensive and therefore mostly limited to a few hydrological events (Botter et al., 2020; Knapp et al., 2020). Therefore, this master thesis examines the chemical composition of soil water as well as groundwater to enhance our understanding of

their spatial variability in an undisturbed sub-catchment of the Studibach catchment in the Alptal in Switzerland. The goal of the thesis is to determine the spatial and temporal variations in soil water and groundwater chemistry, and how change with depth below the surface. More specifically, the change with depth below the surface is related to the topographic characteristics of the study sites, in particular the Topographic Wetness Index (TWI) (Beven & Kirkby, 1979) because it is assumed that soil chemistry varies with wetness conditions. Previous research in the Studibach has shown that groundwater level dynamics are related to topography (Rinderer et al., 2014) and that groundwater chemistry is highly variable and differs between riparian areas and hillslopes (Kiewiet et al., 2019).

The overall research question of this thesis is: **How does the soil water chemistry vary in space and with depth below the surface, and how much does this change after a rainfall event?**

To answer this question, the following sub-questions are addressed:

- **How does soil water chemistry change with depth below the surface?**
    - *Hypothesis: The depth variation depends on the type of solute. Base cation (e.g. Ca, Na) concentrations increase with depth, heavy metal concentrations (e.g. Pb, Zn) are constant with depth, and transition metal (e.g. Mn, Fe) and anion (e.g. NO_3, SO_4) concentrations decrease with depth.*
- **Do the changes in concentrations depend on the topographic wetness index (TWI)?**
    - *Hypothesis: Variations in concentrations with depth are more pronounced for drier sites with a low topographic wetness index.*
- **How does the chemical composition of soil water change during a rainfall event?**
    - *Hypothesis: The difference in the concentrations of samples taken before and after the event are largest near the surface and for the driest sites.*

2 Literature review

2.1 Temporal variability in stream chemistry

The routes that precipitation can take to the stream are numerous. On its way the water reacts with organisms and soils. Many of the biological, chemical, and physical processes that occur in a catchment are illustrated in Figure 2.1. These processes are interconnected. Additionally, the water flow pathway, the residence time, and the materials that the water encounters give it its specific chemical composition. Over the past 30 years, many studies have attempted to unravel the inner workings or mechanics of catchments and to expand knowledge and understanding of these processes (Church, 1997; Li et al., 2021).

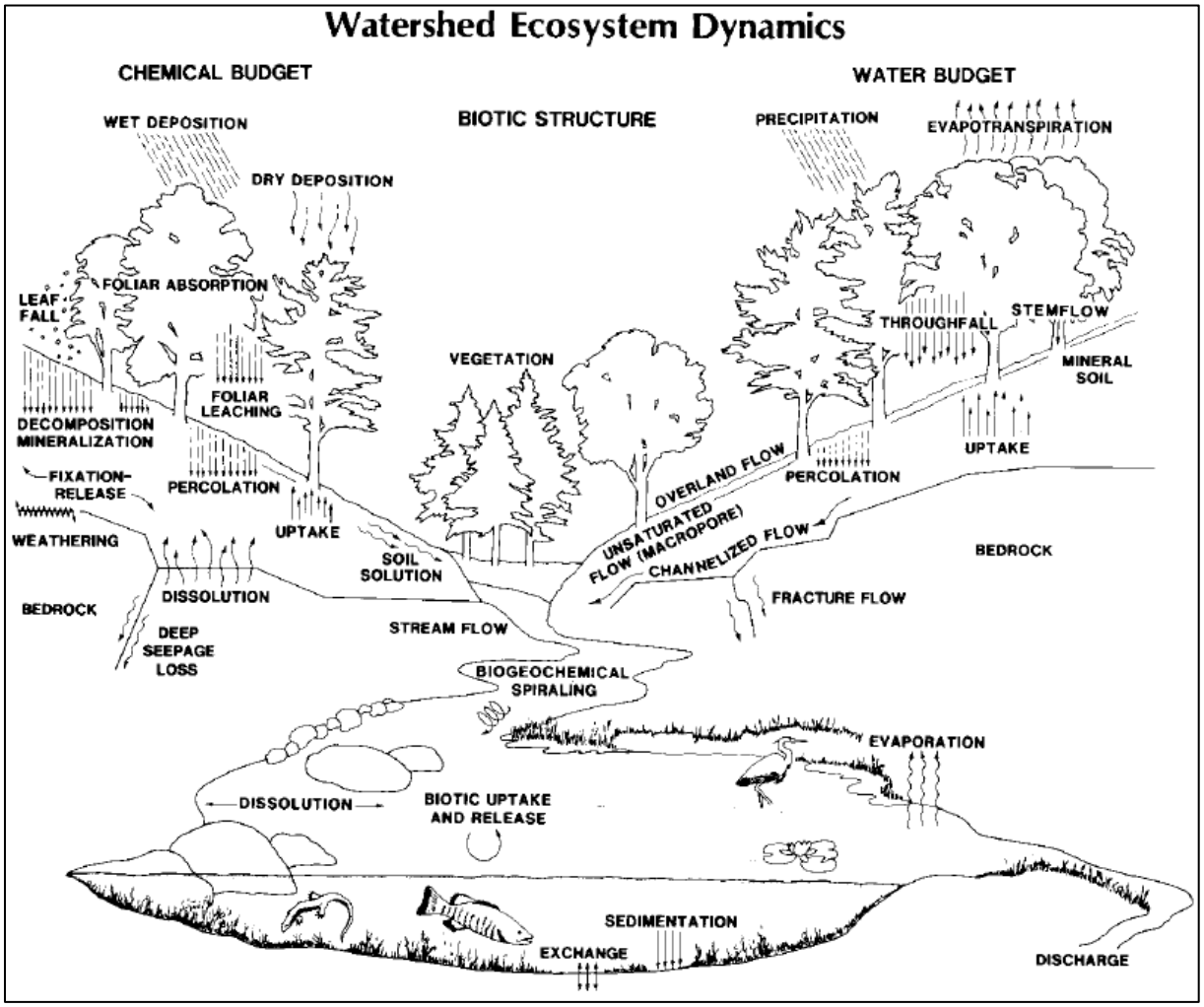

Figure 2.1: Conceptualization of the physical, chemical and biological processes in a catchment (source: Church, 1997; Johnson & Van Hook, 1990)

Stormflow can have taken four basic paths: direct precipitation on the stream, surface runoff, subsurface flow through the soil, or groundwater flow. These pathways and the route the water takes depend on topography, land cover, soil type and geological structure, as well as wetness conditions and precipitation intensity. Once precipitation exceeds the infiltration rate of the soil, overland flow begins, which can lead to a rapid increase in streamflow. Most overland flow still infiltrates into the ground at some point, where it is converted to subsurface flow. Early on, it was

believed that the majority of stormflow came from surface runoff. After the 1960's scientists hypothesized that in small catchments, stormflow is dominated by subsurface flow. And in the 1980s, a combination of hydrometric and isotopic studies determined that groundwater contributes between 60% and 80% of stormflow generation (Church, 1997).

The changes in stream water chemistry during a rainfall event can provide important insights into how catchments store and release water and solutes (Klaus & McDonnell, 2013; Knapp et al., 2020). There are several factors that lead to changes in chemistry during an event. New source areas that were not contributing or directly connected to the stream now start to contribute to the streamflow. Hydrological connectivity is controlled by the distribution of landscape elements and the wetness conditions of the catchment. Previously dry paths fill up with water, and steep hillslope soils cannot absorb the precipitation fast enough so that overland flow is added to the stream. But not only surface spatial variation changes the water chemistry. The subsurface water also changes. With the inflow of new rainwater, the pre-event, also called 'old' soil- and groundwater is mobilized and displaced, and can enter the stream (Kiewiet et al., 2020). During an event most stormflow in the streams is 'old' water (Klaus & McDonnell, 2013). The two-component hydrograph separation of Kiewiet et al. (2020), indicates that this is also the case at in the Studibach.

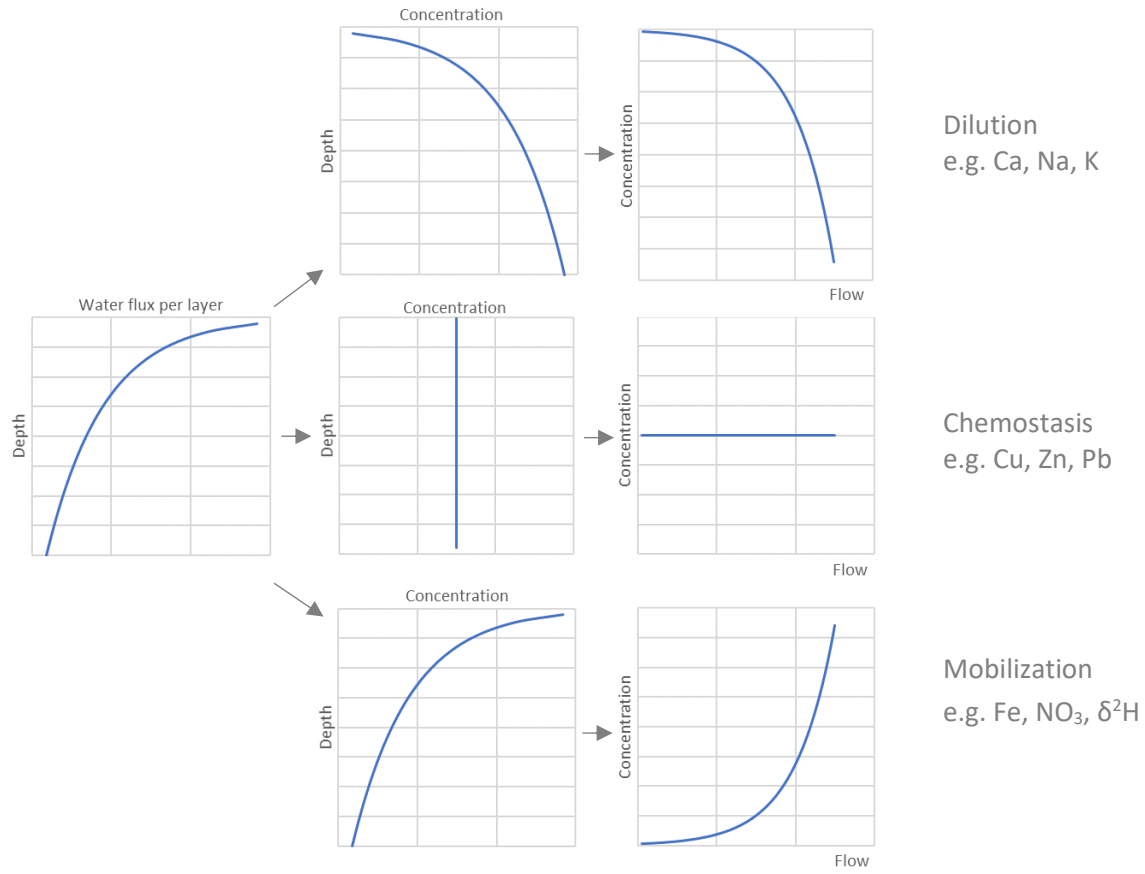

Figure 2.2: Schematic depiction of the concentration variation with depth below the surface (middle) and the resulting concentration-discharge relationship (right) if the flow rate increase near the surface (left) (Figure after Knapp et al. (2020) and Seibert et al. (2009)).

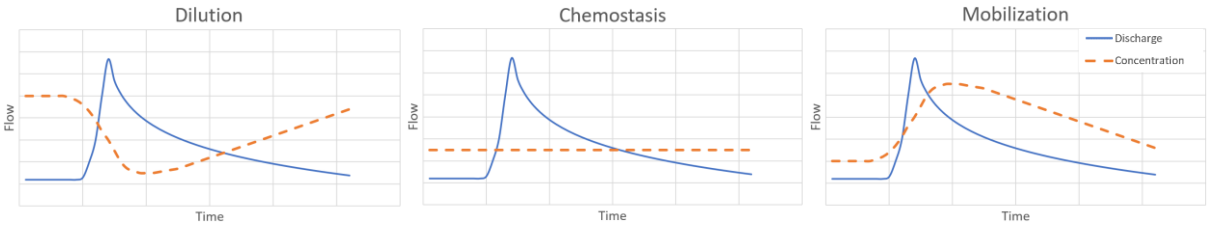

Figure 2.3: Time series of the discharge (blue) and concentration (orange) change in the stream during a rainfall event for dilution (left), chemostatic (middle) and flushing (right) behaviour (Figure after Knapp et al. (2020))

Hillslopes are the largest landscape units in almost all catchments. They carry most of the water as well as most of the solutes to the stream. In many soils, some properties such as the lateral hydraulic conductivity or soil water concentrations vary with soil depth (Seibert et al., 2009). The concentration of the solutes in water within the soil profile is reflected in the stream discharge (Figure 2.3). This connection is called the concentration-discharge (C-Q) relationship (Knapp et al., 2020). In general is the water flux at the soil surface highest during a rainfall event (Figure 2.2). This means that the water from the event that percolates into the soil displaces the old water from before the event. This occurs primarily near the groundwater level. As mentioned before, a major part of the stormflow is generated by 'old' groundwater. Therefore, the fully saturated soil is the first subsurface area from which water enters the stream. As precipitation increases, near-surface water begins to contribute. If the solute concentration is higher at greater soil depths, the stream will also have a high solute concentration at the beginning of the event and during low flow. With increasing discharge, these concentrations then decrease and become diluted (dilution behaviour). However, if the concentration is highest in the shallow soils, the concentration in the stream increases with increasing flow and the solutes get flushed out (mobilization behaviour). But there are also other solutes that essentially remain unchanged even during high flow, the chemostatic behaviour (Knapp et al., 2020; Seibert et al., 2009; Stewart et al., 2022).

2.2 Variations in soil water chemistry with depth

Changes in soil water chemistry with depth below the surface depend on the biological, chemical, and physical processes that affect the solutes (Figure 2.4). Solute concentrations derived from weathering are generally highest farther down the profile or in the groundwater due to the longer contact time, while solute concentrations derived primarily from atmospheric deposition are higher near the surface. Similarly, solutes affected by plant processes (e.g., nutrient cycling or leaching from leaves) are higher near the surface (Jutebring Sterte et al., 2021).

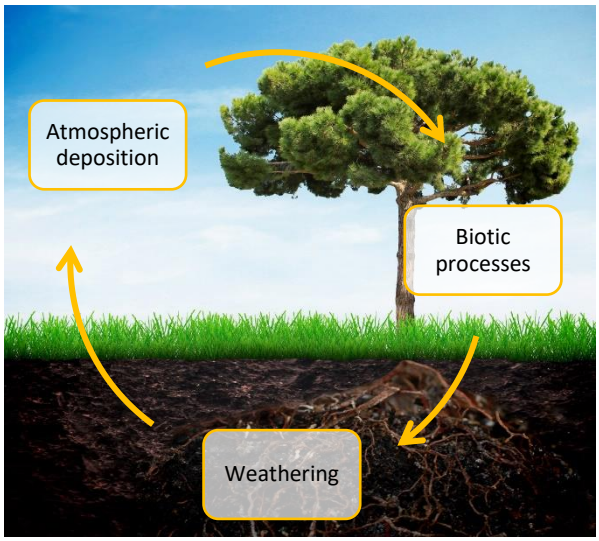

Figure 2.4: Input and processes that affect water solute concentrations in the soil (background picture from Elite Tree Care, n.d.)

2.2.1 Isotopes

Stable water isotopes ($\delta^{18}O$ and $\delta^{2}H$) are part of the water molecule and are therefore ideal tracers. They can be used to gain an understanding of the age and movement of water. During phase changes (e.g., liquid water to vapour), isotopic fractionation occurs. When water evaporates, the lighter molecules ^{16}O and ^{1}H evaporate faster than the rarer and heavier isotopic molecules ^{18}O and ^{2}H. This causes a depletion of Deuterium (^{2}H) and ^{18}O in the clouds. During condensation, the liquid that forms is heavier than the vapour from which it was formed (Mook & Geyh, 2000a). In the end, the water that rains inland is enriched in ^{2}H and ^{18}O compared to the depleted vapor.

The isotope abundance (in ‰) is generally described as a deviation of the isotope ratio of a sample A relative to the ratio of a reference sample or standard r (Mook & Geyh, 2000a):

$$\delta^{2}H = \frac{(\,^{2}H\,/\,^{1}H\,)_{A}}{(\,^{2}H\,/\,^{1}H\,)_{r}} - 1 \qquad \delta^{18}O = \frac{(\,^{18}O\,/\,^{16}O\,)_{A}}{(\,^{18}O\,/\,^{16}O\,)_{r}} - 1 \qquad \text{Equation 2.1}$$

A negative δ indicates a lower abundance of the rarer and heavier isotope in the sample (A) than in the reference material (r). A positive value means a higher abundance of the rare isotope. By definition, both $\delta^{18}O$ and $\delta^{2}H$ are 0‰ for the isotopic water standard (Vienna Standard Mean Ocean Water (VSMOW)).

The Global Meteoric Water Line (GMWL) is an equation that expresses the global average relation between the hydrogen and the oxygen isotope ratios in precipitation. A meteoric water line can also be calculated for a specific area: the Local Meteoric Water Line (LMWL) (Benettin et al., 2018). The points in Figure 2.5 portray the $\delta^{18}O$ and $\delta^{2}H$ for all samples taken in the field: rainfall, stream, soil water and groundwater. The black line indicates the LMWL determined in 2020 for this site by Staudinger et al. (2020). It is apparent that the on-site measurements have a higher deuterium content than the local average. One reason for this could be a slight difference in location or a change in the direction from which the rainfall came from.

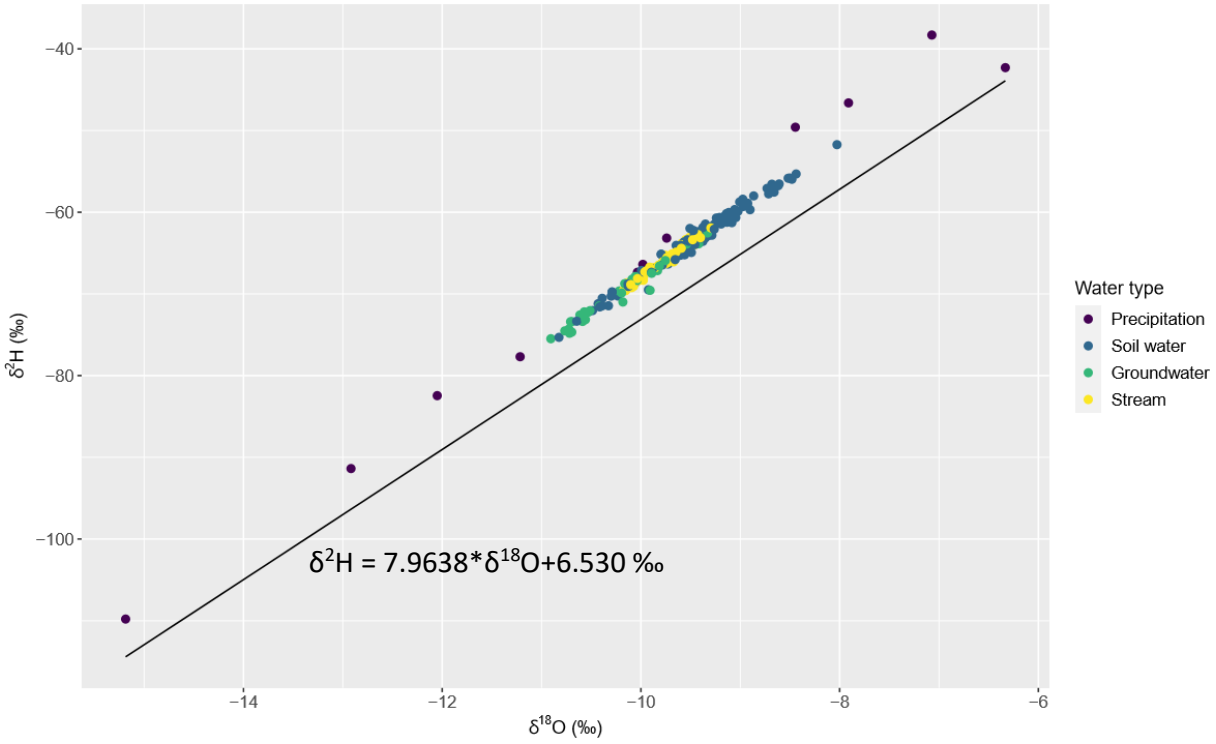

Figure 2.5: The $\delta^{18}O$ and $\delta^{2}H$ for the water samples taken during this study and the Local Meteoric Water Line for the Alptal from Staudinger et al. (2020)

Figure 2.5 also shows that all delta values are negative. This indicates that the vapor was already strongly depleted in the heavier isotopes and only a few rare isotopes reached the Earth's surface by precipitation. The precipitation is widely distributed, but the other three water types are concentrated in the middle to upper right part of the diagram. Their location implies that the samples were primarily taken in the warmer, drier late spring or early autumn months (Benettin et al., 2018).

The spatial variability in the isotopic composition of water below the surface is relatively large and depends on the water source and the degree of mixing within the soil. Therefore, it depends on the incoming precipitation, throughfall, evaporation, water uptake and soil water storage. Spatial variation is usually larger closer to the surface because of more extensive mixing at greater soil depths (Penna & van Meerveld, 2019). The season has a great influence on the change in concentration at the soil depth. Since the samples were taken in autumn, it can be assumed that the soil water at the surface is more enriched in stable water isotopes. Precipitation in winter has a lower abundance of heavy isotopes than the summer precipitation, as there is more fractionation at low temperatures. Last winter's snowmelt is still present in the deeper soil water, while summer rainwater remains closer to the surface. All snowmelt-dominated systems are expected to have the highest isotopic composition at the surface in summer and autumn (Penna & van Meerveld, 2019).

2.2.2 Cations

Positively charged ions can be divided into three groups of different origin: base cations, heavy metals and transition metals (Kiewiet et al., 2019).

2.2.2.1 Base cations

Base cations such as boron (B), calcium (Ca), magnesium (Mg), sodium (Na) and barium (Ba) are partially derived from atmospheric deposition. However, their main source is typically weathering. Magnesium and calcium are vital plant nutrients and an important factor in the structure of freshwater communities. The weathering of base cations is therefore essential for aquatic biota and forest growth (Jutebring Sterte et al., 2021). Field observations in the Krycklan catchment in the boreal region of northern Sweden that were conducted by Jutebring Sterte et al. (2021) indicated that Ca continuously increases with soil depth, as well as soil contact time due to weathering. For Mg the results were not as conclusive. The weathering rate and thus the release of Mg was dampened. Only about half of the Mg exported from the soil originated from the deep soil. For Na, they discovered that the concentration increased rapidly towards the surface after an event, while the weathering rate at the groundwater level declines (Jutebring Sterte et al., 2021).

Potassium (K) is also a base cation but reaches the soil surface through weathering, as well as atmospheric input from vegetation. Conifers are the main source of potassium in the studied sub-catchment, which is why, this cation has been included in the study. Unlike other base cations, potassium can be affected by biotic processes. This element is also known to be retained in soils and it cycles internally within forest stands (Botter et al., 2020; Kiewiet, 2020; Knapp et al., 2020; Tripler et al., 2006). The release of K was strongly linked to soil contact time (Jutebring Sterte et al., 2021). Kiewiet et al. (2020) discovered that K concentrations were highest at relatively dry (forested) sites, in soil water and in groundwater of steep hillslopes.

2.2.2.2 Heavy metals

Heavy metals like copper (Cu), zinc (Zn), and lead (Pb) are considered significant pollutants of aquatic ecosystems due to their toxicity and persistence. They mainly originate from anthropogenic sources (e.g., automobile exhaust gas, industrial wastewater, or coal consumption), loosely bind to the surface of dust particles, and are subsequently returned to the land surface by atmospheric deposition. All heavy metals are poorly soluble (Kiewiet et al., 2019; Li et al., 2021; Rao et al., 2021).

Li et al. (2021) discovered that atmospheric dust inputs are lowest in forests compared to urban areas because they are less affected by human activities. Forested hillslopes and ridges are considered to have higher heavy metal concentrations than downslope areas due to the drier and less diluted deposition from the atmosphere (Kiewiet et al., 2019). The hardly soluble metals can be absorbed relatively easily, depending on the material. This leads scientists to assume that solute concentrations of heavy metals are relatively constant and unchanging over soil depth (Feng et al., 2007; Rao et al., 2021).

2.2.2.3 Transition metals

Transition metals, also called major metals, are iron (Fe), manganese (Mn) and cobalt (Co). These metals are highly mobile and redox-sensitive. Due to their high absorption capacity, excellent oxidation and catalysis activity, they influence and control the release, transfer, availability and toxicity of many nutrient elements and organic contaminants in soil (Feng et al., 2007; Kiewiet et al., 2019; Rao et al., 2021).

The solute concentration of transition metals depends strongly on the water table elevation. Anoxic conditions can reduce the redox potential in the soil resulting in reductive dissolution of the transition metal oxides. The oxygen concentration is higher in the shallower soils, which increases the redox potential and leads to higher transition metal concentrations near the soil surface compared to greater soil depths where oxygen availability is limited (Kiewiet et al., 2019; Rao et al., 2021).

2.2.3 Anions

Anions are negatively charged ions. The anions included in this study are nitrate (NO_3), phosphate (PO_4) and sulphate (SO_4). In agricultural and urban areas, nitrate, phosphate, and sulphate are deposited on the soil surface by fertilization. These man-made sources of anions do not occur in forest catchments that are not fertilized.

In remote forest sites, NO_3 can originate from atmospheric deposition, decomposition of organic matter in shallow soils and leaching from nitrogen-containing rocks (Zhi & Li, 2020). The concentrations of PO_4 in forest soils is generally low. The reason given by Pastore et al. (2020: 1) is that "*[PO_4] either exists within poorly soluble primary minerals or becomes increasingly bound to reactive secondary phases, such as aluminium (Al) and iron (Fe) hydrous oxides with progressing soil development*". Desorption of PO_4 from primary minerals contained in rocks is driven by complexation of mineral cations or acidification of soil solutions (Pastore et al., 2020).

Sulphate in water can have multiple sources. Possible sources in a forested environment include atmospheric deposition, evaporite dissolution, oxidation of sulphide minerals, as well as soil sulphate. In the Studibach, an important source could also be pyrite. Pyrite is a sulphide mineral that is commonly found in rocks, it is very reactive with oxygen and dependent on pH. The products of pyrite oxidation are sulphur and iron (Brown, 1985; Gu et al., 2020). The mobility of SO_4 depends on the absorption capacity, which is affected by the pH of the soil. A higher pH causes lower absorption, which in turn increases the mobility of SO_4 in the soil (Bloem et al., 2001; Zhang et al., 2021).

The origin of the anions determines the concentration at soil depth. For NO_3, it is generally assumed that the solute concentration is higher closer to the surface due to the inputs from atmospheric and organic matter. Zhi & Li (2020) found that in agriculture land NO_3 concentrations were higher in shallow water than in deep water but for remote untreated forests the pattern was the opposite. Frequent rainfall can lead to insufficient nitrogen accumulation in topsoil, resulting in a decrease in the concentration of nitrate in shallow water. Dissolved phosphate concentrations decrease with increasing soil depth, which is strongly negatively related to soil pH. PO_4 availability was found to depend mainly on the mineral hydroxyapatite, from which PO_4 is extracted by acidification (Pastore et al., 2020). The same spatial pattern was detected for SO_4, for which the concentrations are generally higher at the surface than in groundwater. This is caused by the low absorption in the subsurface layer (Calvo et al., 2009; Zhang et al., 2021). However, the pattern can also be reversed if pyrite weathering is a major source of SO_4 (Brown, 1985; Gu et al., 2020).

3 Study Site

3.1 Location

The study area is located in the Studibach catchment, located east of Brunni in the Alptal (Kiewiet et al., 2019; Figure 3.1). The Alptal is a topographically diverse pre-alpine valley in the canton of Schwyz in Switzerland. It is known for its numerous heavy rainfall events and high humidity and is therefore used as a long-term hydrological measurement site in Switzerland (Hegg et al., 2006). The Studibach catchment is an undisturbed headwater catchment that drains into the Zwäckentobel. The Zwäckentobel drains into the Alp, which then flows through the Alptal into the Sihl, the Limmat, the Aare, and finally into the Rhine (Van Meerveld et al., 2018).

The chosen study site for this thesis is the sub-catchment number 21 (in Kiewiet et al. (2019); sub-catchment C3) in the Studibach (Figure 3.1; in turquoise). This location was chosen for its accessibility, diverse vegetation, and size. The sub-catchment is characterized by spruce, clayey and silty gleysols over Schlieren flysch bedrock (Kiewiet et al., 2019).

3.2 Topography

The Studibach catchment stretches over a 20-ha area between 1’270 and 1’650 m a.s.l. and has an average slope of 35% (~19°) (Kiewiet et al., 2019; Rinderer et al., 2014). The topography is shaped by soil creep and landslides, resulting in a terrain with alternating steeper and gentler slopes. The flatter wetlands are characterised by distinct surface micro-topography with hummocks and hollows. The headwater catchments have mostly shallow streams, only the larger streams are incised (about 0.5 m deep) (Kiewiet et al., 2019; Van Meerveld et al., 2018).

3.3 Climate

The frequent rainfall in the Alptal leads to a humid temperate climate. The mean annual temperature is 6°C. The monthly average temperature is 14°C in July and -1°C in January (Van Meerveld et al., 2018). The mean annual precipitation in the Studibach catchment is 2300 mm/y, of which about 30% falls as snow in the winter months (Knapp et al., 2020; Rinderer et al., 2014; Stähli & Gustafsson, 2006; Van Meerveld et al., 2018). Most of the precipitation falls with low intensity and the summer months are wetter than the autumn or winter months (Van Meerveld et al., 2018). Event-related rainfall also varies significantly throughout the region due the high variability in topography and the nearby mountains (Fischer et al., 2017).

3.4 Vegetation

The Studibach catchment consists of 55% coniferous and open forest, 14% dry meadows and 33% wetland (Knapp et al., 2020; Van Meerveld et al., 2018). The steeper parts of the catchment and the ridge are covered by an open coniferous forest, whereas the flatter and concave areas consist of wet grassland and swampy terrain (Kiewiet et al., 2019). The forest is dominated by spruce (Picea abies, Picea rubens), silver fir (Abies alba) and grey alder (Alnus incana) with an understory of blueberries (Vaccinium sp.) on the drier sites and ferns and Equisetum on the wetter sites. Maple and beech are also found at lower altitudes. In terms of ground coverage, Poa trivialis and Carex ferruginea are found in the meadows. The wetlands contain Caltha palustris, Petasites albus,

Poa trivialis and Carex ferruginea (Hagedorn et al., 2000). During the fieldwork, additional plants were spotted; blueberries (Vaccinium myrtillus), different blackberry types (Rubus argutus, vestitus and elegantispiosus), raspberries (Rubus occidentalis), strawberries (Fragaria vesca), as well as coltsfoot (Tussilago farfara), thistle (Cirsium oleraceum), bushgrass (Calamagrostis epigejos) in the meadows and thistle (Cirsium oleraceum) and meadowsweet (Filipendula ulmaria) in the wetlands.

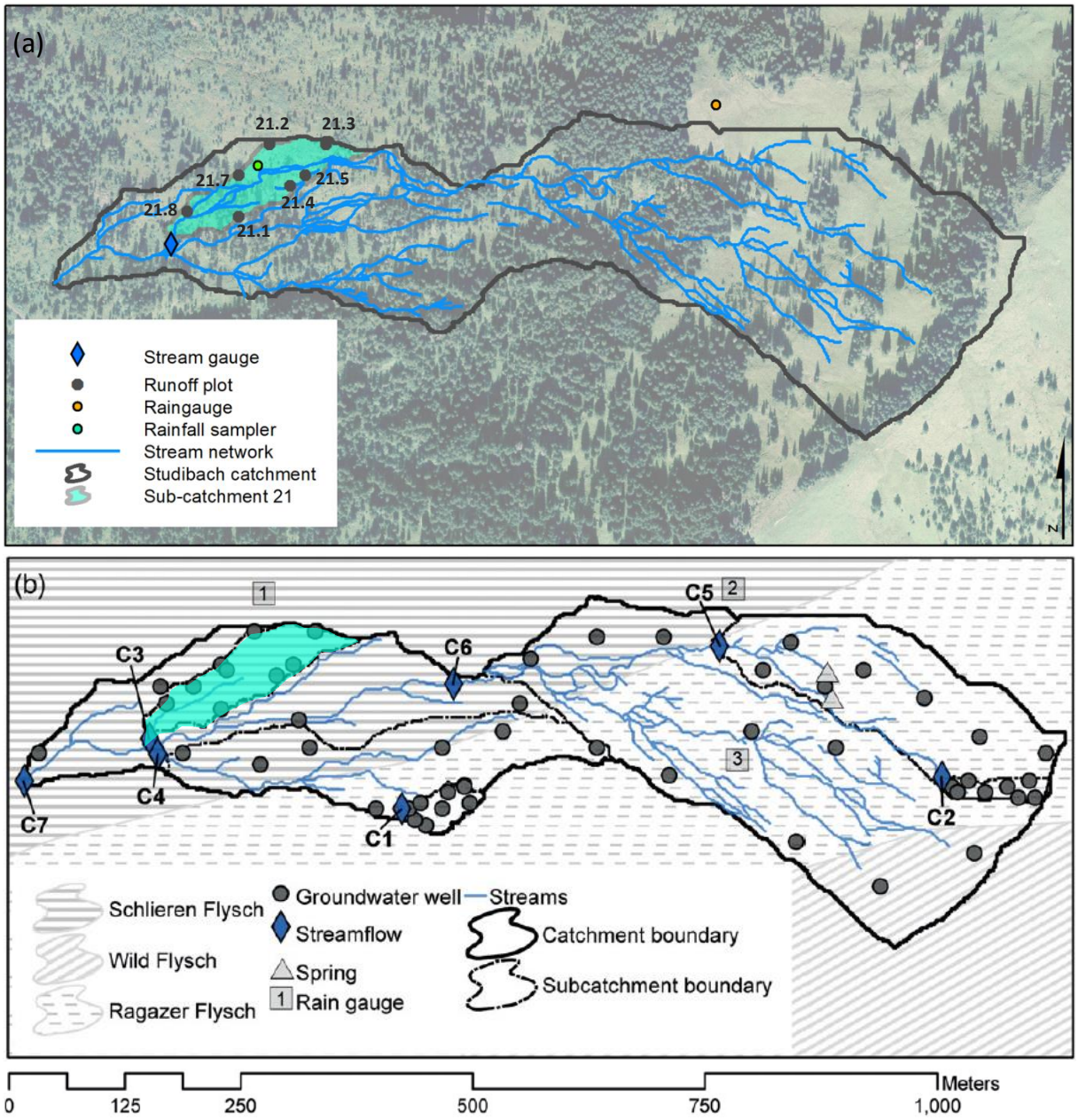

Figure 3.1: Map of the Studibach catchment and the research area (sub-catchment no. 21) in turquoise (a) a satellite image and (b) the catchment and sub-catchments in dashed grey, the streams in blue, stream gauges as blue diamonds, location of the groundwater wells as dark grey dots and the Flysch types in the background (map from Kiewiet et al. (2019) adjusted by Anna Leuteritz).

3.5 Soil and bedrock

The soil depth ranges from 0.5 m at the ridge to 2.5 m in the depressions. The soil consists mainly of clay and silt. The major soil types in the Studibach catchment are mollic and umbric gleysols, which are characterized by a low permeability. The mollic gleysols typically have a permanently reduced B_g horizon, while the umbric gleysols have an oxidized B_w horizon (Hagedorn et al., 2000). The wetlands in the flatter areas contain a thick organic soil horizon up to 1 m deep (Van Meerveld et al., 2018). The gleysols overlay three different types of Flysch: Schlieren Flysch, Ragazer Flysch, and Wild Flysch. Flysch is a "*geologic formation consisting of a sequence of sedimentary rocks deposited in a basin adjacent to a rising mountain belt*" (Van Meerveld et al., 2018; 436) and is usually highly heterogeneous. It is also considered to be poorly permeable. The characteristics of the soil and the bedrock cause the groundwater levels in the Studibach catchment to be shallow (Kiewiet et al., 2019; Rinderer et al., 2014).

3.6 Previous studies in the Alptal

At the beginning of the 20th century, the Swiss Federal Institute for Forest, Snow and Landscape Research (WSL) wanted to better understand how forests influence floods because the poor conditions of the forests at the time were blamed for the severe floods at the end of the 19th century (Hegg et al., 2006). Regions with flysch geology, which are very vulnerable to flooding due to their wet soils and nearly impermeable subsoil, were selected as ideal study areas because they were heavily afforested since the 19th century. The Rappengraben and Sperbelgraben headwater catchments underlain by Flysch geology in the Emmental region were instrumented by the WSL to study the forest's influence on the water balance and flood runoff generation (Badoux et al., 2006; Stähli et al., 2021).

In the early 1960s, a new long-term forest hydrological monitoring programme was established in the Alptal. Eleven catchments were selected for continuous measurements but after a big flood in 1974, measurement stations were reinstalled only in the Vogelbach and Lümpenenbach (in 1975) and the Erlenbach (in 1978). Since then, the Alptal has become a research site for many aspects of hydrology, such as water quality, snow hydrology, bedload transport and the effects of climate change on water supply and runoff generation (Hegg et al., 2006; Stähli et al., 2021). In 2009 the University of Zurich started research in the headwater catchments neighbouring the Erlenbach to better understand the hydrological processes leading to runoff responses and their spatiotemporal variation (Van Meerveld et al., 2018). One of those catchments is the Studibach catchment.

In 2010, Rinderer et al. (2014) installed 51 groundwater (GW) wells to the depth of refusal across the entire Studibach catchment, with eight to nine groundwater wells in each of the seven sub-catchments (Figure 3.1b). The depth of the wells ranges from 0.45 and 2.14 m, depending on the depth of the soil-bedrock interface. Their locations were chosen based on the topographic wetness index (TWI; Beven & Kirkby, 1979), which is defined as:

$$ln \frac{a}{\tan \beta} \qquad \text{Equation 3.1}$$

where α is the upslope contributing area per unit contour length [m] and ß is the local slope [°] (Beven & Kirkby, 1979; Rinderer et al., 2014). The values of the TWI can range from 1 to 15, the higher the value, the wetter the location (Kopecký et al., 2021). The manually installed wells have holes along their entire length up to 10 cm below the surface to allow groundwater to collect within the tubes. Rinderer et al. (2014) investigated the correlation between TWI and the groundwater level. They found that "[…] *median groundwater levels were correlated to slope, curvature, and TWI, but the strength of the correlation depended on whether the indices characterized the local topography or the topography of the upslope contributing area. The correlation between TWI and groundwater levels was not constant over time, but decreased at the beginning of rainfall events, indicating large spatial differences in groundwater responses, and increased after peak flow when groundwater levels could be considered to be spatially in a steady state*" (Rinderer et al., 2014; 6067).

Five years later, Kiewiet et al. (2019) studied the spatiotemporal variability of the hydrochemistry of groundwater in the Studibach catchment. Their focus lay on the electrical conductivity (EC), the stable water isotopic composition and the concentration of major and trace ions. They sampled the groundwater wells of Rinderer et al. (2014), precipitation, and stream water during nine snapshot campaigns under different conditions between May and November 2016 and 2017. They found that the spatial variability was large and greater than temporal variability for almost all parameters. They were able to distinguish "*four shallow groundwater types based on differences from the catchment average concentrations: riparian zone-like groundwater, hillslopes and areas with small upslope contributing areas, deeper groundwater, and sites characterized by high magnesium and sulphate concentrations that likely reflect different bedrock material*" (Kiewiet et al., 2019; 2502).

Kiewiet et al. (2020) compared the chemical composition of stormflow with the composition of rainfall, groundwater and soil water and calculated the mixing fractions. Soil water was sampled from six to 18 suction lysimeters (at depths of at 15, 30 and 50 cm) at four to six sites. "*The findings of this study show that solute concentrations partly reflect the gradual changes in hydrologic connectivity and that it is important to quantify variability in the composition of different source areas*" (Kiewiet et al., 2020; 3381). They also found that for three of the four measured events, the soil water contributions were minimal. In the same year, another paper was published analysing the contribution of 'old' and 'new' water to streamflow by comparing samples before, during and after rainfall event (Kiewiet et al., 2020).

In spring 2021, Anna Leuteritz and Victor Gautier started their PhD thesis at the University of Zurich. Both PhD students are working within the TopFlow project, which focuses on near-surface flow pathways (overland flow and lateral flow through the topsoil) in the Studibach catchment. As part of this project, Anna is studying the spatiotemporal variability in the chemical composition of overland and topsoil interflow and its effect on streamflow and stream chemistry. Victor's research focuses on the connectivity of flow pathways at the surface and in the topsoil. He studies how topography, land-use, topsoil properties and characteristics of precipitation events influence these processes.

Victor and Anna are conducting their studies in sub-catchments number 12, 21 and 32 in the Studibach catchment (sub-catchments C2, C3 and C5 in Kiewiet et al. (2019); see also Figure 3.1b). For their studies, they installed 14 plots within the sub-catchments based on the topographic wetness index. Each plot was located within five meters of a groundwater well that was installed by Rinderer et al. (2014). EC, temperature and flow rate of overland flow and topsoil interflow are measured at each plot location. In addition, precipitation collectors and four automatic water samplers (ISCO; Teledyne ISCO, 6710; 6712) were installed in the three sub-catchments. The ISCOs were pre-programmed to sample overland flow, topsoil interflow or stream water in 24 plastic bottles at specified intervals during a series of rainfall events.

The field work for this thesis was carried out with the help and guidance of Anna Leuteritz, as well as input from Dr. Ilja van Meerveld. The samples were prepared in the laboratory in collaboration with Anna.

4 Methods

4.1 Field Work

4.1.1 Plot selection and characteristics

A total of nine groundwater wells are installed in sub-catchment 21 (Rinderer et al., 2014). Anna Leuteritz and Victor Gautier selected seven of the nine wells to build their plots (see Figure 4.1). Groundwater well 6 was excluded due to inaccessibility and well 9 is located only two meters from well 8 and was therefore also excluded. Finally, GW wells 1, 2, 3, 4, 5, 7 and 8 were chosen to conduct the studies. The seven plots are located within a 5 m radius around the groundwater wells.

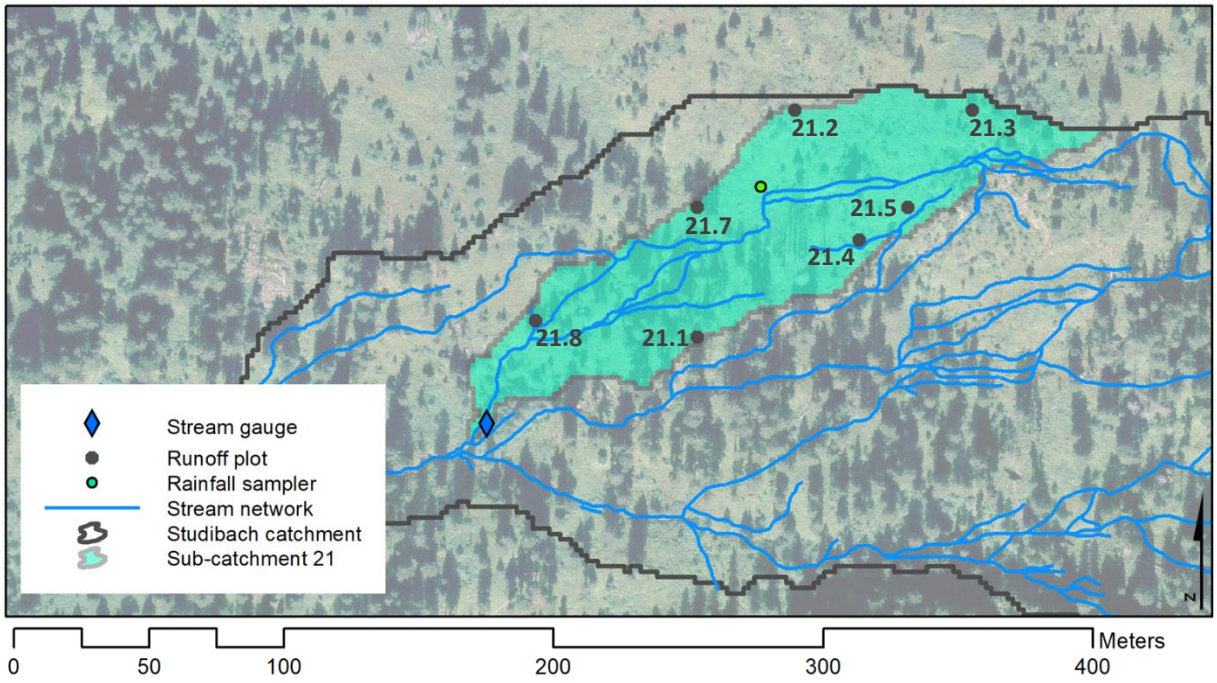

Figure 4.1: Map of the sub-catchment no. 21 in turquoise including the location of the studied plots (map from Kiewiet et al. (2019) adjusted by Anna Leuteritz).

The wells are numbered based on the rank of the TWI values of all pixels within the sub-catchment. For example, 21.1 is the well with the lowest TWI value, whereas 21.8 has the highest TWI (see Table 4.1; Rinderer et al., 2014). The wells are located in three different vegetative sites. The wettest plot is situated in grassland, the other six plots are either in the forest or in a clearing.

Table 4.1: Overview of the topographic attributes of the seven studied plots

Site	TWI	Latitude	Longitude	Slope (°)	Landuse
21.1	3.39	47.03882° N	8.72088° E	15.6	Forest
21.2	4.08	47.03957° N	8.72137° E	21.0	Clearing
21.3	4.40	47.03956° N	8.72224° E	12.6	Clearing
21.4	4.83	47.03913° N	8.72167° E	25.6	Forest
21.5	5.23	47.03924° N	8.72191° E	21.0	Forest
21.7	5.97	47.03920° N	8.72097° E	17.7	Clearing
21.8	6.96	47.03888° N	8.72009° E	8.5	Grassland/ wetland

4.1.2 Lysimeter installation

Three suction lysimeters were installed at different soil depths in each plot on the 26th of August 2021 to obtain soil water samples. The smaller lysimeters (Ø 31mm) were deployed at a depth of 12.5 cm (L12.5) and 20 cm (L20), while the larger tubes (Ø 63mm) were installed at 30 cm (L30) depth (Figure 4.3). All lysimeters were installed within a five-meter radius to the groundwater wells. The shallowest L12.5 lysimeter was positioned inside the plot, while L20 and L30 were placed next to it.

A suction lysimeter is "*a device for collecting water from the pore spaces of soils*" (Soilmoisture Equipment Corp., n.d.). The sampler consists of a grey plastic tube attached to the white ceramic cup at the bottom (see Figure 4.2). The ceramic cup is porous and is the most important component of the lysimeter. It must have a hydrophilic (water loving) surface with numerous pores to allow transport soil water fluids into the reservoir without alteration or leakage (Soilmoisture Equipment Corp., n.d.).The holes for each lysimeter were dug using an auger (see Figure 4.5a). Some of the moist soil was used to form a tight ball around the lower end of each lysimeter to ensure the absence of large air pockets near the ceramic cup. The lysimeter was then carefully pushed as deep as possible into the holes. After ensuring the correct measuring depth, the area around the tube was sealed with moist soil to prevent water from draining directly into the holes (see Figure 4.5a, and Figure 4.3). This process was repeated until all 21 lysimeters were properly installed.

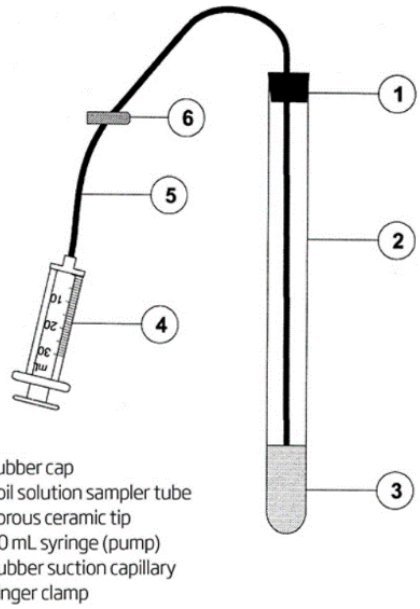

Figure 4.2: Ceramic suction lysimeter (Real Nitrition, n.d.)

Figure 4.3: Lysimeters L20 and L30 installed at plot 21.3

In order to use the lysimeter, a vacuum must be created inside the tube. A vacuum hand pump was used to create a suction of 50 mbar inside the tube. The plastic hose is sealed airtight with a

finger clamp. From then on, the soil water is slowly sucked into the tube through the porous ceramic cup and stored in the reservoir until it is emptied. During the two-week adaptation time, the lysimeters were emptied four times to equilibrate. After this time, the lysimeters were ready to be used for the study (Figure 4.3).

4.1.3 Water sampling

4.1.3.1 Precipitation events and sampling period

Sampling was conducted within a seven-week period from the 15th of September to the 25th of October 2021. Four out of six precipitation events that occurred during this period were monitored and sampled (see Figure 4.4). The first event (39 mm) lasted from the 15th to the 17th of September, the second event (32 mm) from the 19th to the 20th of September, the third event (39 mm) from the 3rd to the 7th of October and the fourth and last event (39 mm) from the 20th to the 21st of October.

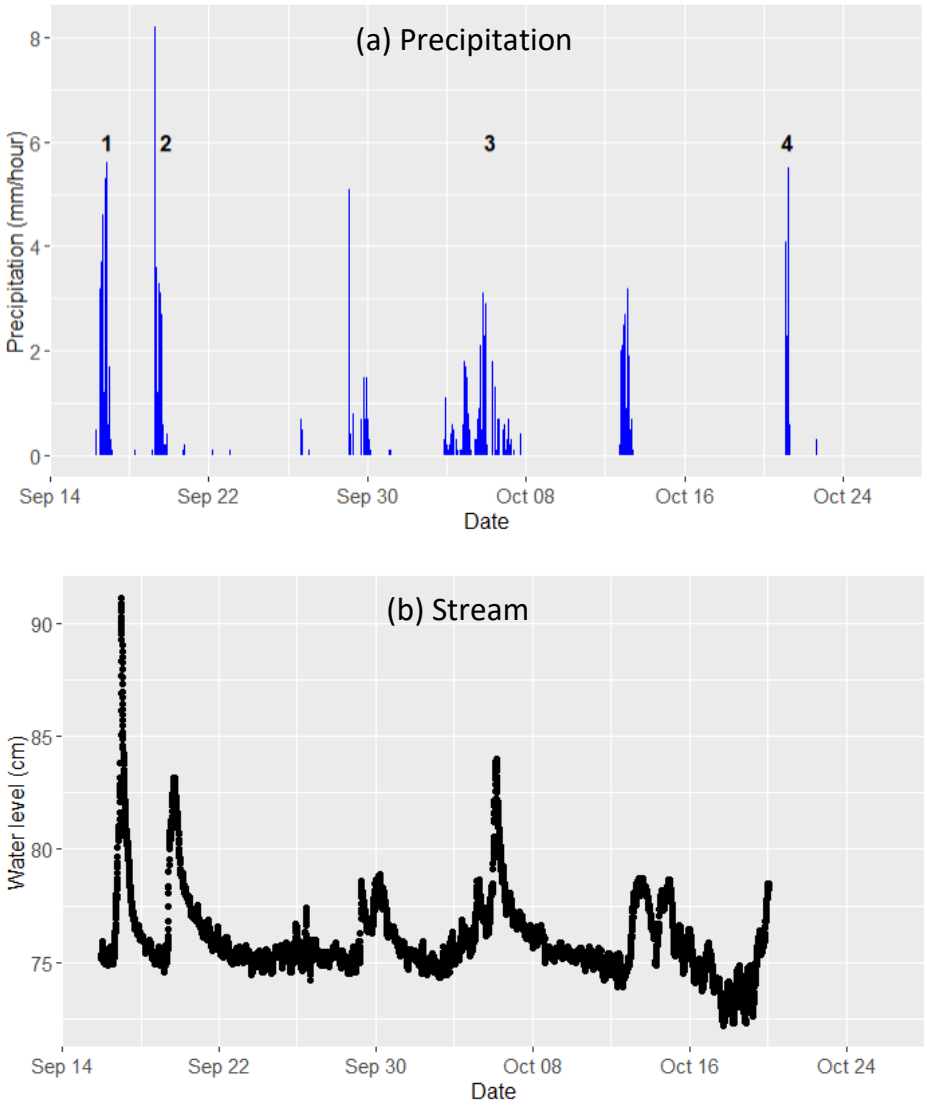

Figure 4.4: (a) Hourly precipitation and (b) stream level during the study period. The four sampled events are indicated with a number.

Samples of the precipitation, stream, lysimeters and groundwater wells were taken before and after each event (total of seven sampling campaigns). Because the first and second events were close to each other, the samples taken on the 18th of September are considered both the post-event samples for the first event and the pre-event samples of the second event.

At the end of the sampling period, there were supposed to be 147 lysimeter samples, 49 groundwater samples, 103 stream water samples and at least four precipitation samples. Due to insufficient filling time of the lysimeters and groundwater wells, there were only 135 ion and 111 isotope samples from soil water: and only 44 ion and 38 isotope samples from the groundwater wells. The ISCO did not work properly during the second rainfall event, resulting in 14 missing stream water samples from the second event. As for the rain sampler, a total of eight precipitation samples were taken for ion and 11 samples for isotope analysis.

4.1.3.2 Purging and sample collection

To obtain fresh samples directly from the soil and groundwater, the lysimeters and groundwater wells were emptied before and after each event. In the morning, the lysimeters were emptied completely. The groundwater wells were emptied as much as possible, but some filled again so quickly that a complete emptying was impossible. The lysimeters were emptied with a 50 cm long plastic hose (Ø 2 mm) attached to a 60 ml syringe. For the groundwater wells, another 60 ml syringe was used with a 2 m long hose. The lysimeters and wells were then given enough time to refill with fresh water before the actual sample was taken (within 4 to 24 hours after the tubes were emptied). The wells and lysimeters were usually sampled in the same order as they were emptied to give the tubes the maximal amount of time to refill. Before each sampling, the syringes were rinsed with some sample water before the actual sample was taken.

The electrical conductivity (EC) and the water temperature were measured directly on site using a digital portable electrical conductivity meter (Multi 3420 conductivity probe: WTW Measurement Systems Inc). This meter was put directly into the lysimeters to measure. For the GW wells a plastic centrifuge tube filled with well water was used to facilitate the measurement.

The stream that runs through sub-catchment 21 was also sampled before and after each event. In addition, the stream water was sampled at hourly intervals during each event by an ISCO stationed at the outlet (see Figure 4.1; stream gauge). Samples were collected from the 24 polyethylene bottles (600 ml) from the ISCO during each post-event sampling (Kiewiet et al., 2019).

The precipitation was gathered in a rain sampler placed in the middle of the sub-catchment (see Figure 4.1). After each event, the water in the rain sampler was taken. Depending on the amount of precipitation, one to four samples were taken per event.

4.1.3.3 Sample storage

The sampled waters were put into two separate containers: Falcon 50 mL Conical Centrifuge Tubes and 20 ml glass vials. The centrifuge tube was used for the ion samples, the glass vial for the isotopes. The glass vials had to be filled without any head space and be airtight to prevent fractionation.

The water samples were stored at 4°C in a refrigerator at the laboratory of the Geographical Institute of the University of Zurich before processing to reduce and prevent biochemical reactions. The water samples were processed within one week after their collection (Kiewiet et al., 2019).

4.1.4 Soil sampling

In addition to the water samples, 21 soil samples were collected on the 28th of October 2021. Three samples were taken per plot at a depth of 0-12.5 cm, 12.5-20 cm, and 20-30 cm. These sampled soil depths correspond with the three depths of the lysimeters. In order not to disturb the plots, the soil samples were taken directly next to the plots in an undisturbed area.

A soil auger was used to collect the soil samples (see Figure 4.5a). The soil in the auger was divided between the three lysimeter depths (see Figure 4.5b). Two to four auger contents were sampled per site and depth to obtain about 130 g of soil per sample.

Figure 4.5: (a) Auger used to install lysimeters and take soil samples and (b) soil sample that was divided into three depth sections.

4.2 Lab Work

4.2.1 Water samples

In the laboratory, the water samples were filtered (0.45 µm, SimplepureTM Syringe Filter) into a 15 ml centrifuge tube using a 60 ml syringe. Pipettes were then used to redistribute the water sample into three different vials to measure cation and anion concentrations and isotopic composition. For the anion and isotope analysis, two 2 ml glass vials were each filled with sampled water. For the cation analysis, a 15 ml centrifuge vial was filled with 8 ml of the sampled water. The cation samples were then acidified with about 7 µl of Nitric Acid 65% and shaken to mobilize trace metals and reduce microbial activity (Kiewiet et al., 2019).

The ion samples were analysed at the Physics of Environmental Systems laboratory at ETH Zurich (Switzerland). An ion chromatograph (861 Advanced Compact IC, Metrohm AG) was used for the anion and a mass spectrometer (ICP-MS 9700, Agilent Technologies) for the cation samples (Kiewiet et al., 2019). Calibration curves were obtained from measurements with five (for anion) to seven (for cation) calibration standards before, during and after measuring the samples.

The isotope samples were analysed in the isotope laboratory of the Chair of Hydrology using a Cavity Ring-Down Spectrometer (L1102-I Picarro Inc.). The reported accuracy is ±0.16‰ for $\delta^{18}O$ and ±0.6‰ for $\delta^{2}H$.

4.2.2 Soil samples

4.2.2.1 Preparation

The soil samples were prepared and analysed in in the laboratory of the Geographical Institute of the University of Zurich. After the fresh wet soil was weighed, the crushed soil samples were dried in the oven at 65°C for 48 hours. The dry soil samples were then weighed again before the skeletal material (stones, roots, and biomass) was separated from the soil aggregates. The dried soil was then mortared and sieved into fine soil to a particle size < 2 mm. The fine soil and skeletal material were again weighed separately (Table 4.2; Egli et al., 2016).

Subsequently, 10g of the fine soil was milled in a Wolfram cup in the horizontal mill with two wolfram-balls per sample. Each sample was milled for 12 minutes at a frequency of 30 Hz into a grain size < 63 µm (Egli et al., 2016).

The soil samples were studied and analysed for their chemical properties by measuring the total carbon content (TC), the proportion of organic material, the hydrogen ion concentration (pH) and the total elemental content of the soil.

Table 4.2: Characteristics of the soil samples

Site	Depth (cm)	Wet soil (g)	Dry soil (g)	Fine earth <2mm (g)	Soil moisture (%)	Skeleton (%)
21.1	0 - 12.5	145	62	60	57	3.4
21.1	12.5 - 20	139	71	71	49	0.8
21.1	20 - 30	159	90	87	43	3.6
21.2	0 - 12.5	107	39	38	64	2.8
21.2	12.5 - 20	76	32	31	58	4.1
21.2	20 - 30	115	62	61	46	3.0
21.3	0 - 12.5	139	62	61	55	2.4
21.3	12.5 - 20	116	61	60	47	2.0
21.3	20 - 30	177	112	110	37	1.6
21.4	0 - 12.5	175	77	75	56	3.1
21.4	12.5 - 20	133	70	69	47	1.0
21.4	20 - 30	109	59	59	46	0.3
21.5	0 - 12.5	113	53	50	53	5.3
21.5	12.5 - 20	116	64	63	45	1.9
21.5	20 - 30	110	61	58	45	4.0
21.7	0 - 12.5	157	60	56	62	5.9
21.7	12.5 - 20	86	26	24	70	9.2
21.7	20 - 30	119	38	37	68	3.9
21.8	0 - 12.5	140	30	29	78	4.6
21.8	12.5 - 20	144	25	24	83	3.6
21.8	20 - 30	119	30	29	75	2.3

4.2.2.2 Combustion method

The total carbon (C_{tot}) and nitrogen (N_{tot}) content were measured using the combustion method. For the measurement, two tin capsules were filled with 3-4 mg of the milled soil samples (< 63 µm). These capsules were then all analysed with the Flash HT Plus elemental analyser.

4.2.2.3 Loss on ignition

The organic content of the soil can be determined by the loss on ignition. The weight loss due to combustion of the sample quantifies the organic content. The crucibles used were weighed and 2.0 g of fine soil (< 2 mm) was added. All samples were then heated in a muffle oven at 550°C for 6 hours to burn off the organic material contained. After cooling, the crucible including the burnt ash (inorganic material) was weighed again. The weight loss due to combustion represents the organic matter (Egli et al., 2016).

4.2.2.4 pH measurements

To measure the acidity of the soil, the soil samples had to be suspended. 5.0 g of the fine soil (< 2 mm) was weighed into a 50 ml beaker and 12.5 ml of 0.01 mol/l $CaCl_2$ was added. The solution was then stirred four times within 30 minutes and left to settle for an additional 30 minutes to allow the solids to sink. The $CaCl_2$ solution was then filtered into a 15 ml beaker (Egli et al., 2016). The pH meter was calibrated twice before the pH of the soil solution was measured four times. The mean value from the four measurements is used to represent the pH of the soil.

4.2.2.5 XRF

The total elemental content of the soil samples was measured by X-ray Fluorescence (XRF). To analyse the elements, 5.0 g of the milled soil (< 63 µm) was placed in prepared cups. The cups

were then placed into the Multi-Channel-Analyzer where the elemental content was measured over a period of four hours (Egli et al., 2016).

4.3 Data evaluation

The data analyses were performed with the software R-Studio (version 1.4.1106) A confidence level of 95% was used for all analyses (Kiewiet et al., 2020; Rinderer et al., 2014). The logarithmic scale was applied to some of the boxplots, to better illustrate the data range.

4.3.1 Statistical differences between depths or sites

To test for the normality of the solute concentrations and EC, the Shapiro-Wilk normality test was applied (Kiewiet et al., 2019) on all data values per depth and site. The Kruskal-Wallis test for one-way analysis of variance was used to determine whether there was a statistically significant difference between the independent non-parametric mean values of the concentrations at the four depths, the seven sites, and finally the depth and site. This test does not assume normality of the data and only ordinal scale was a necessary requirement. If the results of the Kruskal-Wallis test showed a statistically significant different mean value for the groups, The Dunn multiple comparison test was applied to determine which groups differed significantly. To control the family-wise error rate that could occur with this method, the Bonferroni Adjustment was used. For this, the p-value was adjusted by multiplying it with the total number of comparisons being made (Zuecco et al., 2019).

4.3.2 Relation between concentrations and site characteristics

The relationship between the mean solute concentration and plot location was examined using the Spearman's rank correlation analysis. Instead of the depth in cm, a depth factor was applied for this analysis (1, 2, 3 and 4 for L12.5, L20, L30 and GW, respectively). The ρ of Spearman's rank correlation shows how closely two variables vary; it ranges from -1 to 1. A positive ρ indicates a mutually reinforcing relationship, 0 means no correlation and a negative ρ shows that one variable is increasing, while the other is decreasing (Rinderer et al., 2014).

4.3.3 Change in solute concentration with depth

The relations between solute concentrations and soil depth showed that concentrations generally became more similar with increasing depths regardless of the solute. Therefore, logarithmic regression was used to describe the variation in concentration with depth.

$$C_z = C_0 \times e^{-\alpha z} \qquad \text{Equation 4.1}$$

Where C is the concentration in µg/l, z is the soil depth in cm, C_z is a solute concentration (µg/l) at depth z (in cm), C_0 is the solute concentration at the soil surface and α describes how quickly the solute concentration changes with depth. The value that is the most interesting in terms of research question 1 is the α. The value of α was therefore related to the TWI to determine how the change in solute concentrations with depth depends on topography. The logarithmic regression also indicated the p-value as well as the R-squared (R^2), which describes how well the data fit the logarithmic regression model (goodness of fit). The logarithmic regression was applied

twice, once for only the lysimeter data (L12.5, L20, L30) and once with for both the soil- and the groundwater (L12.5, L20, L30, GW).

It is assumed that heavy metals do not change over the soil depth. Therefore, linear regression was chosen to find α for the solutes Cu, Zn and Pb.

4.3.4 Changes in concentrations during events

To check general temporal changes in solute concentrations during the events, the paired sample Wilcoxon test was performed. This test checks if there is a significant difference between the mean concentrations before and after the precipitation event. The concentrations of the four events were analysed individually per depth and site using the one sample t-test. For this, the concentration changes during the four events were averaged and the t-test was used to determine whether the average concentration change was statistically different from zero (Kiewiet et al., 2020).

Spearman rank correlation was used to examine the change in concentrations of the solutes in the stream and the water level in the stream.

5 Results

5.1 Precipitation and streamflow

The total amount of precipitation during the four events was 39, 32, 39 and again 39 mm, and the events had a duration of within 20, 27, 82 and 6 hours respectively (Figure 4.4a and Table 5.1). The total precipitation amount was thus very similar for all four sampling periods, but the average intensities differed greatly: 1.8, 1.2, 0.5 and 2.6 mm h^{-1}, respectively.

Table 5.1: Hydrological characteristics during the four sampling events (n.a. in Event 4 due to missing measurements)

			Event 1	Event 2	Event 3	Event 4
	Event period		15.-18.09.21	18.-21.09.21	02.-08.10.21	18.-25.10.21
	Date precipitation event		16.-17.09.21	19.-20.09.21	03.-07.10.21	21.10.2021
Precipitation	Duration	h	20	27	82	6
	Total amount	mm	39	32	39	39
	Average intensity	mm h^{-1}	1.8	1.2	0.5	2.6
	Number of precipitation samples	-	2	2	4	3
Streamflow	Number of peaks during sampling period	-	1	1	1	n.a.
	Min stream level	cm	74	75	74	72
	Max stream level	cm	91	83	84	n.a.
	Mean stream level	cm	77	77	76	n.a.
	Number of streamflow samples	-	25	11	26	27

The stream reacted within two to four hours after the start of precipitation (Figure 4.4). The stream level increased to its maximum height at 91, 83, 84 cm throughout the first three rainfall events. The highest water level was generally reached three to eight hours after the maximum precipitation amount. Table 5.1 shows that the highest stream level of 91 cm was reached during the first event. This is due to the higher average rainfall intensity during the entire precipitation event than the total amount of rainfall that fell in an hour (which was measured during event 2).

5.2 Groundwater level

The topographic wetness index of the seven plot sites ranges between 3.4 for plot 21.1 to 7.0 for plot 21.8. The slope angle is steepest at plot 21.4 within the forest, and the flattest plot is at 21.8, which is located in an open wetland (see Table 4.1). Therefore, the groundwater level at the plot with highest TWI value (21.8) was also closest to the surface, whereas the lowest GW level was measured at the site with the steepest slope angle (21.4). At site 21.4, the groundwater well was empty (>120 cm) at almost at every sampling time, which made groundwater sampling difficult.

Overall, groundwater levels varied between 228 and 8 cm below the surface and among wells (Table 5.2). The topographic attributes (Table 4.1) can explain some of the hydrometric characteristics such as groundwater levels (Rinderer et al., 2016). On plot 21.3 the groundwater level logger stopped working before the start of the study period, resulting in the data gap (Table 5.2).

Not only the water level but also the skewness and the time period during which the water level rose above the sampling depths of 30, 20 and 12.5 cm below the surface varied (Table 5.2). Only

three wells had water levels rising within 30 cm below the surface. The wettest site, plot 21.8 had the highest groundwater level, that was for almost half of the sampling time within 30 cm from the surface. At plot 21.5, the water level rose the most. During the first rainfall event, the level rose up to 8 cm below the surface and remained above the 12.5 cm mark for more than five hours. The low permeability of the bedrock and the frequent input of new precipitation result in relatively high median groundwater levels at all sites, which is also reflected in the high soil moisture (see chapter 5.3).

Table 5.2: Overview of the groundwater dynamics at the seven sites measured between September and October 2021

Site	Median GW level below surface (cm)	Skewness of the frequency distribution of the GW level	Fraction of time GW level > - 30 cm (%)	Fraction of time GW level > - 20 cm (%)	Fraction of time GW level > - 12.5 cm (%)
21.1	103	0.7	0	0	0
21.2	78	-0.7	8.2	3.1	0
21.3					
21.4	>119*	-1.3	0	0	0
21.5	33	-0.6	8.7	3.1	1.3
21.7	60	0.4	0	0	0
21.8	30	6.7	48.6	16.1	0

*groundwater level was above the well depth only during half of the study period

5.3 Pedological plot characteristics

The general soil characteristics are described by the pH, skeletal fraction, and the amount of organic material (see Appendix: Table 9.2).

The soil moisture at the time of sampling varied from 37% at plot 21.3 to 83% at plot 21.8 (Figure 5.1a). Plots 21.1, 21.3, 21.4 and 21.5 had similar mean soil moisture contents between 37 and 57%. As expected, the two sites with the highest TWI also had the highest moisture content but the second driest plot according to its TWI actually had a higher moisture content than expected (46-64%).

There is some variation in the pH of the soil with TWI (Figure 5.1b). Most soil samples were slightly acidic with a pH between 5.3 and 7.0. Only three samples were slightly basic. Soils at the drier sites show a consistent acidic pH across the measured depths. Medium-dry locations show a slight increase in pH with increasing soil depth, with samples at 30 cm even being slightly basic. The wettest site, on the other hand, becomes increasingly acidic with increasing soil depth.

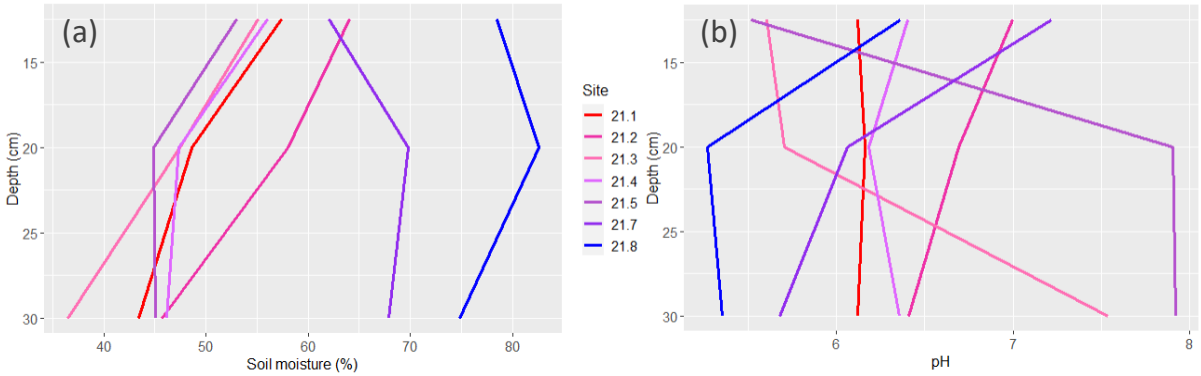

Figure 5.1: (a) Moisture content and (b) pH as a function of depth for each site (color-coded based on topographic wetness index). The sample taken from 0-12.5 cm, 12.5-20 cm, and 20-30 cm are plotted at 12.5 cm, 20 cm and 30 cm depth, respectively.

The soil skeleton was composed of stones, roots, and biomass. The number of roots and stones in the soil was quite low. A maximum of 1% of the soil samples were plant roots, and the highest number of roots was found in the soil closest to the surface (0-12.5 cm). The stone content was slightly higher (0-4% of the weight of the dried soil). Overall, the stone content was higher in the deeper soil samples (at 12.5-30 cm depth). The biomass recovered in all soil samples consists of grass blades, moss, dried leaves, pieces of branches and wood. Grass, moss, and dried leaves were mostly found in the top layer of the soil, the pieces of branches and wood were located further down.

The loss on ignition shows that the organic matter content generally decreased with soil depth. In the topsoil it was about 30%. At the drier sites, the content decreased with increasing soil depth down to 10-15%. At the two wettest sites, loss on ignition was highest at 33-53 %. This was probably due to the high biomass fraction that was observed for these soil samples.

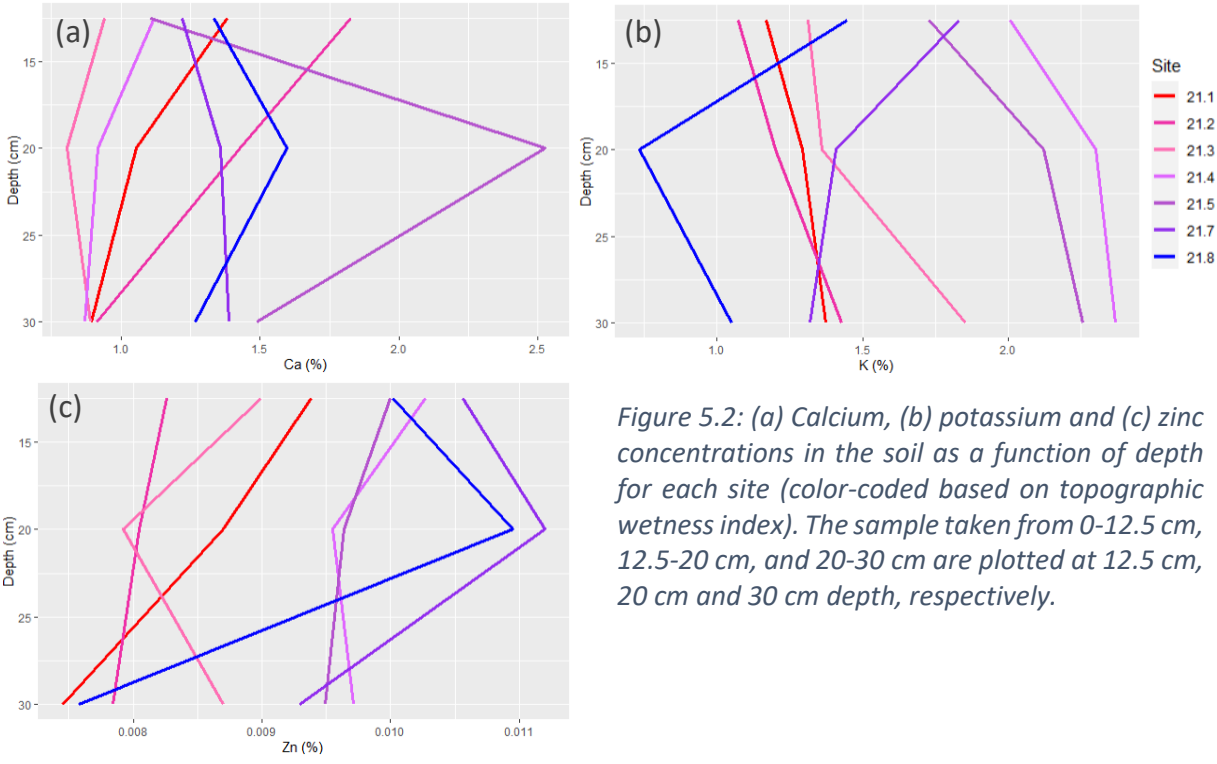

Figure 5.2: (a) Calcium, (b) potassium and (c) zinc concentrations in the soil as a function of depth for each site (color-coded based on topographic wetness index). The sample taken from 0-12.5 cm, 12.5-20 cm, and 20-30 cm are plotted at 12.5 cm, 20 cm and 30 cm depth, respectively.

The concentrations of the elements in the soil are given in % of the dry soil sample. Figure 5.2 shows that the concentrations generally vary with depth and location. Calcium and Potassium concentrations vary with soil depth in opposite ways, while variation in zinc concentrations were more similar to those of calcium. The calcium concentration was highest at the surface and decreased with increasing depth. The concentration was higher at the wetter locations (blue), whereas at the dry locations (red) the calcium concentrations in the soil were very low at a depth of 20-30 cm. An outlier is in plot 21.5, where the concentration is particularly high at 12.5-20 cm depth. Potassium was more abundant in dry locations at greater soil depths, while the two wettest locations had lower potassium concentrations at 30 cm than at the surface. Overall, the potassium concentrations at the surface were higher at the wetter locations. Zn concentrations were also highest at the surface of the wetter locations.

The concentration of calcium and potassium in the soil was similar at all seven plot locations (0-2.5 %). In comparison, the zinc concentration was much lower at only 0.007-0.012 %. Soil water showed similar concentration ranges for these three elements, but in µg/l. Calcium and potassium concentrations were high, while only traces of zinc were measured (see Appendix: Table 9.1).

5.4 Spatial variability in soil water and groundwater chemistry

5.4.1 Overall hydrochemical variation with depth and site

The most abundant solutes (>500 µg/l) found regardless of soil depth were calcium, magnesium, potassium, sodium, iron, manganese, sulphate, and phosphate. The most dominant solute was Ca, followed by Mg. Trace metals present in low concentrations (<10 µg/l) in soil- and groundwater included lead, cobalt, and copper.

Figure 5.3 shows how some of the measured concentrations change with soil depth. Electrical conductivity and calcium concentration increase with depth, indicating dilution behaviour. The opposite process is observed for deuterium and iron. The stable water isotopic composition and the concentration of transition metals decrease with increasing soil depth, which could suggest their mobilization with rising water levels and increased moisture content. These are only a few selected solutes that display the assumed hydrochemistry change over the soil depth below the surface.

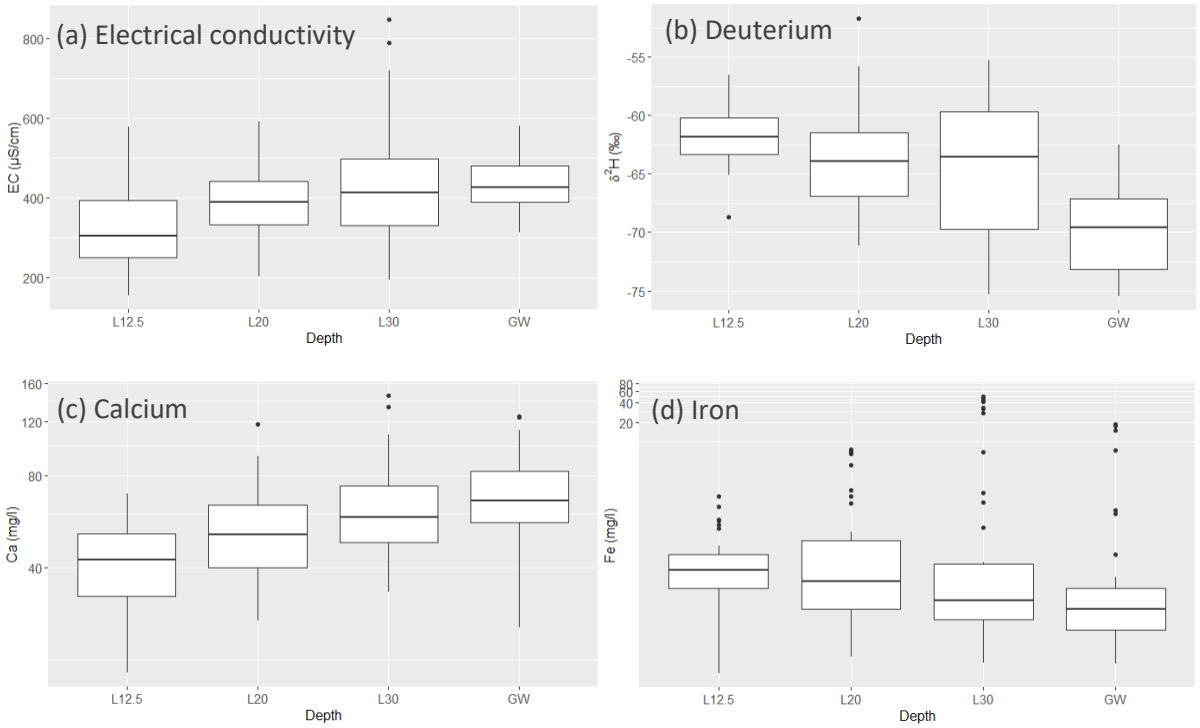

Figure 5.3: Boxplots showing (a) the electrical conductivity, (b) deuterium, and concentrations of (c) calcium and (d) iron for all the samples taken at the three different soil depths and the groundwater (GW). The box represents the interquartile range, the line the median, and the whiskers extend to 1.5 times the interquartile range and the points the outliers.

The spatial variability in electrical conductivity, stable isotopic composition and ion solute concentrations were generally large and for most solutes larger than the temporal variability. The median spatial range was measured based on the seven plot locations, while the median temporal range was determined through the seven sampling times. For 56% of the different solutes and sampling depths, the median spatial range was larger than the temporal range, and for 31% the temporal range was bigger. For the remaining 12.5% the two ranges were similar (see Appendix: Table 9.1). For most solutes, there was no consistent median spatiotemporal range over the four depths. Only for the lead concentration were the median temporal and spatial ranges similar for

all four soil depths. The one solute for which there was a consitently greater spatial than temporal variation was cobalt.

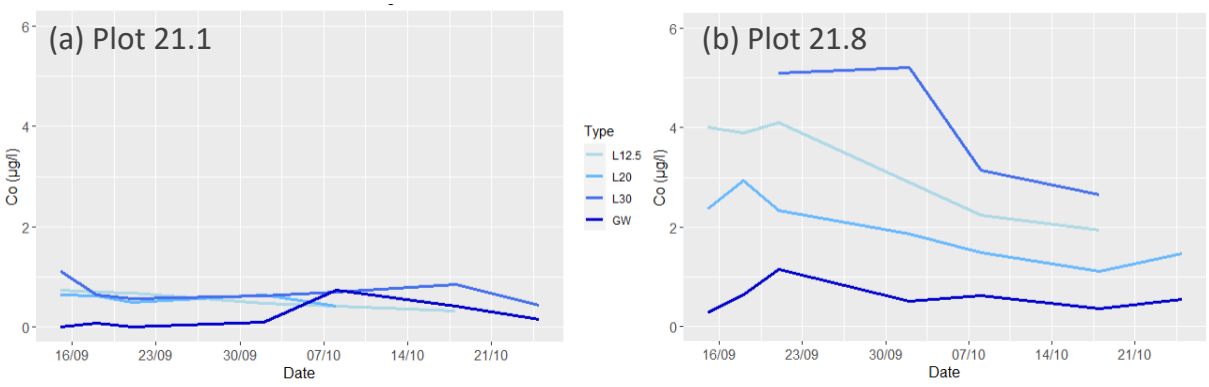

Figure 5.4: Spatiotemporal variability of cobalt concentration for the three soil depths and groundwater (GW) at the (a) driest and (b) wettest plot location.

For cobalt, there is no clear change in concentration with soil depth (Figure 5.4). At the driest site (plot 21.1 with a TWI value of 3.4) soil water concentrations appear to be almost identical over the entire period, with a slightly lower concentration in the groundwater. At the wettest site (plot 21.8 with a TWI value of 7), the cobalt concentration in soil water (L12.5, L20 and L30) is clearly elevated. At this site, the solute concentration appears to decrease with increasing soil depth with one exception at 30 cm depth. Solute concentrations also decrease slightly over time.

The Kruskal Wallis test of significance revealed that there was no statistically significant change in the mean concentrations with depth for boron and nitrate (Table 5.3); for the other fourteen solutes, the p-value was less than 0.05. The Dunn's test was applied to these to determine for which depths the mean values were statistically different. For almost all solutes, the concentrations in the groundwater differed from those in the soil. However, there was no statistical significance between the mean concentrations at the three soil water depths themselves. This behaviour makes sense because the samples from the lysimeters were taken at a distance between 7.5 and 17.5 cm, whereas the groundwater samples were taken further down at a depth of 40 to 120 cm below the surface. It is thus to be expected that the solute concentrations of the groundwater differ significantly from those of the soil water samples.

Table 5.3: Statistical significance between the mean concentrations measured at different soil depths (blue=statistically significant)

Solute	L12.5 vs. L20	L12.5 vs. L30	L12.5 vs. GW	L20 vs. L30	L20 vs. GW	L30 vs. GW
$\delta^{18}O$						
$\delta^{2}H$						
B						
Ca						
Na						
Mg						
K						
Cu						
Zn						
Pb						
Fe						
Mn						
Co						
NO_3						
PO_4						
SO_4						

Table 5.4: Statistical significance of the mean concentrations between different sites (blue = statistically significant; p < 0.05)

Solute	21.1 vs 21.2	21.1 vs 21.3	21.1 vs 21.4	21.1 vs 21.5	21.1 vs 21.7	21.1 vs 21.8	21.2 vs 21.3	21.2 vs 21.4	21.2 vs 21.5	21.2 vs 21.7	21.2 vs 21.8	21.3 vs 21.4	21.3 vs 21.5	21.3 vs 21.7	21.3 vs 21.8	21.4 vs 21.5	21.4 vs 21.7	21.4 vs 21.8	21.5 vs 21.7	21.5 vs 21.8	21.7 vs 21.8
$\delta^{18}O$																					
$\delta^{2}H$																					
B																					
Ca																					
Na																					
Mg																					
K																					
Cu																					
Zn																					
Pb																					
Fe																					
Mn																					
Co																					
NO_3																					
PO_4																					
SO_4																					

Statistical significance was also tested between the mean concentrations for the different plot locations was also tested (

Table 5.4). Mean concentrations did not vary between sites for magnesium, zinc, boron, and nitrate. For manganese and sulphate concentrations differed between most of the seven sampling sites.

5.4.2 Concentration changes with soil depth

5.4.2.1 Overall pattern

The soil- and groundwater depth related characteristics of the sixteen ion solutes and isotope concentrations studied, such as mean, standard deviation, median, minimum, maximum, spatial, and temporal range can be found in Appendix: Table 9.1.

Table 5.5: Spearman rank correlation between solute concentration and soil depth. Positive correlations are indicated in blue and negative correlations in red.

Solute	21.1	21.2	21.3	21.4	21.5	21.7	21.8
$\delta^{18}O$	-1.0	-0.8	-0.4	-0.4	-0.2	-0.4	-1.0
$\delta^{2}H$	-1.0	-0.8	-0.4	-0.4	-0.2	-0.4	-1.0
B	-0.8	0.4	-0.4	0.8	1.0	-0.2	1.0
Ca	0.8	0.4	1.0	1.0	0.8	1.0	0.4
Na	0.2	0.2	1.0	1.0	0.8	0.8	1.0
Mg	-0.6	-0.4	-0.2	-0.8	-0.8	-0.8	-0.8
K	-0.8	-0.8	-1.0	-0.8	-1.0	-1.0	-0.8
Cu	-0.8	0.4	0.4	0.2	0.4	0.2	-0.2
Zn	0.8	0.2	0.4	0.8	0.8	0.8	-0.4
Pb	-0.8	0.4	-0.4	0.4	0.2	0.2	0.4
Fe	0.4	-0.2	-0.4	0.0	-0.4	-0.4	0.8
Mn	-0.8	-0.8	-0.8	-0.4	0.4	-0.8	-0.4
Co	-0.4	-0.8	-1.0	-0.8	-0.2	-0.2	-0.4
NO_3	0.4	-0.8	0.2	1.0	0.4	0.4	-0.8
PO_4	-0.8	-1.0	-0.2	0.5	-0.4	-0.5	-0.4
SO_4	0.8	0.8	0.2	0.4	0.2	0.4	0.2

The correlation (ρ; Table 5.5) between solute concentration and sampling depth was calculated using the Spearman rank analysis. Even though for the majority of the solutes, there is a concentration trend with soil depth, none of the Spearman rank correlations are statistically significant. The reason is the non-monotonic change in the concentrations with depth, except for the heavy metals. Even for the heavy metals (Cu, Zn and Pb), the Spearman correlation coefficients are often between -0.4 and 0.4. Only for plot 21.1 was there a higher correlation coefficient for all three heavy metals. And zinc has a stronger trend leaning towards increasing with soil depth compared to the other two heavy metals. Regardless, rows that are predominantly blue (positive) indicate that the concentrations increase with depth. Rows that are predominantly red (negative) indicate that the concentrations decrease with depth. The lines where the colour changes indicate that there is no clear gradient with depth, that the trend depends on the site or is influenced by outliers. Solutes for which there is no clear depth trend are boron, copper, lead, iron, nitrate, and phosphate. Solutes for which there was a strong correlation with depth at almost all sites are calcium, sodium, magnesium, and potassium, all of which are base cations.

The concentrations of six solutes ($\delta^{2}H$, Ca, K, Zn, Mn and SO_4) are studied in more detail to show the spatial variations. Each solute is used as a representative for its group.

The abundance of deuterium decreases with increasing soil depth (Figure 5.3b and Figure 5.5a). At a depth of 12.5 cm below the surface, the mean δ^2H was -62‰; the mean at 20 and 30 cm depth was almost identical at -64‰. The δ^2H was the lowest for the groundwater with a of -70‰ (Appendix: Table 9.1). These numbers indicate that the deeper the sample was taken, the rarer is the isotope ^2H (Figure 5.5a). The same behaviour could be detected for oxygen as the mean $\delta^{18}O$ which decreased of -9.3 to -10.2‰ with increasing soil depth. The spatial pattern for the different plot locations is less clear. The δ^2H and $\delta^{18}O$ were similar at a depth of 12.5 cm for all sites, but for the other three depths. The isotope composition was lower at plots 21.1, 21.2, 21.7 and 21.8, and it increases measurably in the three middle plots 21.3, 21.4 and 21.5.

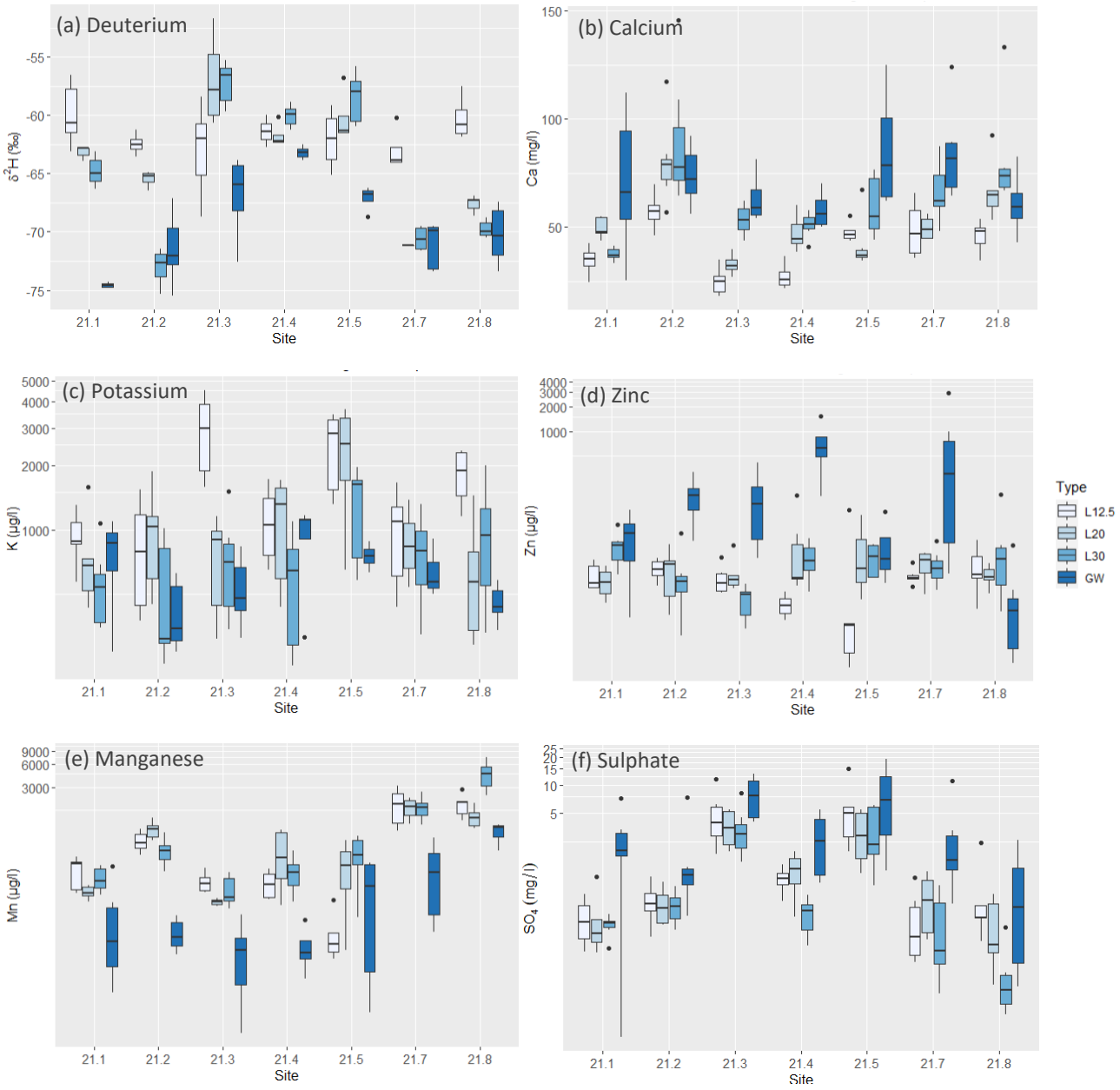

Figure 5.5: Boxplots showing the variation in (a) deuterium, and the concentrations of (b) calcium, (c) potassium, (d) zinc, (e) manganese and (f) sulphate for the four depths (three soil water and groundwater samples) for the different sites. Note the log-scale for c-f and the solutes in b and f are in mg/l.

The variation in base cation concentrations with soil depth can be divided into two types. For boron, calcium and sodium concentrations increase, while for magnesium and potassium the concentrations decrease with increasing soil depth. The concentration trend is clearest for calcium (Figure 5.5b). In the lysimeter closest to the surface, the mean Ca concentration was 41'480 µg/l, the mean for the second highest lysimeter was 53'559 µg/l and for the lowest it was 62'494 µg/l. The mean concentration was highest for the groundwater with a Ca concentration of 70'830 µg/l (Figure 5.3c and Appendix: Table 9.1). No other solute showed such high concentrations in soil- or groundwater. The change in calcium concentration with depth is similar for three of the seven measured sampling sites. Only at plots 21.2 and 21.8 was the concentration of dissolved calcium at L20 and L30 higher than in the groundwater. The amount of calcium is very similar at all seven plot locations.

The concentration of potassium in the sampled water is also high, but much lower than that of calcium. The highest concentration of K was measured closest to the surface at 1'617 µg/l. With increasing depth, the mean potassium concentration changed to 1'089, 764 and finally 618 µg/l in the groundwater. Figure 5.5(b) and (c) also clearly show that the range of calcium concentration in relation to the mean concentration is much smaller than that of potassium. Especially at 20 and 30 cm below the surface, the interquartile range (IQR) of K concentration is large, but there are few outliers overall. The standard deviation of potassium is generally large and does not appear to depend on site either. The amount of potassium is similar at all seven plot locations. Only 21.3 has an exceptionally high concentration at a depth of 12.5 cm (Figure 5.5c).

Zinc is used as a representative of the heavy metals. Its concentration generally increased with increasing soil depth (Figure 5.5d). The median concentration increases from 16, 17 and 20 µg/l in L12.5, L20 and L30, respectively to 69 µg/l in the groundwater. The amount is consistent at all seven plot locations for the lysimeters. Only the groundwater differed somewhat, with lower concentrations at 21.4 and 21.8. This pattern is not so pronounced for copper and lead. The median copper concentration decreases slightly in the soil water samples between 12.5 and 30 cm (1.6 to 1.2 µg/l, respectively), but then increased in the groundwater (up to 3.4 µg/l). The concentrations of lead were highest at 12.5 cm depth and in the groundwater, but the concentration change was generally minimal over depth with median concentrations between 0.01 and 0.05 µg/l. It is notable, that the mean groundwater concentrations are much higher than the median concentration for all three solutes. This is because site 21.4 seems to have an abnormally high concentration of heavy metals in the groundwater (Figure 5.5d). The mean groundwater concentrations at plot 21.4 are 727 µg/l for zinc, 176 µg/l for copper and 8 µg/l for lead. Without this location, the mean groundwater concentration would be 188 µg/l, 6.7 µg/l and 0.13 µg/l, respectively.

The transition metal manganese has the tendency to decrease its concentration in the soil (Figure 5.5e). Groundwater contains the lowest manganese concentration at all but one plot locations, with a mean concentration of 216 µg/l. However, the highest median manganese concentration is found at 20 cm (609 µg/l) instead of 12.5 cm (315 µg/l) depth. Below 20 cm the median concentration decreases with increasing depth. The mean concentration of L30 deviates strongly from the median. Calculating the overall mean value for L30 yields a concentration of 1'052 µg/l

as the mean value. This outlier is caused by the huge concentration of manganese found on plot 21.8 at 30 cm soil depth (Appendix: Table 9.1). On average, the mean concentration of L30 at this location is 1'868 µg/l, whereas the median concentration for all locations is 333 µg/l (Figure 5.5e). Exactly the same outlier is found for the iron concentration. The median values indicate a decreasing iron concentration over soil depth from 105 µg/l at L12.5 to 27 µg/l in groundwater. The outlier in L30 in plot 21.8 results in a mean concentration of 5'305 µg/l for L30, whereas the median concentration is only 36 µg/l. The cobalt concentration is the lowest at only 0.3 to 2.3 µg/l. As can be seen in Figure 5.4, the cobalt concentration increases with depth, with the lowest concentration in groundwater. The median concentration change with soil depth of the three transition metals differs from the mean solute concentrations due to the large outlier in plot 21.8 at 30 cm depth. For cobalt, there is another outlier in plot 21.7, also at 30 cm depth (Appendix: Table 9.1).

The anions show a similar uncertain concentration change as the transition metals. The median sulphate concentration decreases in the soil water (from 2'074 to 1'157 µg/l), but the highest concentrations were found in the groundwater (3'656 µg/l; Appendix: Table 9.1). This pattern is similar for all seven plot locations. It is also apparent that the groundwater concentration has the widest range of all depths, and for sulphate there are several large outliers (Figure 5.5f).

Mean nitrate concentration generally increases with soil depth from 48 to 76 µg/l, but the solute concentration is slightly higher at L20 (67 µg/l) than at L30 (51 µg/l). The NO_3 concentration range is generally high for all locations and depths and has even more outliers than sulphate. The standard deviation is correspondingly large. Phosphate is the solute with the greatest uncertainty range, as many samples have a concentration below the detection limit of 1 µg/l. Only 55% of the 172 soil and groundwater samples had a measurable phosphate concentration.

5.4.2.2 Fitting exponential (or linear) functions

*Table 5.6: Slope of logarithmic resp. linear regression of solute concentration with soil depth (where * = linear regression, bold = statistically significant, grey = $R^2 < 0.4$). The column Expect indicated if the decrease (red) or increase (blue) in concentrations matched the expectations (as described in chapter 2.1).*

Solute	21.1	21.2	21.3	21.4	21.5	21.7	21.8	Expect.
$\delta^{18}O$	**-0.8**	-0.6	0.9	0.0	-0.3	-0.3	-0.9	✓
$\delta^{2}H$	**-6.4**	-4.8	6.7	-0.8	-2.7	-3.3	-7.4	✓
B	-48	21	-123	18	**107**	7	**40**	(✓)
Ca	15'104	6'434	32'142	11'600	31'746	**20'039**	13'881	✓
Na	39	58	27	161	293	119	5'924	✓
Mg	-3'542	-2'039	2'950	-2'868	-15'561	-2'850	-2'702	×
K	-49	-276	-2'606	-88	-1'578	**-195**	-881	×
Cu*	**-0.003**	**0.189**	-0.028	**1.764**	0.050	**0.217**	-0.007	(✓)
Zn*	0.3	**2.2**	-0.5	**7.2**	0.5	**9.9**	-0.2	×
Pb*	-0.001	0.007	-0.010	**0.078**	-0.002	0.000	0.001	(✓)
Fe	18	-139	-317	-15	-16	-26	12'953	(✓)
Mn	-65	-361	-40	-114	146	-832	2	(✓)
Co	-0.2	**-0.5**	-0.4	-0.4	0.3	-1.6	-1.2	✓
NO_3	3	-27	112	**66**	142	7	-14	✓
PO_4	-520	-240	**1'446**	261	-105	-43	-7	(✓)
SO_4	1'081	721	-1'801	868	1'373	1'424	-9	(✓)

The slope α of the concentration as a function of soil depth was calculated using Equation 4.1. Similar to the Spearman rank correlation, α indicates whether the solutes per site increase or decrease with depth. A large discrepancy is visible between Table 5.5 and Table 5.6 for plot 21.3. The reason for this is missing data. The groundwater level could not be measured at this site, therefore the column for plot 21.3 in Table 5.6 does not contain information on the concentration of the solute in the groundwater. There are also some additional deviations for lead and cobalt in plot 21.5, boron in plot 21.7 as well as manganese and sulphate in plot 21.8. These deviations between the two tables are due to the solutes' irregular behaviour over the soil depth. The correlation and the slope are very close to zero in all five cases and the goodness of fit is less than 0.4, therefore uncertainties and small deviations have a large impact on both the Spearman rank correlation and α. Table 5.6 also shows that even though the goodness of fit is reasonable for most slopes, there are few statistically significant values. However, the majority of solutes follow the expected change in concentration over soil depth.

The mean concentration (over site and depth) is shown for deuterium, calcium, and potassium in the left plots of Figure 5.6. These figures show that the mean groundwater level is closer to the surface at the wetter locations. The plots on the right-hand side of Figure 5.6 portray the concentration change over depth (slope α) for the three solutes compared to the proportion of time that the groundwater level was within the top 30 cm of the soil. The groundwater at the wettest site was above the 30 cm mark most of the time, which causes the data to be skewed.

For $\delta^{2}H$, the most negative concentration change with depth were observed at the wettest and driest sites (Figure 5.6a). However, in contrast to plot 21.8, where the groundwater level was

almost 50% of the time within the upper 30 cm, groundwater at plot 21.1 was always below this level. The only positive change in concentration was observed for plot 21.3 (+ 6.7 ‰ between 12.5 and 30 cm) but could not be shown in the figure since the groundwater level was not measured.

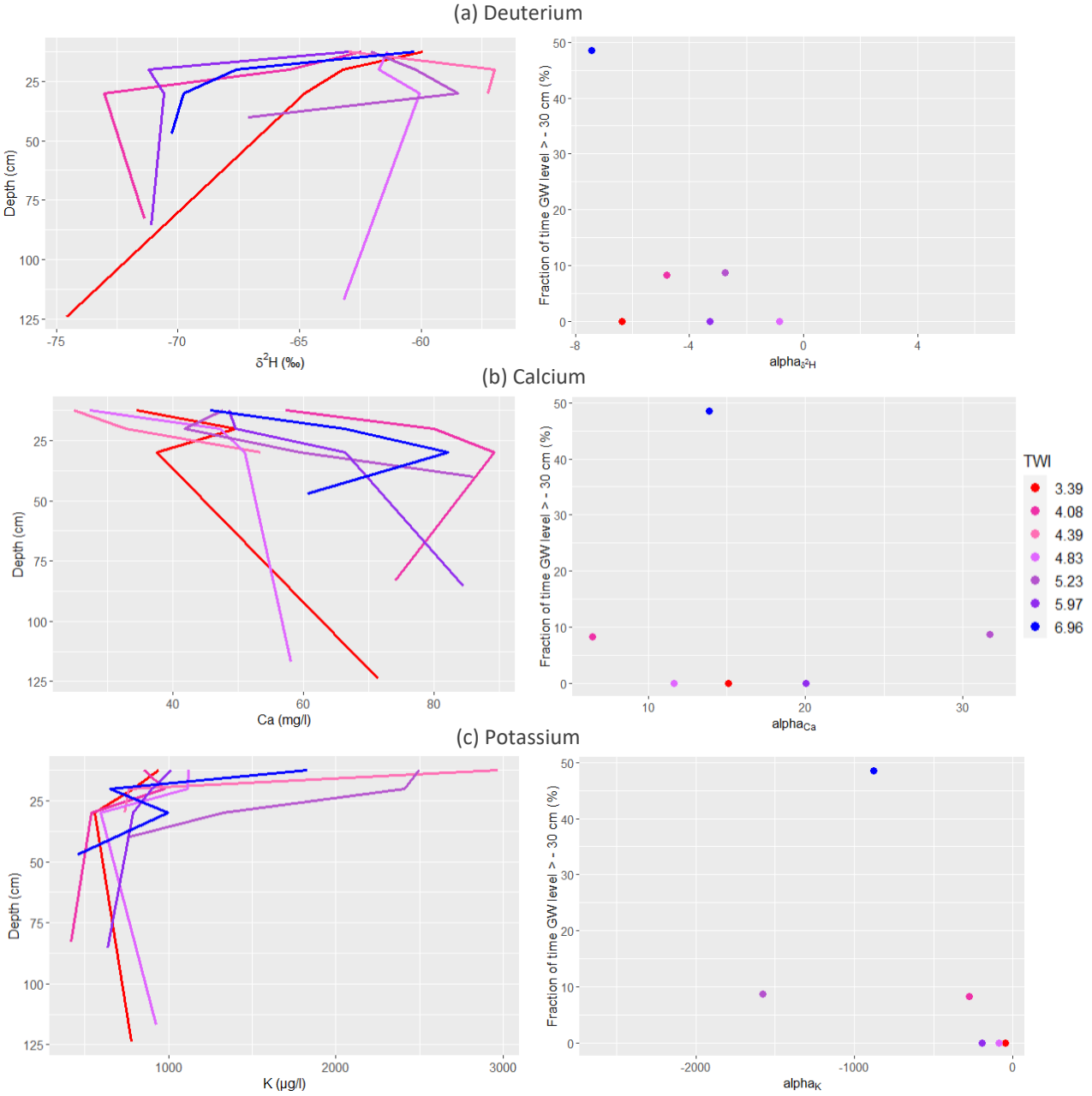

Figure 5.6: Site specific concentration change with depth (left) and the slope α of the concentration compared to the fraction of time the GW level was above 30 cm depth (right) for (a) deuterium, (b) calcium and (c) potassium. Note the different units and 21.3 is not displayed in the figures on the right.

For calcium, the results are similar to those of deuterium, except that the slope of concentration change with depth is positive (increasing with depth; Figure 5.6b). The concentration changes with depth were larger for the wetter plots, where the water level was closer to the surface. The higher groundwater level could therefore have influenced the calcium concentration in the soil water.

Figure 5.6c shows the decreasing potassium concentration over soil depth with very high concentrations at the surface. The corresponding figure on the right shows that the strongest most

negative decrease over depth were observed for plots 21.8 and 21.5, while at the other five locations the concentrations were almost constant over depth. The groundwater level at these locations practically never reached 30 cm below the surface. The slope was most negative for plot 21.3 but it is not shown in the figure because the data on GW level is missing.

5.4.3 Topographic and hydrodynamic influences on water chemistry

To test the influence of the topographic and hydrodynamic site attributes on the depth variation in the concentrations, the locations' topography (topographic wetness index as well as the slope angle) and the hydrodynamic effect (the median groundwater level) were related to the slope value α using Spearman rank correlation.

The influence of the TWI on the change in solute concentration over soil depth was found to be relatively small. The Spearman's rank correlation between α and the TWI ranged from -0.50 to 0.79 (Table 5.7). Changes in the isotopes, and the concentration changes over depth for potassium and cobalt were higher at the relatively dry sites, whereas for the other base cations (B, Ca, and Na), transition metals (Fe, Mn) and anions, the changes in concentrations with depth were highest at the wetter locations (Table 5.7). Only for boron, sodium and cobalt was the Spearman rank correlation higher than 0.5 and only for sodium was the correlation statistically significant. Changes in sodium concentrations with depth rise significantly with increasing wetness (0.79), while for cobalt they decrease (-0.5). The correlation between the alpha value for boron and the wetness index is 0.5, for this solute there is no clear or significant concentration change with soil depth (Table 5.5). For the other dissolved substances the variation in α cannot be explained by the different wetness indices (Table 5.7).

The slope appears to have an equally small influence on the change in solute concentration with depth. The most affected solutes are the heavy metals (>0.5). The change in concentrations with depth for heavy metals is higher at the plot locations with steeper slopes. But the slope's influence is not statistically significant for any of the solutes.

The groundwater level attribute had the strongest influence on the change in solute concentration (α) at depth. For the base cations boron, calcium and sodium, changes in concentrations generally increase with an increasing water table (see Table 5.6). This means that the base cation concentration change is higher within the groundwater when the water table is closer to the surface. That is reasonable since water facilitates the weathering of the bedrock and soil water mixes with the groundwater when the water table is high. A higher water table has the opposite effect on the variation in the base cation potassium and the heavy metals copper and zinc with depth. For these solutes the variation in concentration with depth is greater if the water table is low. This can be due to accumulation of these ions on the surface and less flushing by the groundwater. But none of the slope values α had a statistically significant correlation with the groundwater level.

Table 5.7: Spearman rank correlation between the change in solute concentration over soil depth, as indicated by α (Equation 4.1) and topographic wetness index, slope, and groundwater level, as well as correlation between the variation with depth and TWI (where bold = $p < 0.05$, grey = $R^2 < 0.4$)

	change in concentration			**variation with depth**		
Solute	α vs. TWI	α vs. slope	α vs. GW level	SD vs. TWI	IQR vs. TWI	Range vs. TWI
$\delta^{18}O$	-0.11	0.40	0.43	-0.64	-0.29	-0.39
$\delta^{2}H$	-0.11	0.40	0.43	-0.64	-0.32	-0.36
B	0.50	0.29	-0.66	-0.50	-0.39	-0.29
Ca	0.14	-0.38	-0.43	-0.21	-0.04	0.21
Na	**0.79**	0.13	-0.66	0.18	0.14	0.11
Mg	-0.04	-0.41	-0.14	-0.43	-0.61	-0.21
K	-0.32	0.32	0.83	0.32	0.39	0.25
Cu	0.07	0.85	0.60	-0.07	-0.43	-0.07
Zn	0.00	0.65	0.60	0.25	-0.57	0.32
Pb	0.25	0.56	0.26	-0.50	**-0.86**	-0.50
Fe	0.29	-0.18	-0.14	0.43	0.46	0.43
Mn	0.21	-0.34	-0.43	0.68	0.71	0.68
Co	-0.50	0.18	0.26	**0.86**	**0.86**	**0.82**
NO_3	0.14	0.22	0.09	-0.43	-0.71	-0.54
PO_4	0.43	-0.16	-0.09	**-0.93**	-0.75	**-0.89**
SO_4	0.14	0.45	0.09	-0.14	-0.25	-0.14

The relation between the TWI and the standard deviation (SD), interquartile range (IQR) and total range in generally match the results for α, except for calcium and zinc (Table 5.7). The SD and IQR for calcium are higher at the wetter locations, while the overall range is higher at the drier sites. For zinc, the SD is greater than the IQR due to the high concentration of zinc in the groundwater at location 21.7 (Figure 5.5d). This causes the standard deviation to be higher at wetter sites, while the IQR is higher at the drier sites.

The variation in isotope, lead, and anion (nitrate, phosphate, and sulphate) concentrations are higher overall at drier locations. The opposite is true for the variation in the concentrations of sodium, potassium, and transition metals (iron, manganese, and cobalt), which are higher at wetter locations.

5.5 Temporal variability in soil water and groundwater chemistry

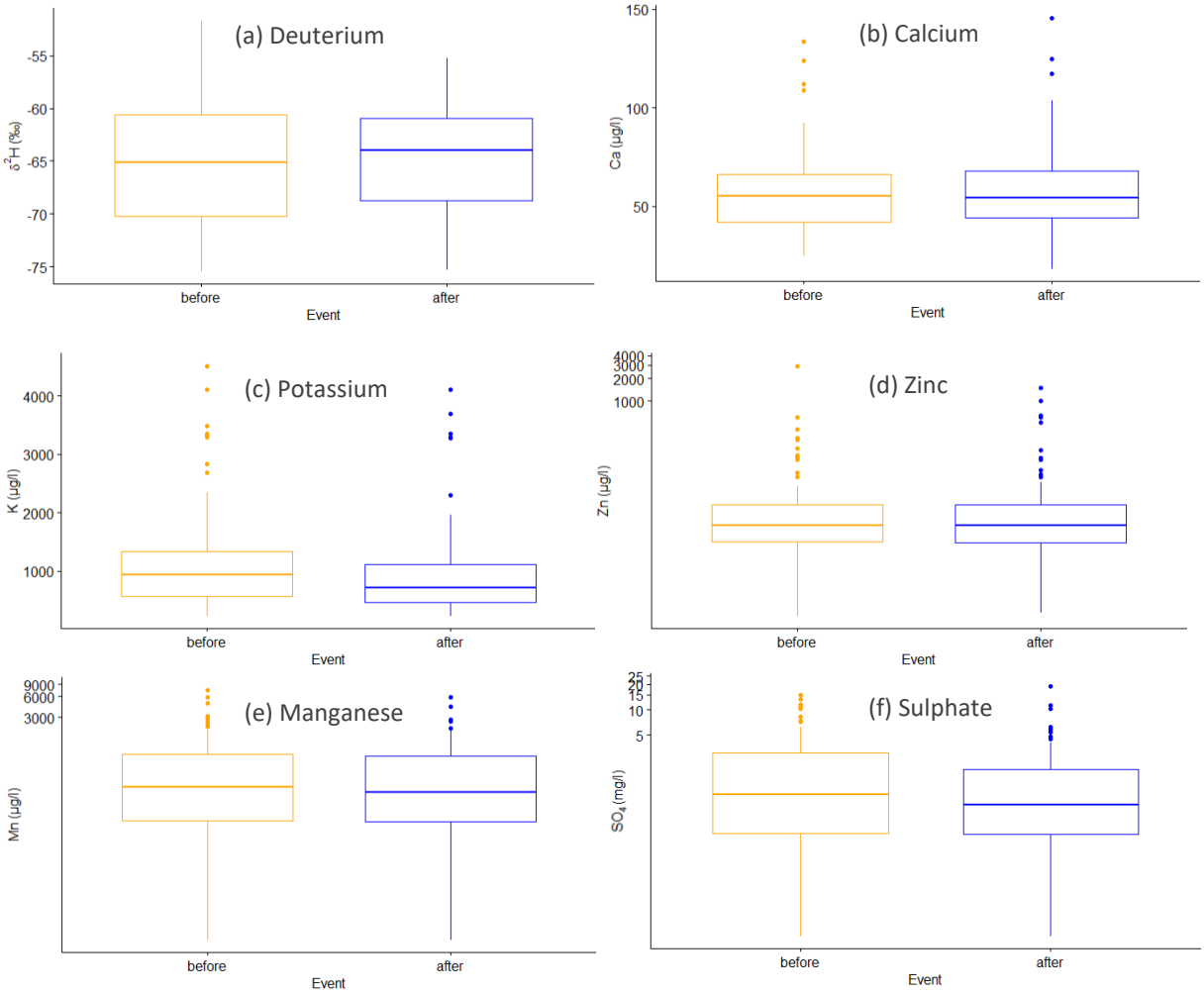

Figure 5.7: Boxplots of the solute concentration before and after precipitation event for (a) deuterium, (b) calcium, (c) potassium, (d) zinc, (e) manganese and (f) sulphate. Note the log-scale for d-f and the solutes in b and f are in mg/l.

The temporal variation in the six representative dissolved substances is shown in Figure 5.7. It shows how the average concentrations of solute differ between the samples taken before and after the event. The soil- and groundwater concentrations change only minimally with a slight increase during the event for the isotopes and a slight decrease for the base cations, transition metals and anions. The concentrations of heavy metals did not change during any of the four events. The interquartile range for the solutes in Figure 5.7 is also practically equal and a similar number of high outliers can be seen in the boxplots.

The Shapiro Wilk test of normality showed that all solutes, except phosphate were not normally distributed. Therefore, the paired samples Wilcoxon test was used to determine the significance of the changes before and after the events. The samples taken on the 18th of September were used once as pre-event and once as post-event samples. The paired samples Wilcoxon test showed that only for boron, magnesium, and potassium there was a significant difference in the mean concentration before and after the event.

The paired sample t-test was applied for each site and depth for each of the four individual events. Out of the 448 statistical comparisons (16 solutes at seven sites over four depths during four

events), only 18 (=4%) were significantly different from zero. A statistical decrease during the events was detected for $\delta^{18}O$ in plot 21.2 in groundwater, copper in plot 21.7 at 30 cm depth, lead in plot 21.5 at 12.5 cm depth, and cobalt in plot 21.8 in groundwater. A statistical increase during the events was recorded for calcium in plot 21.3 at 12.5 cm and plot 21.7 at 30 cm depth, zinc in plot 21.2 in groundwater and 21.7 at 20 cm depth, manganese in plot 21.4 and 21.8 at 30 cm and in plot 21.7 at 12.5 cm depth, cobalt in plot 21.4 at 30 cm depth, nitrate in plot 21.1 at 30 cm depth, phosphate in plot 21.1 at 20 cm and in plot 21.3 at 12.5 and 20 cm depth, and finally for sulphate in plot 21.3 in groundwater and plot 21.4 at 20 cm depth (see Appendix: Table 9.3). In summary, the results suggest that there is no consistent temporal change in concentration at all at any of the four events.

6 Discussion

6.1 Temporal variability in hydrochemistry

A temporal variability between the solute concentrations before and after the precipitation event could not be detected. Only 4% of the analysed temporal changes during the four rainfall events were significantly different from zero. There is practically no significant change in solute concentration during the rainfall event. Most of the statistically significant changes in solute occurred at 30cm soil depth. But since these are only six of the 448 statistical comparisons, there is no evidence that the difference in concentrations of samples taken before and after the event is greater anywhere in the total soil depth. Therefore, we have to reject the hypothesis for the third research question from the Introduction that there is a significantly greater difference closer to the surface or at the drier locations.

This is a confirmation that the spatial variability in solute concentration in soil water and groundwater is much greater and thus should get much more attention than the temporal variability. It does not matter whether the soil water and groundwater samples were taken before, during or after the event. This also explains the greater number of research papers on the spatial variability, whereas temporal variability has often been neglected or simply less researched. Even Kiewiet et al. (2019) investigated both spatial and temporal variability of hydrochemistry in the Studibach catchment, and the only conclusion they could draw about changes over time was that spatial variability was greater than temporal variability.

However, the chemical composition of the stream water can change considerably over time, especially during rainfall events. The incoming amount of precipitation and the duration of the rainfall influence the hydrological connectivity of the catchment, which in turn leads to different contributions of soil- and groundwater to the stream. This makes the composition of the stream water very unpredictable, and it is very difficult to trace it back to its source.

6.2 Spatial variability of hydrochemistry

The change in solute concentration in soil- and groundwater with soil depth depends strongly on the dissolved substance studied and its origin. Most solutes behave as expected over the soil depth. Their concentration changes significantly from the soil water to the groundwater level, but the change is not statistically significant within the first 30 cm below the surface. The logarithmic slope α (see Table 5.6), which was formed from the mean value of the concentration over the soil depth, portrays the individual increase or decrease well, but was not always consistent at the different plot locations and only statistically significant in individual cases. The results show that the spatial variability of isotopic composition and solute concentrations in a headwater catchment can be very large.

6.2.1 Variation in hydrochemistry over soil depth

The average concentration range of the sixteen measured solutes largely coincide with the groundwater measurements carried out by Kiewiet et al. at the same locations in 2016 and 2017. Only the heavy metal and anion concentrations differ significantly. The groundwater concentrations of Zn, Cu, Pb, Fe, NO_3 and PO_4 were about four times higher in the sampling

campaigns of Kiewiet et al. (2019) in 2016/17 than the samples taken in 2021. The decrease in heavy metals in soil- and groundwater could very well be connected to the global COVID-19 lockdown and restrictions in 2020. The pandemic-related lockdown led to a decrease in human activities such as travel by car or plane. This improved the air quality in the atmosphere and apparently also the quality of the groundwater. Atmospheric dust inputs in autumn 2021 were cleaner and their deposition was less polluted than in 2016/17. The same phenomenon was observed by Aravinthasamy et al. (2021) in South India. Where heavy metal pollution in shallow groundwater decreased significantly between February and June 2020. The pandemic could also have caused the decrease in Fe concentration but the weather in summer 2021 could have influenced it as well. The summer in 2021 was unusually wet with a high number of storms (WSL, n.d.). The heavy rainfalls caused the soil to be more saturated compared to previous years during the summer. This increase in wetness reduces the redox potential in the soil whereby the dissolved Fe concentration is reduced within the groundwater (Rao et al., 2021). The heavy rainfall in the summer of 2021 may also have led to a reduction in the NO_3 concentration in the groundwater. The wet summer leached the dissolved substance out of the soil. And new nitrate could not be produced fast enough due to the diminished microbial activity caused by the lower temperatures in the topsoil. The PO_4 concentration is extremely low for the same reason. It is already poorly soluble, and the diminished microbial activity makes it almost undetectable (Pastore et al., 2020).

Almost all the solutes investigated behave as expected over depth. The concentrations of the stable water isotopes $\delta^{18}O$ and $\delta^{2}H$ decrease with increasing soil depth. Precipitation water is more depleted in $\delta^{18}O$ and $\delta^{2}H$ than soil water at the surface. The lighter isotopes in the upper soil water might have evaporated resulting in a slightly higher isotope abundance compared to precipitation. Since evaporation occurs mainly at the soil surface, the lower soil water and groundwater samples of old snowmelt were more depleted in the heavier isotopes ^{18}O and ^{2}H and therefore had lower concentrations of stable water isotopes (Mook & Geyh, 2000a).

The concentration of the base cations was supposed to increase with depth. This was only the case for the concentrations of B, Ca, and Na, which were formed by weathering through contact with the bedrock. The acidic soil leads to more dissolution of the carbonate bedrock, which increases the concentration of most base cations in the groundwater (Jutebring Sterte et al., 2021; Kiewiet et al., 2019). The fact that the bedrock is the source of these base cations also explains their very low concentrations in the precipitation compared to the much higher concentrations in the stream (see Appendix: Table 9.1). The source of Mg and K must come from the atmosphere, but not from precipitation, since the mean concentration of magnesium in the rainfall was 34 µg/l, whereas the concentration in topsoil was 9’795 µg/l. Mg and K are in generally influenced by plant uptake, because they are macro nutrients. In the soil water, the mean concentrations are clearly the highest at a depth of 12.5 cm. The Mg and K concentrations in the soil samples taken are also higher above 12.5 cm than between 12.5 and 20 cm. This is surprising as the roots in the topsoil should absorb the magnesium and potassium in the soil, which would lower the concentration in the topsoil compared to 12.5 - 20 cm. The elevated concentrations of magnesium and potassium in the soil and the high dissolved magnesium concentration in the soil water cannot be explained (Jutebring Sterte et al., 2021). The source of Mg is not clear as Jutebring Sterte et al. (2021) assume that it comes from the decomposition of rocks. However, very few stones were found in the

topsoil. Only 0.7% of the soil samples within 20 cm below the surface were stones. Although the source of K seems to be as expected the potassium rich needles of conifers (Tripler et al., 2006).

The concentration of heavy metals remains constant in the first 30 cm of soil below the surface in both the hydrological and pedological samples (Appendix: Table 9.1 and Table 9.2). Only the concentrations in the groundwater are slightly higher than expected, especially for Zn. The source of the increased Zn concentration in groundwater appears to be natural due to erosion of minerals from rocks and soil, and not anthropogenic (Rao et al., 2021). Zn is poorly soluble. But in combination with the slightly elevated Pb concentration in groundwater, the increased natural Zn concentration seems reasonable (Li et al., 2021).

The only transition metal that shows the assumed change over depth is iron. This metal has its highest concentration at the surface, where the redox reaction was strongest due to high oxygen availability (Kiewiet et al., 2020). This led to the oxidation of pyrite and other minerals (Brown, 1985; Gu et al., 2020). Mn and Co have the highest concentration at 20 cm below the surface, and the second highest in 30 cm depth. Co generally has very low concentrations, often below 0.1 µg/l. Mn has higher concentrations in soil- and groundwater but is hardly detectable in precipitation or in the stream due to its insolubility. Soils contain less than 0.1% Mn and less than 0.005% Co.

The three anions nitrate, phosphate and sulphate cannot be grouped due to their change in concentration over depth. There is little to no anthropogenic input of NO_3 in the study area, since no agricultural or livestock farming in sub-catchment 21 is occurring. Therefore, the source is most likely leaching from nitrogen-bearing rocks. The NO_3 concentration in the soil itself is higher closer to the surface, but in soil water it increases with increasing soil depth. Heavy rainfalls flush the available nitrogen from the topsoil and leach it into the groundwater and stream (Zhi & Li, 2020). PO_4 concentrations are generally low, very often they were undetectable (less than 0.01 µg/l). Overall, the highest concentration was measured at a depth of 20 cm. The availability of PO_4 correlates negatively with the pH value. This is consistent with the findings of Pastore et al. (2020) in five forests in Germany. The more acidic pH at 20 cm depth causes PO_4 to be extracted from the hydroxyapatite mineral. It is also possible that the high Fe concentration in the uppermost 12.5 cm causes the lower PO_4 availability. Iron oxyhydroxides can bind and absorb phosphate, causing the PO_4 concentration to drop sharply, while the Fe-oxide concentration remains practically the same (Herndon et al., 2020). SO_4 appears to have two sources, since the concentration is very high in groundwater and topsoil, but quite low at 30 cm depth. The oxidation of the before mentioned pyrite increases the concentration of SO_4 and lowers the pH at the same time. The slightly more acidic soil in turn increases the dissolution of evaporite, which further increases the concentration of SO_4. The anions are clearly the most diverse group of ions analysed in this thesis.

The soil samples taken from 0–12.5, 12.5–20 and 20–30 cm depth show the opposite change in concentration over soil depth compared to the water samples taken from the same depths. If the concentration of the dissolved substance increases with increasing soil depth, the concentration in the soil shows a decreasing behaviour. This phenomenon seems contradictory at first glance, but it is logical. Readily soluble substances are easily leached out of the soil and enter the water

directly. Poorly soluble substances such as heavy metals or phosphate have a higher concentration in the soil and appear only in traces in the soil water.

The entire environment of atmospheric input, surface vegetation, topography, subsurface attributes, soil, groundwater level and rock minerals have their individual influence on the stable isotope composition and solute concentration in soil- and groundwater in this sub-catchment. And as Kiewiet et al. (2019) has shown, this large spatial variability applies to the entire pre-alpine headwater catchment.

6.2.2 Variation in hydrochemistry with space

The spatial variability at the different plot locations is much less pronounced than in soil depth. Topographic site attributes have a relatively small influence on solute concentrations. Only the groundwater level correlates more strongly with some of the dissolved substances studied. Even though the topographic wetness index has little influence on the solute concentration itself, the variation of the concentration with depth is influenced by the wetness index of the site. For most solutes, concentration variations are more pronounced at sites with a low topographic wetness index.

The differences in solute concentrations at the seven sites are generally not very pronounced, with some isolated outliers. But these outliers cannot be explained as some kind of measurement error, as all seven samples taken during the sampling period from these specific sites (and depths) had equally high divergent concentrations from the mean. The concentration of the base cation Na in plot 21.8 differs significantly from all other plots over the entire depth (see Figure 6.1a). It is possible that the high humidity at this site led to increased salt weathering of the bedrock, which caused the eight times higher Na concentration in the groundwater at well 21.8 compared to the mean groundwater concentration of the other six wells (Sato & Hattanji, 2018). The heavy metal concentration was several times higher in the groundwater level of plot 21.4 than the others plots (see Figure 6.1b). For Zn, the concentration in the groundwater of plot 21.7 was equally high. The reason for the extremely high concentration of these three solutes (Cu 8x higher, Zn 3x higher and Pb 9x higher) is unknown since their origin should be from atmospheric deposition. But at site 21.4 the concentration appears to be related to the groundwater and it is apparently spatially variable. The transition metals are highest over the whole depth at the two sites 21.7 and 21.8 (see Figure 6.1c). The increased concentration is caused by the heavy wetness at the two sites, which accelerates the redox reaction (Feng et al., 2007; Rao et al., 2021). The last solute that also shows an unexpected increased concentration over the entire depth at plots 21.3 and 21.5 is SO_4 (see Figure 6.1d). Its mean concentration is about four times higher in groundwater at these two sites, while the difference is smaller closer to the surface. It could be that there is more pyrite in the bedrock at these two locations, the oxidation of which is causing the increased SO_4 concentration in the groundwater. However, the reason the concentration at the surface is also higher at these two locations is unknown.

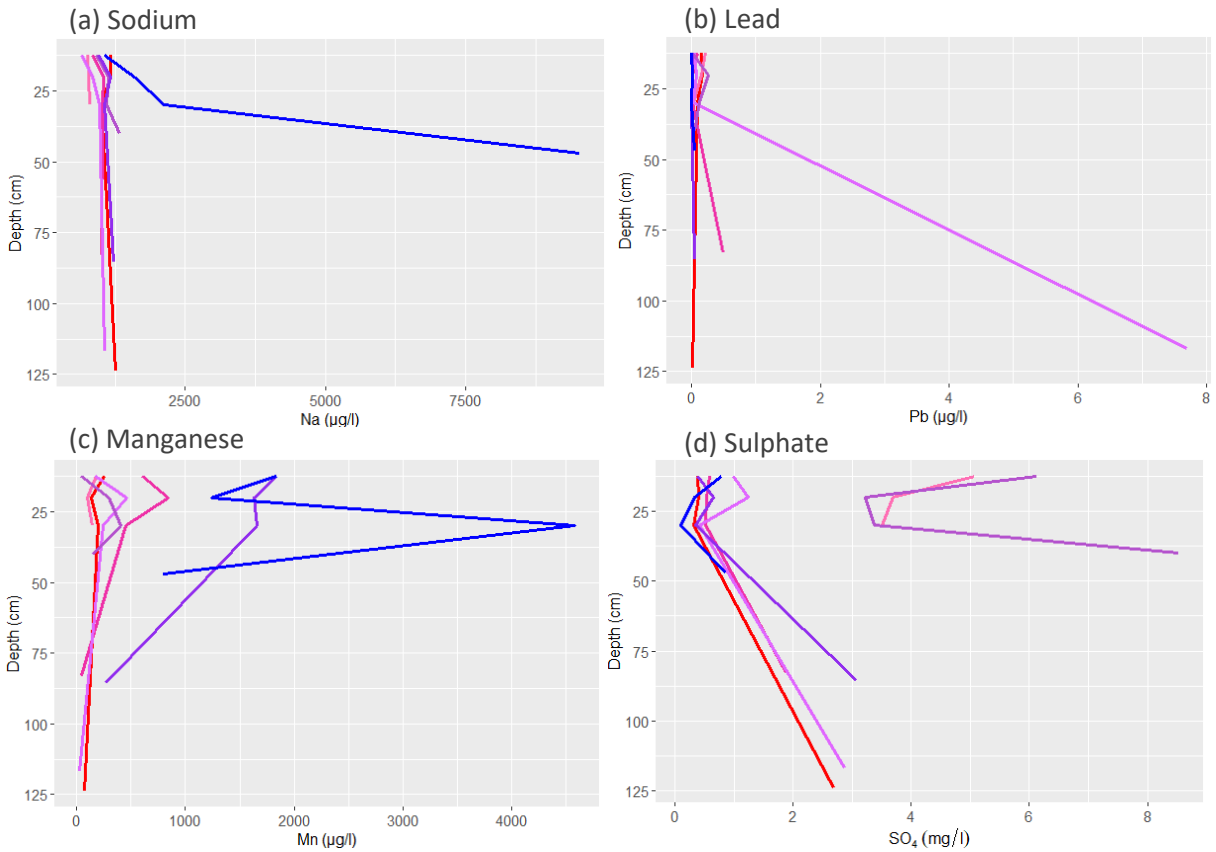

Figure 6.1: Solutes which showed site-specific abnormal concentrations including (a) sodium, (b) lead, (c) manganese and (d) sulphate. Note the solutes in b and f are in mg/l.

Kiewiet et al. (2019; 2515) were able to spatially "*distinguish four shallow groundwater types based on the mean relative differences in the concentrations from the catchment average*". Type I was the riparian-like groundwater, characterized by above-average concentrations of transition metals and below-average concentrations of heavy metals, trace metals and Ca. Only site 21.8 from sub-catchment 21 was included in this cluster. Type II was hillslopes and areas with small rising areas including sites 21.2 and 21.4, which had higher concentrations of heavy metals and isotopes. The third groundwater type was deeper groundwater on steeper slopes, which included sites 21.1, 21.3 and 21.7. And the last groundwater type was sites with elevated magnesium and sulphate concentrations and below-average concentrations of transition and heavy metals. Only well 21.5 was included in cluster IV (Kiewiet et al., 2019). The groundwater samples taken in 2021 from the same sites in sub-catchment 21 could mostly be assigned to the same cluster as in 2019, with the exception of site 21.7. The second wettest plot had a below-average Mg concentration, was low in isotopes and had above-average heavy metal, transition metal and SO_4 concentrations. Therefore, this site cannot be assigned to any of the four groundwater types. However, if it had to be assigned to one of the types, it would still be part of groundwater type III, although the Mn and Co concentrations were above instead of below the sub-catchment's average concentration. The spatial variability at the seven sites measured in 2021 is thus quite similar to that of Kiewiet et al. (2019) from 2017.

Topography appears to have some influence on the solute concentrations in the soil. But the correlation between the three topographic and hydrodynamic attributes and the concentration of the dissolved substances is quite weak. Rinderer et al. (2014) did not yet investigate the

concentration of solutes in soil and groundwater but focused mainly on the influence of topography on groundwater levels. Their topographic attributes were limited to slope, curvature, and topographic wetness index. They found that topography has a significant influence on the median groundwater level in the entire Studibach catchment. The results of this thesis show that there is a non-significant correlation between TWI and the median GW level (ρ = -0.77, p = 0.1). A higher wetness index usually coincides with a very shallow groundwater level near the surface. The only site where this does not seem to be the case is plot 21.4, which has an uncharacteristically low groundwater table. The correlation between the GW level and the slope was lower, with a ρ value of 0.55, and the TWI and the slope have an even weaker correlation of only -0.2. It is surprising that the slope and the TWI have such a low correlation, since the slope is integrated in the calculation of the wetness index (Equation 3.1). But the TWI values used in this study were calculated by Rinderer et al. in 2014. Therefore it is possible that the contributing upslope area or the slope could have changed slightly since then. This concideration is supported by the constantly changing landscape due to landslides and soil creep caused by heavy rainfalls (Kiewiet et al., 2019).

Kiewiet et al. (2019) examined even more topographic and hydrodynamic attributes, including slope, plan curvature, profile curvature, average flow path length, elevation above stream, accumulated area and again TWI. They found (2019; 2511) that "*[…] the heavy metal, transition metal, and potassium concentrations were relatively well correlated with the topographic and hydrodynamic attributes. The heavy metal concentrations were higher at sites that were predominantly dry, whereas the transition–metal concentrations were usually higher at sites that were predominantly wet. Potassium concentrations were strongly correlated with multiple hydrodynamic and topographic attributes and were higher at drier sites."* The same cannot be determined in the results of this thesis (see Table 5.7). With few exceptions, the change in concentration over the soil depth is not strongly correlated with the topographic and hydrodynamic attributes. The correlation of the concentration is generally greater at the wet locations, contrary to what Kiewiet et al. (2019) discovered. The earlier assumption that the copper concentration is higher at the dry sites while the iron concentration is higher at the wet locations could not be fully confirmed. It was suspected that Cu and Zn were higher at dry sites due to the atmospheric input getting less flushed out causing higher accumulation. For Fe, its concentration was assumed to be higher at wet location because of increased reactions between the water and oxygen causing the release of Fe from Pyrite (Brown, 1985; Gu et al., 2020). But in reality, the Fe concentration is only slightly higher at the wet location, which is probably due to the extremely high concentration at plot 21.8. Heavy metals are slightly higher overall at predominantly wet sites, contrary to the study of Kiewiet et al. (2019). This group of solutes has very low concentrations at the driest and the wettest site, but it has increasingly large concentrations in the groundwater of plot 21.4. This is the well with the lowest groundwater level. Thus, groundwater elevation and slope seem to be the most influential attributes for the heavy metal concentration in soil- and groundwater. However, the concentration variations with depth (SD, IQR and range) compared to the wetness index are more pronounced at the dry locations. This is true for almost all solutes studied. Only Na, K and the transition metals vary stronger in the wetlands.

There are other potential wetness indices such as the calculated topographic index (CTI; EPA, 2021). This index also involves the flow accumulation and the slope. But it makes more sense to apply the topographic wetness index instead of the CTI, since the TWI has already been applied twice before by Rinderer et al. in 2014 and Kiewiet et al. in 2019 which provides comparable data. The CTI, on the other hand, would have been difficult to interpret in complete isolation without comparable reference values.

Overall, it is clear that there are some topographic and hydrographic influences on soil- and groundwater chemistry, although it is almost impossible to identify the exact attribute causing the change, as the individual attributes could have collective influences on the solute concentrations.

6.3 Variation reflected in stream chemistry

6.3.1 Concentration-discharge relationship with depth

The response of the stream to a rainfall event is highly variable. The temporal variability of the stream's water chemistry was analysed during the four rainfall events, using the stream level for orientation. Unfortunately, the stream level measurement device failed at the beginning of the fourth event, therefore the change in concentration for this last event could not be evaluated.

Stream chemistry should generally reflect the change in concentration over soil depth, since the concentration-discharge relationship was demonstrated by Knapp et al. (2020). This was true for about half of the analysed solutes. The change in concentration in the stream is compared with the stream level in Table 6.1. The blue positive values in Table 6.1 indicate a mobilizing behaviour of the solutes, the negative red values portray a diluting behaviour, and the almost white cells indicate a chemostatic behaviour. It is visible that the individual events mostly show the same composition within the stream as the overall composition, which includes all three events. Only the dissolved substances Zn, NO_3 and especially SO_4 have a deviating change in solute concentration with increasing stream level. This is caused by the differences in intensity of the three precipitation events (see Table 5.1).

The first event had a higher intensity than the second or third event, resulting in a higher stream level and slightly higher SO_4 concentrations in the stream during this event. Yet this specific solute concentration in the stream was generally higher during low flow. This led to a decrease in concentration during the individual events when the flow was high, but overall the mean concentrations are higher when the level of the stream is elevated.

Table 6.1: Spearman rank correlation between solute concentration in the stream and stream level (bold font indicates statistically significant correlation; blue shading a positive correlation, red shading a negative correlation, and grey shading $R^2 < 0.4$)

Solute	Event1	Event2	Event3	**Overall**	original expect.	expectation based on soil water chemistry
$\delta^{18}O$	0.19	0.29	**0.48**	**0.68**	✓	✓
$\delta^{2}H$	0.11	0.43	**0.47**	**0.66**	✓	✓
B	0.12	-0.27	-0.14	0.04	×	×
Ca	-0.41	-0.53	**-0.59**	**-0.77**	✓	✓
Na	-0.36	-0.60	**-0.58**	**-0.78**	✓	✓
Mg	-0.41	-0.52	**-0.66**	**-0.78**	✓	×
K	-0.06	0.62	0.25	0.26	×	✓
Cu	0.35	0.12	0.08	**0.60**	×	×
Zn	-0.10	0.17	0.01	**-0.51**	×	×
Pb	-0.12	0.43	0.23	**0.30**	×	×
Fe	0.23	0.18	**0.52**	**0.58**	✓	✓
Mn	-0.34	-0.10	0.04	**-0.57**	×	×
Co	-0.36	NA	0.35	0.03	(✓)	(✓)
NO_3	0.15	-0.37	**0.58**	**0.59**	×	×
PO_4	NA	NA	-0.04	-0.09	(✓)	×
SO_4	-0.33	-0.50	-0.13	**0.37**	×	×

The expectation on how the solute concentrations should behave with increasing streamflow has changed with the findings of how the concentrations actually change in the soil. Both the original expectation (see Figure 2.2) and the adjusted expectation after the spatial variability analysis (see Appendix: Table 9.1) are shown in Table 6.1. The reality in solute concentration over soil depth, which contradicted the original expectation, was detected for the solutes Mg, K, Zn, NO_3 and SO_4. Therefore, the stream chemistry expectations for these five solutes have also changed. Especially Mg stands out since it does not occur in the soil as expected of all base cations, but it shows the expected dilutive behaviour in the stream for all three events. It is even a statistically significant behaviour with the increase of stream level. But as Kiewiet et al. already mentioned in 2019, it is nearly impossible to determine the active contribution of specific areas within the catchment to solute concentration in the stream without also measuring hydrological connectivity as well as hydrograph separation of individual sources (Kendall et al., 2001; Kiewiet et al., 2019). The chemical composition in stream water can only indicate which landscape characteristics potentially contribute to baseflow.

The solute concentrations in the stream during an event cannot be explained solely by the mixing of the baseflow with the incoming precipitation (see Appendix: Table 9.1). Stormflow always has slightly to significantly higher concentrations than precipitation or baseflow, which can only arise when new source areas with different solute concentrations contribute to the stormflow (Knapp et al., 2020; Welsch et al., 2001). Figure 6.2 indicates that different precipitation intensities lead to different concentrations of distinct solutes in the stormflow. Event one had the highest intensity (1.8 mm/h) followed by the second (1.2 mm/h) and third event. The third event (0.8 mm/h) lasted the longest and had the lowest intensity. The low rainfall intensity led to only a small increase in

stream level. The diluting and mobilizing behaviour of the solutes are well visible in Figure 6.2. The 'old' groundwater begins to contribute to stormflow shortly after the onset of the rainfall event. For this reason, the blue points show low concentrations for δ^2H and Fe and high concentrations for Ca. The first and second event have higher rainfall intensities, which results in the soil water contributing to faster stormflow (Knapp et al., 2020; Seibert et al., 2009; Stewart et al., 2022).

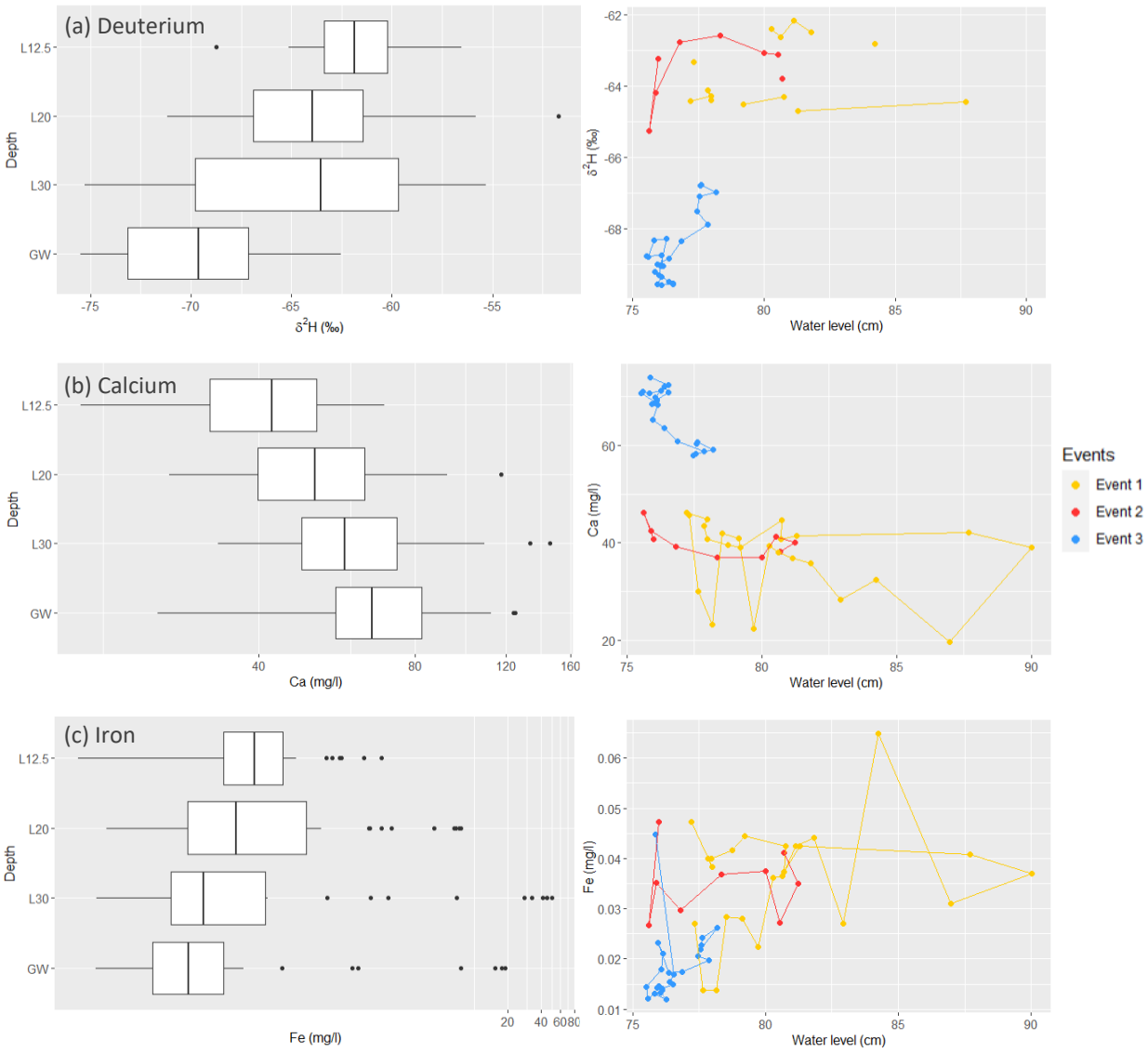

Figure 6.2: The concentration variation with depth below the surface (left) and the resulting concentration-discharge relationship (right) for (a) deuterium, (b) calcium and (c) iron

The figures on the right side of Figure 6.2 show another interesting pattern. Connecting the measurements over time shows the slow change in deuterium, calcium, and iron concentration in the stream as the stream level responded to the rainfall event. D^2H had at low flow a more negative abundance in the stream. During peak flow at 90 cm and immediately after the abundance increased. Only when the stream approached its pre-event levels did d^2H abundance start to become more negative again (Figure 6.2a). Calcium showed a flushing behaviour with very high concentrations before the event at low flow. The concentration in the stream decreased slightly during the peak flow and decreased further when the stream level dropped again. Only at the end of the event was the Ca concentration back at its original level (Figure 6.2b). Iron and

deuterium behaved very similar. The concentration of Fe was lowest at the beginning of the event and started to increase as soon as the stream level rose, reacting to additional discharge. However, the Fe concentration was still quite high when the stream level sank down to 76 cm after the event (Figure 6.2c).

Most solutes display a similar concentration range in the stormflow as in soil- and groundwater, only Na, K and SO_4 have uncharacteristically high concentration in stormflow, possibly caused by spatial variation by site rather than per depth. It is also assumed that the deviation in expectation for the concentration-discharge relationship in Table 6.1 is due to spatial variation across space.

6.3.2 Concentration-discharge relationship across space

The composition of the stream water is different for each precipitation event. This is an indication that several areas of the sub-catchment contribute to the stream at any given time, but they are constantly changing. Seibert et al. (2009) identified the riparian zone as the area most in control of stream water chemistry dynamics. It means that the soil-and groundwater closest to the stream has the greatest influence on stream chemistry. In this sub-catchment, plots 21.3, 21.5, 21.7 and 21.8 are closed to the stream (see Figure 4.1). The last one being the closest. Since plot 21.8 has such a high wetness index and is located in the riparian zone, it can be assumed that it has the greatest influence on the stream chemistry of the seven plots. The other six plots, on the other hand, have a larger distance to the stream and contribute less. Kiewiet et al. (2020) studied the isotopic composition of the river using hydrographs to determine its source during baseflow and rainfall. They found large differences in the proportion of water from before the event and many uncertainties because the separation of the hydrographs depends on the number and location of the groundwater samples taken. A higher number of groundwater samples from the pre-event facilitates the separation of the different sources in stormflow during the rainfall event.

In this study the most peculiar solute is magnesium. It does not behave as expected over the soil depth at any of the sites, but its concentration change in the stream during the event is as expected (see Table 6.1). Therefore, Mg seems to come from somewhere else. Only seven selective locations were sampled in the entire sub-catchment. It is very likely that there are other locations where Mg changes with depth as expected and causes the discovered concentration changes in the stream water.

6.3.3 Implications for understanding stream chemistry and limiting factors

Stewart et al. (2022) claimed that stream water originates mainly from soil - and groundwater and that the contribution of precipitation water is negligible. This can be confirmed, since the solute concentrations in precipitation were mostly much lower than the concentrations in soil-, groundwater or stream water during stormflow (Appendix: Table 9.1). Stewart et al. (2022; 1) also claimed that "*the streams mirror subsurface waters: stream chemistry can be used to infer scarcely measured subsurface water chemistry, especially where there are distinct shallow and deep end members*." This assertion is not entirely true for the Studibach. The concentrations within the soil water are highly depth and site dependent. As shown in Table 6.1 , for only seven of the sixteen solutes did the expected stormflow chemistry agree with the depth distribution of solute concentrations in soil- and groundwater. But again, only seven selected locations were sampled. It is possible that other locations have different concentration changes over depth, which are

reflected in the stream. More likely though, the changes in stream water concentrations do not only reflect changes in flow pathways with depth below the surface but also changes in the spatial sources of streamflow across the catchment and connectivity of different sources. However, the results of this study suggest that the chemical composition of stream water can give some indication on how the concentration generally changes over soil depth and that this change is strongly dependent on space and cannot be estimated without direct measurement. As Penna & van Meerveld (2019; 3) said: "*Often the determination of the isotopic composition of a water source or compartment relies on sampling at one or a few locations. In practice, this approach assumes that the spatial variability in the isotopic composition of a given hydrological compartment is negligible, and that samples taken at one or a few locations are representative for that compartment. However, this assumption is rarely tested.*" This was a statement in the introduction of their paper, and they later showed that the spatial variability in the isotopic composition of soil water is large. This study can thus confirm their findings. Furthermore, the finding of Kiewiet et al. (2020) that the change in the composition of the runoff during a rainfall event indicate that the water before the event dominates the runoff could also be confirmed. The contributions of the different sources could not be distinguished in this study either.

6.4 Uncertainties in the hydrochemical conditions

A number of samples could either not be taken due to the time to fill the lysimeters and groundwater wells, or they were lost after sampling because they exploded in the refrigerator. Furthermore, some equipment malfunctions prevented a complete dataset: e.g., groundwater levels, stream level or sampling of stream water with the ISCO. This missing information caused unbridgeable data gaps.

This study was based on seven samplings over a period of six weeks in autumn 2021. Each sample was taken only once but since each site and depth was sampled seven times, the samples could be compared, and no major measurement errors were detected. Since soil- and groundwater sampling took place in sub-catchment 21 at only seven specific locations and on only seven sampling dates, it is impossible to make general statements about soil- and groundwater chemistry for the sub-catchment, or the entire Studibach catchment. Interpolation or extrapolation of the measured solute concentrations to other locations or depths is not possible, as the variability is too great. General statements about the chemical composition of precipitation, soil water, groundwater and baseflow are possible, but should be treated with caution. The concentrations of the different solutes themselves can be spatially very variable, and the poor correlations with topographic and hydrodynamic attributes make extrapolation with these proxies difficult. It is assumed that for the seven sub-catchments of the Studibach the soil and stream concentrations differ (e.g., Kiewiet et al., 2020) because the sources of the various solutes in the soil vary greatly and depend on the environment: atmospheric input, vegetation, soil composition, bedrock, season, temperature, etc.

These different sources of uncertainty in the hydrochemical composition of precipitation, soil water, groundwater and stream water can be large and need to be considered when analysing the results. Expanding the sampling locations and sampling times can reduce uncertainty not only in the accuracy of measurements, but also in the spatial variability of solute concentrations.

The exact source of the various solutes in soil- and groundwater is speculative. The assumptions about where the solutes analysed in this study come from were merely based on the findings of other researchers such as Feng et al. (2007), Jutebring Sterte et al. (2021), Kiewiet et al. (2019), Mook & Geyh (2000); Pastore et al. (2020) Rao et al. (2021) or Zhi & Li (2020). In order to determine this, the atmospheric deposition needs to be measured at all sites, and leaching experiments need to be performed for the soil and bedrock.

6.5 Future research

In future, the separation of the hydrographs in the stream should be intensified in in order to investigate the origin of the solutes in the stream more precisely. More detailed sampling of the subsurface water will make it easier to determine the origin of the water. And the power law slope could give a new insight into the relationship of solute concentrations in soil water compared to groundwater.

Since the spatial differences in soil- and groundwater are so large, it would be interesting to select more locations for sampling. The hydrograph separation that Kiewiet et al. (2019) already started could be extended within the catchment using the stable water isotopes as well as hydrochemical tracers. In this way, the hydrological connectivity of the entire catchment to the stream will be better known. As Kiewiet et al. (2019) have already done, it is practical to group the different locations together based on their solute concentrations. The seasonal aspect, especially in isotopic composition, would also be interesting to investigate. But the focus should be on spatial rather than temporal variability.

Another method that could be applied is the one used by Stewart et al. (2022). They calculated the power law slope (*b*) for each solute by extending the ratio between the mean soil water concentration and the mean groundwater concentration for their two study sites. They found that *b* values mostly increase with the ratio between soil water and groundwater concentrations, suggesting that the ratio influences export patterns (Stewart et al., 2022).

7 Conclusions

In this study, the spatial and temporal variability in soil water and groundwater chemistry in the Alptal was investigated. The spatial variation in solute concentrations is large and far greater than the temporal variation.

The change in solute concentration in soil- and groundwater with soil depth strongly depends on the dissolved substance and its origin. Most solutes varied with soil depth in the way that was expected. While the abundance of two stable isotopes both decreased with soil depth, the base cations had to be divided into two sub-groups. One group consists of boron, calcium, magnesium, and sodium, which increased from the surface towards the groundwater, whereas for magnesium and potassium the concentrations were highest at the soil surface. Concentrations of the heavy metals were mostly constant independent of soil depth, with the exception of zinc, which had unexpectedly high concentrations in groundwater. For the transition metals the concentrations were highest closer to the surface (at either 12.5 or 20 cm depth). And for the anions (phosphate, sulphate and nitrate) the concentrations with depth varied and were inconsistent.

The spatial variation in mean solute concentrations (i.e., by site) was less pronounced than expected. The solute concentrations were only weakly related to the topographical attributes of the sampled locations (TWI and slope), and slightly better correlated to the hydrodynamic attribute, the median groundwater level. The variation in concentration (SD, IQR and range) were largest at the sites with a low topographic wetness index.

A change in solute concentrations before and after the four measured rainfall events could not be detected. Only very few of the numerous comparisons were statistically significant. This suggests that it does not matter whether the samples are taken before or after the precipitation event, which facilitates future sampling. Instead of measuring the sites before as well as after every rainfall event, the effort can be used to sample more sites.

The results, further confirm previous findings by Kiewiet et al. (2019) that the stream water chemistry is highly influenced by hydrological connectivity and that stormflow is a composition of soil water and groundwater, as evidenced by solute concentrations in the steam.

The large and strongly site- and depth-dependent changes in concentration make it very difficult to make general assumptions for other catchments in the same valley or even for other locations in the Studibach. But it was proven, that the concentration change over depth can be reasonably determined from the solute change in the stream water during an event.

The study could be improved by extending the number of studied locations within the same catchment or an application of tracers in the soil water and groundwater to determine the source of the water in the stream. Another uncertainty that could be minimised is to look at the median concentrations instead of the mean concentration change with depth. This method makes the findings more robust against potential outliers that skew the data. Fortunately, there were only few strong outliers, which affected the mean concentrations of iron and the heavy metals.

Overall, this thesis shows the large and complex variation of the solute concentrations in the Studibach catchment in the Alptal. The spatial change over depth is very pronounced for each solute and strongly dependent on its source. The contribution of the different water sources to the stream is also not clear, mainly due to the big spatial variability. However, further sampling is expected to provide a better picture of the complicated spatial variation of the sources of stream water in the Studibach catchment.

8 References

Aravinthasamy, P., Karunanidhi, D., Shankar, K., Subramani, T., Setia, R., Bhattacharya, P., & Das, S. (2021). COVID-19 lockdown impacts on heavy metals and microbes in shallow groundwater and expected health risks in an industrial city of South India. *Environmental Nanotechnology, Monitoring & Management*, *16*(March), 100472. https://doi.org/10.1016/j.enmm.2021.100472

Badoux, A., Witzig, J., Germann, P. F., Kienholz, H., Lüscher, P., Weingartner, R., & Hegg, C. (2006). Investigations on the runoff generation at the profile and plot scales, Swiss Emmental. *Hydrological Processes*, *20*(2), 377–394. https://doi.org/10.1002/hyp.6056

Benettin, P., Volkmann, T. H. M., Von Freyberg, J., Frentress, J., Penna, D., Dawson, T. E., & Kirchner, J. W. (2018). Effects of climatic seasonality on the isotopic composition of evaporating soil waters. *Hydrology and Earth System Sciences*, *22*(5), 2881–2890. https://doi.org/10.5194/hess-22-2881-2018

Beven, K. J., & Kirkby, M. J. (1979). A physically based, variable contributing area model of basin hydrology. *Hydrological Sciences Bulletin*, *24*(1), 43–69. https://doi.org/10.1080/02626667909491834

Bloem, E., Haneklaus, S., Sparovek, G., & Schnug, E. (2001). Spatial and temporal variability of sulphate concentration in soils. *Communications in Soil Science and Plant Analysis*, *32*(9–10), 1391–1403. https://doi.org/10.1081/CSS-100104201

Botter, M., Li, L., Hartmann, J., Burlando, P., & Fatichi, S. (2020). Depth of Solute Generation Is a Dominant Control on Concentration-Discharge Relations. *Water Resources Research*, *56*(8), 1–18. https://doi.org/10.1029/2019WR026695

Brown, A. D. (1985). Chemical Weathering of Pyrite in Soils. *Utah State University*. https://digitalcommons.usu.edu/etd/4345

Calvo, N. I. R., Echeverría, H. E., & Rozas, H. S. (2009). Determination of sulfate concentration in soil: Depth of sampling. *Communications in Soil Science and Plant Analysis*, *40*(9–10), 1624–1633. https://doi.org/10.1080/00103620902831917

Church, M. R. (1997). Hydrochemistry of forested catchments. *Annual Review of Earth and Planetary Sciences*, *25*, 23–59. https://doi.org/10.1146/annurev.earth.25.1.23

Corp., S. E. (n.d.). *What is a Lysimeter Anyway?* Retrieved May 30, 2022, from https://www.soilmoisture.com/what_is_Lysimeter/

Egli, M., Brandová, D., Sandra, R., Woodhatch, I., & Zollinger, B. (2016). Geochronology laboratory methods. *University of Zurich, Department of Geography*, *January*.

EPA United States Environmental Protection. (2021). *Watershed Index Online, WSIO Indicator Data Library Data Tables , Services and Downloads*. https://www.epa.gov/wsio/wsio-indicator-data-library#:~:text=The Wetness Index is a Computed Topographic Index,%2B 3x3 mean of ln %28flow accumulation%2Ftan %28slope%29%29%2F2.

Feng, X. H., Zhai, L. M., Tan, W. F., Liu, F., & He, J. Z. (2007). Adsorption and redox reactions of heavy metals on synthesized Mn oxide minerals. *Environmental Pollution*, *147*(2), 366–373. https://doi.org/10.1016/j.envpol.2006.05.028

Fischer, B. M. C., van Meerveld, H. J. (Ilja), & Seibert, J. (2017). Spatial variability in the isotopic composition of rainfall in a small headwater catchment and its effect on hydrograph separation. *Journal of Hydrology*, *547*, 755–769. https://doi.org/10.1016/j.jhydrol.2017.01.045

Gu, X., Heaney, P. J., Reis, F. D. A. A., & Brantley, S. L. (2020). Deep abiotic weathering of pyrite. *Science*, *370*(6515). https://doi.org/10.1126/SCIENCE.ABB8092/SUPPL_FILE/ABB8092-GU-SM.PDF

Hagedorn, F., Schleppi, P., Waldner, P., & Flühler, H. (2000). Export of dissolved organic carbon and nitrogen from Gleysol dominated catchments - The significance of water flow paths. *Biogeochemistry*, *50*(2), 137–161. https://doi.org/10.1023/A:1006398105953

Hegg, C., McArdell, B. W., & Badoux, A. (2006). One hundred years of mountain hydrology in Switzerland by the WSL. *Hydrological Processes*, *20*(2), 371–376. https://doi.org/10.1002/hyp.6055

Herndon, E., Kinsman-Costello, L., Di Domenico, N., Duroe, K., Barczok, M., Smith, C., & Wullschleger, S. D. (2020). Iron and iron-bound phosphate accumulate in surface soils of ice-wedge polygons in arctic tundra. *Environmental Science: Processes & Impacts*, *22*(7), 1475–1490. https://doi.org/10.1039/D0EM00142B

Johnson, D. W., & Van Hook, R. I. (1990). Analysis of Biogeochemical Cycling Processes in Walker Branch Watershed. *Journal of Environmental Quality*, *19*(3), 630–630. https://doi.org/10.2134/JEQ1990.00472425001900030046X

Jutebring Sterte, E., Lidman, F., Balbarini, N., Lindborg, E., Sjöberg, Y., Selroos, J. O., & Laudon, H. (2021). Hydrological control of water quality – Modelling base cation weathering and dynamics across heterogeneous boreal catchments. *Science of the Total Environment*, *799*. https://doi.org/10.1016/j.scitotenv.2021.149101

Kaushal, S. S., Gold, A. J., Bernal, S., Johnson, T. A. N., Addy, K., Burgin, A., Burns, D. A., Coble, A. A., Hood, E., Lu, Y. H., Mayer, P., Minor, E. C., Schroth, A. W., Vidon, P., Wilson, H., Xenopoulos, M. A., Doody, T., Galella, J. G., Goodling, P., … Belt, K. T. (2018). Watershed 'chemical cocktails': forming novel elemental combinations in Anthropocene fresh waters. *Biogeochemistry*, *141*(3), 281–305. https://doi.org/10.1007/s10533-018-0502-6

Kendall, C., McDonnell, J. J., & Gu, W. (2001). A look inside "black box" hydrograph separation models: A study at the hydrohill catchment. *Hydrological Processes*, *15*(10), 1877–1902. https://doi.org/10.1002/hyp.245

Kiewiet, L. (2020). *Searching for the source: using shallow groundwater chemistry to determine the sources for streamflow in a pre-alpine catchment*. *I*. www.zora.uzh.chyear:2020

Kiewiet, L., van Meerveld, H. J. (Ilja), & Seibert, J. (2020). Effects of Spatial Variability in the Groundwater Isotopic Composition on Hydrograph Separation Results for a Pre-Alpine Headwater Catchment. *Water Resources Research*, *56*(7), 1–22. https://doi.org/10.1029/2019WR026855

Kiewiet, L., Van Meerveld, H. J. (Ilja), Stähli, M., & Seibert, J. (2020). Do stream water solute concentrations reflect when connectivity occurs in a small, pre-Alpine headwater catchment? *Hydrology and Earth System Sciences*, *24*(7), 3381–3398. https://doi.org/10.5194/hess-24-3381-2020

Kiewiet, L., von Freyberg, J., & van Meerveld, H. J. (Ilja). (2019). Spatiotemporal variability in hydrochemistry of shallow groundwater in a small pre-alpine catchment: The importance of landscape elements. *Hydrological Processes*, *33*(19), 2502–2522. https://doi.org/10.1002/hyp.13517

Klaus, J., & McDonnell, J. J. (2013). Hydrograph separation using stable isotopes: Review and evaluation. *Journal of Hydrology*, *505*(December 2018), 47–64. https://doi.org/10.1016/j.jhydrol.2013.09.006

Knapp, J. L. A., von Freyberg, J., Studer, B., Kiewiet, L., & Kirchner, J. W. (2020). Concentration-discharge relationships vary among hydrological events, reflecting differences in event characteristics. *Hydrology and Earth System Sciences Discussions*, *24*(5), 1–27. https://doi.org/10.5194/hess-2019-684

Kopecký, M., Macek, M., & Wild, J. (2021). Topographic Wetness Index calculation guidelines based on measured soil moisture and plant species composition. *Science of the Total Environment*, *757*, 143785. https://doi.org/10.1016/j.scitotenv.2020.143785

Li, L., Sullivan, P. L., Benettin, P., Cirpka, O. A., Bishop, K., Brantley, S. L., Knapp, J. L. A., van Meerveld, H. J. (Ilja), Rinaldo, A., Seibert, J., Wen, H., & Kirchner, J. W. (2021). Toward catchment hydro-biogeochemical theories. *Wiley Interdisciplinary Reviews: Water*, *8*(1), 1–31. https://doi.org/10.1002/wat2.1495

Li, Y., Zhou, S., Jia, Z., Liu, K., & Wang, G. (2021). Temporal and spatial distributions and sources of heavy metals in atmospheric deposition in western Taihu Lake, China. *Environmental Pollution*, *284*(May), 117465. https://doi.org/10.1016/j.envpol.2021.117465

Mook, W. G., & Geyh, M. (2000a). Environmental isotopes in the hydrological cycle, principles and applications. Volume IV: Groundwater. *IHP-V, Technical Document*, *39*(3), 196. http://www.unesco.org/ulis/cgi-bin/ulis.pl?catno=121542&set=0054BFA545_1_47&gp=1&lin=1&ll=1

Mook, W. G., & Geyh, M. (2000b). Environmental isotopes in the hydrological cycle. Volume I: principles and applications. *IHP-V, Technical Document*, *39*(3), 196. http://www.unesco.org/ulis/cgi-bin/ulis.pl?catno=121542&set=0054BFA545_1_47&gp=1&lin=1&ll=1

Pastore, G., Kaiser, K., Kernchen, S., & Spohn, M. (2020). Microbial release of apatite- and goethite-bound phosphate in acidic forest soils. *Geoderma*, *370*(April), 114360. https://doi.org/10.1016/j.geoderma.2020.114360

Penna, D., & van Meerveld, H. J. (2019). Spatial variability in the isotopic composition of water in small catchments and its effect on hydrograph separation. *Wiley Interdisciplinary Reviews: Water*, *6*(5), 1–33. https://doi.org/10.1002/wat2.1367

Rao, K., Tang, T., Zhang, X., Wang, M., Liu, J., Wu, B., Wang, P., & Ma, Y. (2021). Spatial-temporal dynamics, ecological risk assessment, source identification and interactions with internal nutrients release of heavy metals in surface sediments from a large Chinese shallow lake. *Chemosphere*, *282*(January). https://doi.org/10.1016/j.chemosphere.2021.131041

Real Nitrition. (n.d.). *Lysimeter - Irrigation and Fertigation Management Tools*. Retrieved July 26, 2022, from https://www.real-nutrition.co.za/lysimeter-fertigation/

Rinderer, M., van Meerveld, H. J., & Seibert, J. (2014). Topographic controls on shallow groundwater levels in a steep, prealpine catchment: When are the TWI assumptions valid? *Water Resources Research*, *50*(7), 6067–6080. https://doi.org/10.1002/2013WR015009

Rinderer, M., van Meerveld, H. J., Stähli, M., & Seibert, J. (2016). Is groundwater response timing in a pre-alpine catchment controlled more by topography or by rainfall? *Hydrological Processes*, *30*(7), 1036–1051. https://doi.org/10.1002/hyp.10634

Sato, M., & Hattanji, T. (2018). A laboratory experiment on salt weathering by humidity change: salt damage induced by deliquescence and hydration. *Progress in Earth and Planetary Science*, *5*(1). https://doi.org/10.1186/s40645-018-0241-2

Seibert, J., Grabs, T., Köhler, S., Laudon, H., Winterdahl, M., & Bishop, K. (2009). Linking soil- and stream-water chemistry based on a Riparian Flow-Concentration Integration Model. *Hydrology and Earth System Sciences*, *13*(12), 2287–2297. https://doi.org/10.5194/hess-13-2287-2009

Stähli, M., & Gustafsson, D. (2006). Long-term investigations of the snow cover in a subalpine semi-forested catchment. *Hydrological Processes*, *20*(2), 411–428. https://doi.org/10.1002/hyp.6058

Stähli, M., Seibert, J., Kirchner, J. W., von Freyberg, J., & van Meerveld, H. J. (Ilja). (2021). Hydrological trends and the evolution of catchment research in the Alptal valley, central Switzerland. *Hydrological Processes*, *35*(4), 1–16. https://doi.org/10.1002/hyp.14113

Staudinger, M., Seeger, S., Herbstritt, B., Stoelzle, M., Seibert, J., Stahl, K., & Weiler, M. (2020). The CH-IRP data set: A decade of fortnightly data on δ2H and δ18O in streamflow and precipitation in Switzerland. *Earth System Science Data*, *12*(4), 3057–3066. https://doi.org/10.5194/essd-12-3057-2020

Stewart, B., Shanley, J. B., Kirchner, J. W., Norris, D., Adler, T., Bristol, C., Harpold, A. A., Perdrial, J. N., Rizzo, D. M., Sterle, G., Underwood, K. L., Wen, H., & Li, L. (2022). Streams as Mirrors: Reading Subsurface Water Chemistry From Stream Chemistry. *Water Resources Research*, *58*(1), 1–20. https://doi.org/10.1029/2021WR029931

Tripler, C. E., Kaushal, S. S., Likens, G. E., & Todd Walter, M. (2006). Patterns in potassium dynamics in forest ecosystems. *Ecology Letters*, *9*(4), 451–466. https://doi.org/10.1111/j.1461-0248.2006.00891.x

Van Meerveld, H. J. (Ilja), Fischer, B. M. C., Rinderer, M., Stähli, M., & Seibert, J. (2018). Runoff generation in a pre-alpine catchment: A discussion between a tracer and a shallow groundwater hydrologist. *Geographical Research Letters*, *44*(2), 429–452. https://doi.org/10.18172/cig.3349

Welsch, D. L., Kroll, C. N., McDonnell, J. J., & Burns, D. A. (2001). Topographic controls on the chemistry of subsurface stormflow. *Hydrological Processes*, *15*(10), 1925–1938. https://doi.org/10.1002/hyp.247

Wohl, E. (2017). The significance of small streams. *Frontiers of Earth Science*, *11*(3), 447–456. https://doi.org/10.1007/s11707-017-0647-y

WSL. (n.d.). *Floods and landslides in 2021: wet summer resulted in highest damage costs since 2007 - WSL*. Retrieved July 22, 2022, from https://www.wsl.ch/en/news/2022/06/floods-

and-landslides-in-2021-wet-summer-resulted-in-highest-damage-costs-since-2007.html

Zhang, J., Jin, M., Cao, M., Huang, X., Zhang, Z., & Zhang, L. (2021). Sources and behaviors of dissolved sulfate in the Jinan karst spring catchment in northern China identified by using environmental stable isotopes and a Bayesian isotope-mixing model. *Applied Geochemistry*, *134*(October), 105109. https://doi.org/10.1016/j.apgeochem.2021.105109

Zhi, W., & Li, L. (2020). The Shallow and Deep Hypothesis: Subsurface Vertical Chemical Contrasts Shape Nitrate Export Patterns from Different Land Uses. *Environmental Science and Technology*, *54*(19), 11915–11928. https://doi.org/10.1021/acs.est.0c01340

Zuecco, G., Rinderer, M., Penna, D., Borga, M., & van Meerveld, H. J. (2019). Quantification of subsurface hydrologic connectivity in four headwater catchments using graph theory. *Science of the Total Environment*, *646*, 1265–1280. https://doi.org/10.1016/j.scitotenv.2018.07.269

9 Appendix

Table 9.1: Hydrochemical characteristics per soil depth

Parameter (Units) and Depth (cm)	Mean	Standard Deviation	Median	Min.	Max.	Median spatial range	Median temporal range	Mean Precipitation	Mean Stream Baseflow
EC (µS/cm)									382.0
12.5	328	108	305	154	577	332	309		
20	389	101	389	203	590	386	390		
30	430	162	412	193	847	416	422		
GW	437	68	427	313	581	438	435		
$\delta^{18}O$ (‰)								-10.1	-9.9
12.5	-9.3	0.4	-9.3	-10.1	-8.6	-9.3	-9.2		
20	-9.5	0.5	-9.5	-10.4	-8.0	-9.4	-9.5		
30	-9.6	0.7	-9.4	-10.8	-8.4	-9.6	-9.5		
GW	-10.2	0.4	-10.2	-10.9	-9.3	-10.2	-10.2		
$\delta^{2}H$ (‰)								-66.8	-67.0
12.5	-61.7	2.6	-61.9	-68.7	-56.5	-62.0	-61.6		
20	-63.5	4.2	-64.0	-71.2	-51.7	-62.8	-64.0		
30	-64.3	5.9	-63.6	-75.3	-55.3	-65.0	-64.7		
GW	-69.8	3.6	-69.6	-75.5	-62.5	-69.9	-69.6		
Dex (‰)								13.8	12.2
12.5	12.6	0.6	12.5	11.4	14.1	12.7	12.8		
20	12.3	0.6	12.3	11.0	13.5	12.3	12.3		
30	12.1	0.7	12.1	9.9	13.3	12.2	12.1		
GW	11.8	0.6	12.0	9.7	12.7	11.8	12.0		

BDL = detection limit

continues

Parameter (Units) and Depth (cm)	Mean	Standard Deviation	Median	Min.	Max.	Median spatial range	Median temporal range	Mean Precipitation	Mean Stream Baseflow
B (µg/L)								319	205
12.5	176	112	206	22	385	209	222		
20	176	122	193	17	455	187	190		
30	187	121	204	13	462	201	202		
GW	187	117	210	10	438	199	210		
Ca (µg/L)								400	58’183
12.5	41’480	13’642	42’377	18’134	69’775	46’490	42’382		
20	53’559	18’684	51’305	26’835	117’184	47’802	49’493		
30	62’494	23’028	58’458	33’341	145’627	54’730	56’998		
GW	70’830	20’859	66’009	25’453	124’916	66’115	69’041		
Na (µg/L)								719	4’418
12.5	913	261	847	509	1’417	847	822		
20	1’103	448	968	517	2’181	913	946		
30	1’137	573	981	441	2’774	935	1’000		
GW	2’511	4’052	1’222	368	20’531	1’261	1’134		
Mg (µg/L)								34	3’575
12.5	9’795	7’137	8’414	2’323	32’464	8’115	8’078		
20	7’949	5’414	5’669	1’868	21’199	6’593	6’593		
30	7’598	8’063	5’798	927	38’453	5’732	6’062		
GW	2’976	1’387	2’802	1’136	6’796	3’214	2’363		
K (µg/L)								221	925
12.5	1’617	1’054	1’321	373	4’510	1’094	1’226		
20	1’089	808	834	288	3’689	899	820		
30	764	463	687	230	1’999	704	751		
GW	618	257	564	266	1’171	567	505		

BDL = detection limit

continues

Parameter (Units) and Depth (cm)	Mean	Standard Deviation	Median	Min.	Max.	Median spatial range	Median temporal range	Mean Precipitation	Mean Stream Baseflow
Cu (µg/L)								0.8	0.7
12.5	1.9	1.0	1.6	0.1	4.3	2.0	1.7		
20	1.7	1.3	1.7	BDL	5.4	1.9	1.7		
30	1.3	0.9	1.2	BDL	5.0	1.3	1.0		
GW	23.1	63.7	3.4	BDL	375.7	4.1	3.8		
Zn (µg/L)								32	2
12.5	19	18	16	1	110	14	16		
20	26	28	17	6	166	17	18		
30	28	27	20	3	171	27	21		
GW	250	514	69	2	2’915	129	77		
Pb (µg/L)								0.1	0.0
12.5	0.08	0.09	0.05	BDL	0.33	0.04	0.04		
20	0.10	0.18	0.02	BDL	0.91	0.02	0.02		
30	0.04	0.05	0.01	BDL	0.24	0.02	0.02		
GW	0.86	3.39	0.05	BDL	21.52	0.05	0.05		
Fe (µg/L)								4	16
12.5	207	302	105	3	1’458	135	125		
20	987	2’151	72	5	7’589	123	114		
30	5’305	13’420	36	4	50’255	47	47		
GW	1’485	4’617	27	4	18’944	22	27		
Mn (µg/L)								2	3
12.5	731	863	315	17	3’159	302	302		
20	651	575	609	22	2’192	363	652		
30	1’052	1’615	333	60	7’412	392	396		
GW	216	306	51	2	979	33	48		

BDL = detection limit

continues

Parameter (Units) and Depth (cm)	Mean	Standard Deviation	Median	Min.	Max.	Median spatial range	Median temporal range	Mean Precipitation	Mean Stream Baseflow
Co (µg/L)								BDL	0.0
12.5	1.5	1.5	0.7	0.1	6.0	0.8	0.8		
20	1.7	1.5	1.4	0.2	7.1	1.5	1.4		
30	2.3	2.5	0.9	0.1	9.4	0.8	0.9		
GW	0.3	0.3	0.2	BDL	1.2	0.2	0.2		
NO_3 (µg/L)								226	244
12.5	48	99	18	2	586	19	15		
20	67	143	23	4	880	24	18		
30	51	99	20	3	627	21	17		
GW	76	110	32	2	571	43	33		
PO_4 (µg/L)								30	18
12.5	423	459	247	BDL	1’844	323	360		
20	1’038	1’100	791	BDL	3’611	575	576		
30	803	1’099	406	BDL	4’545	240	469		
GW	3	5	BDL	BDL	13	1	BDL		
SO_4 (µg/L)								245	3’419
12.5	2’074	3’200	687	126	14’934	540	954		
20	1’450	1’632	809	73	5’543	581	847		
30	1’157	1’782	401	35	8’266	449	410		
GW	3’656	4’276	1’761	20	19’086	1’983	2’225		

BDL = detection limit

Boxplots of the stable isotope composition and solute concentration change with depth

Mean stable isotope composition and solute concentration change by site and depth

Mean stable isotope composition and solute concentration change in the stream during events

Deuterium

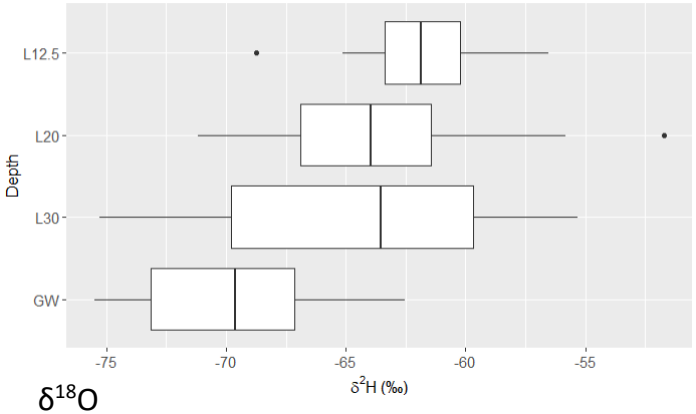

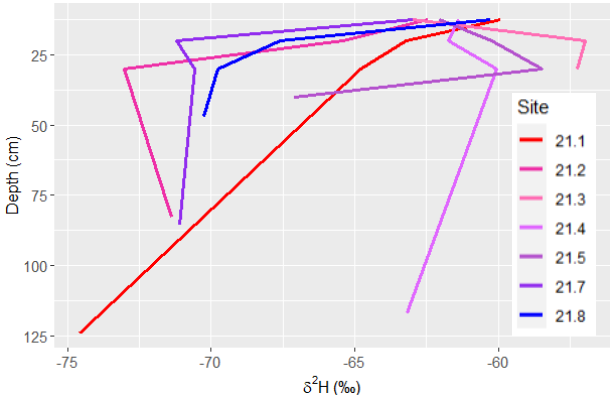

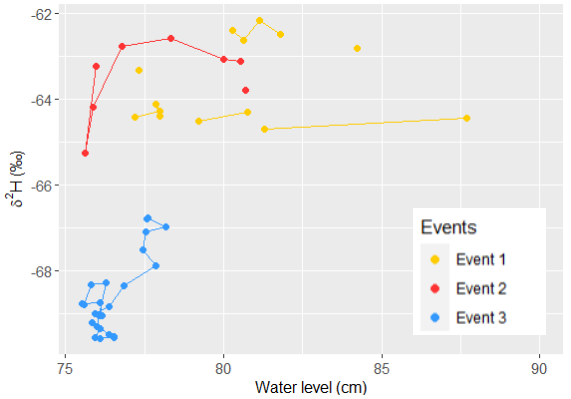

δ^{18}O

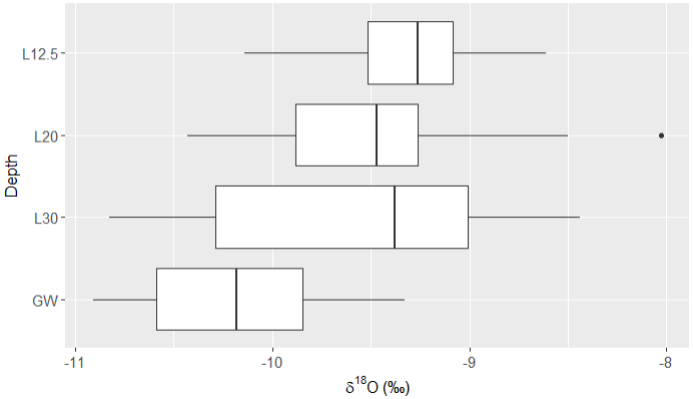

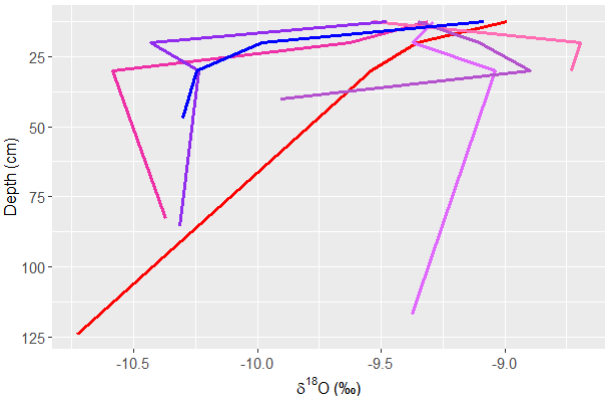

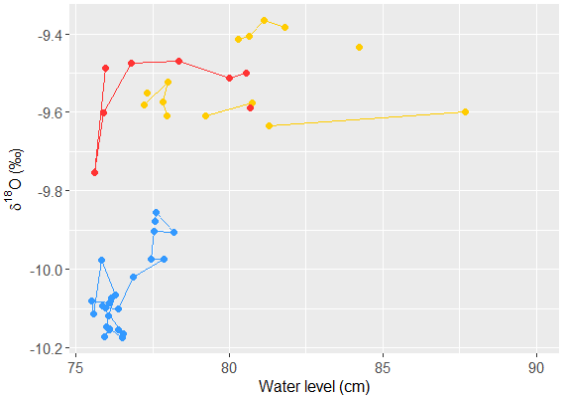

continues

Boron

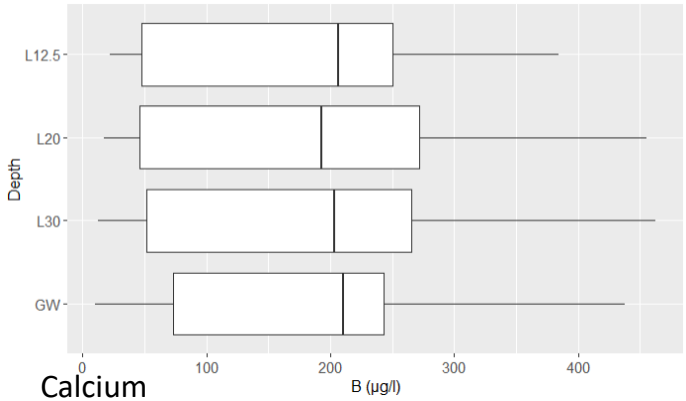

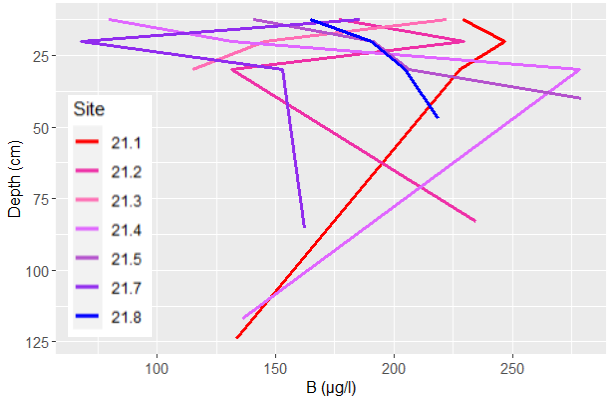

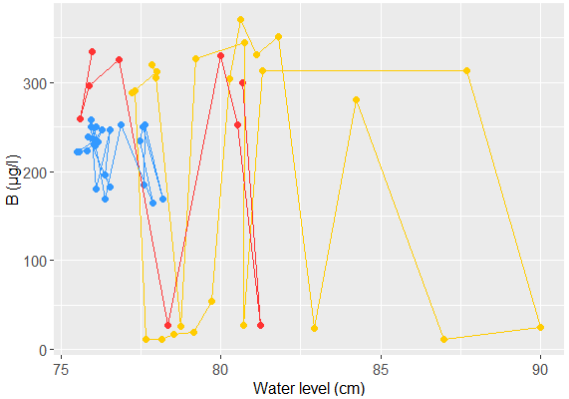

Calcium

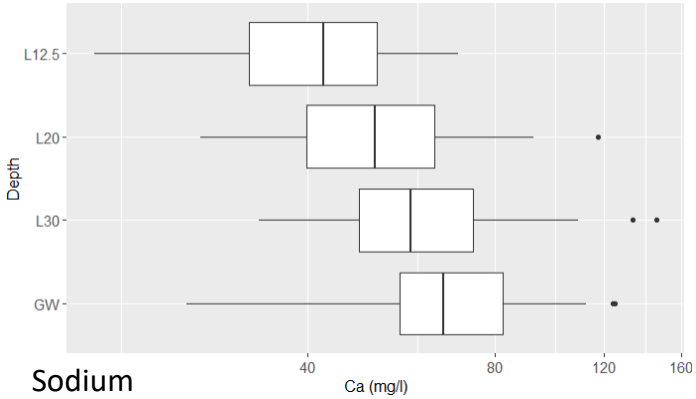

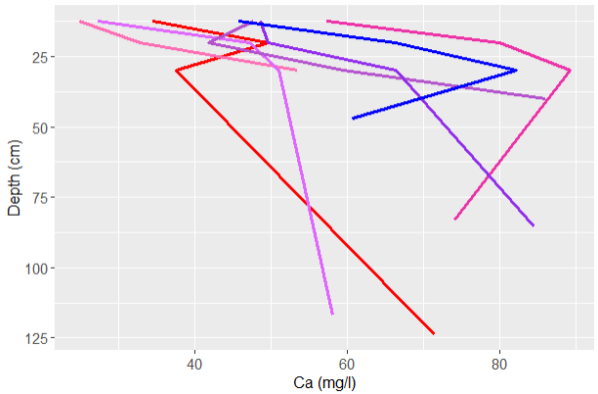

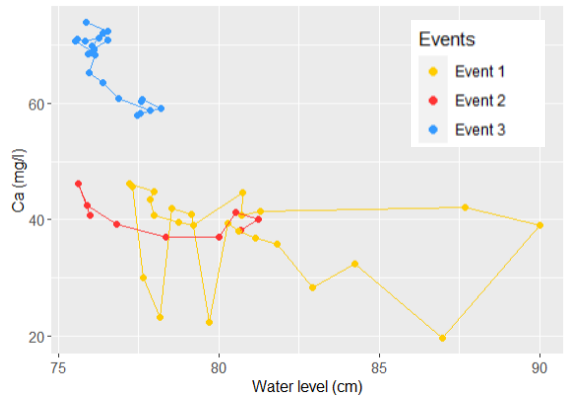

Sodium

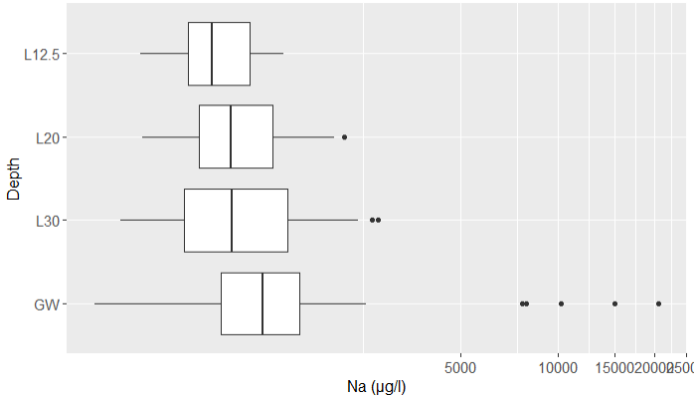

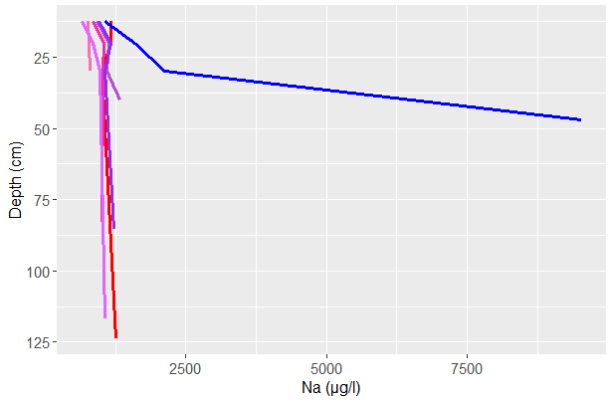

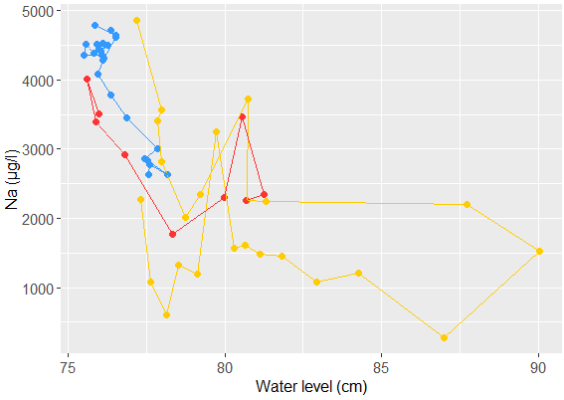

continues

Magnesium

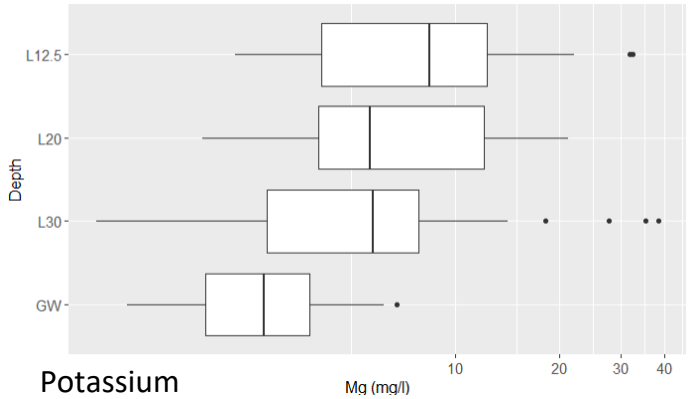

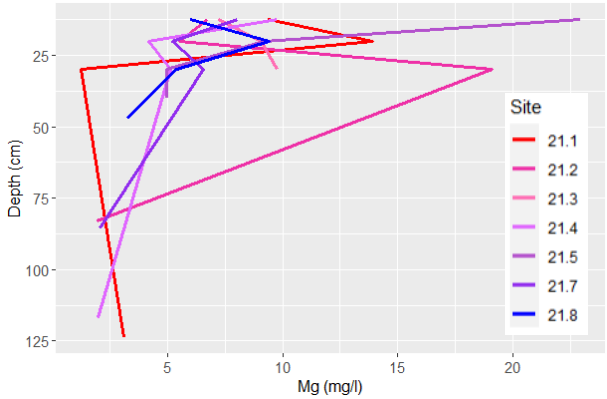

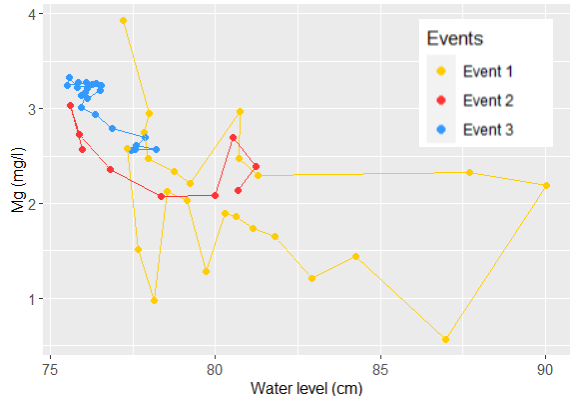

Potassium

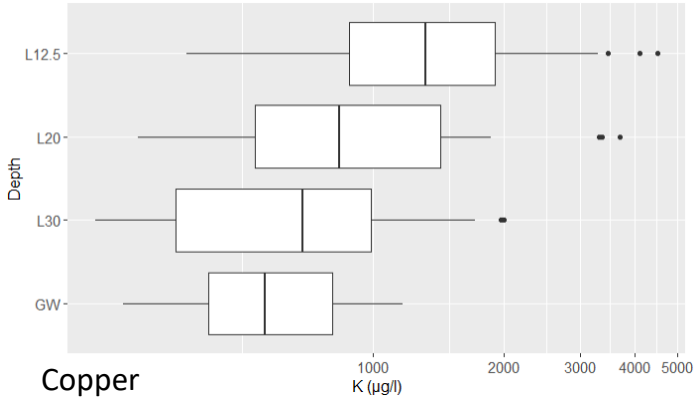

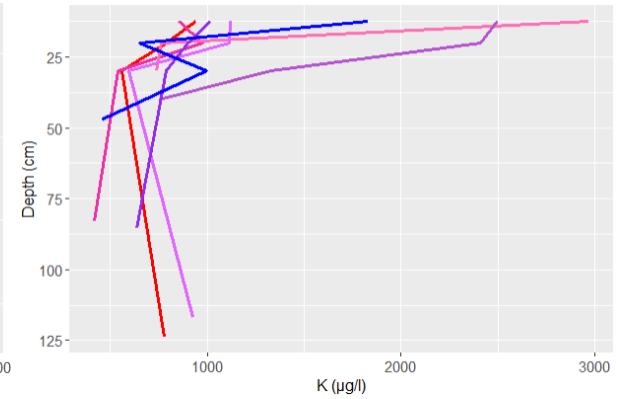

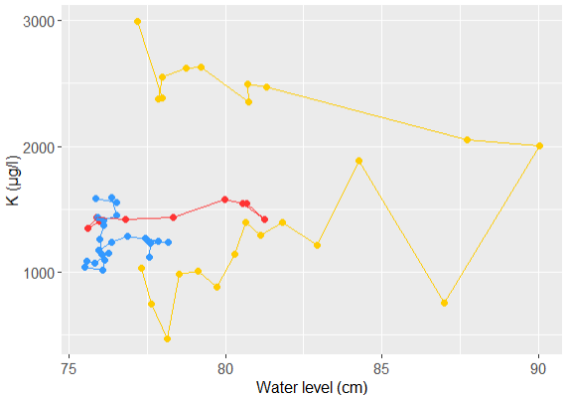

Copper

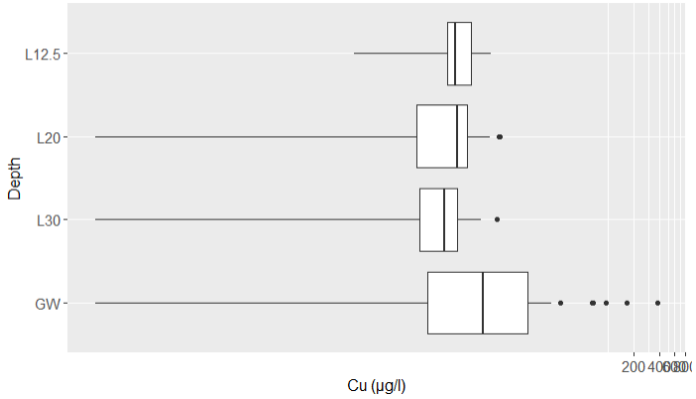

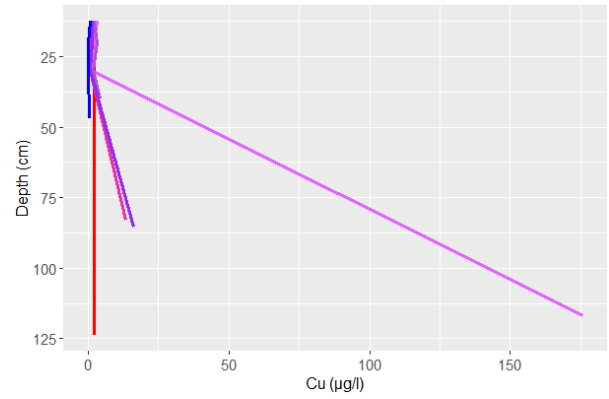

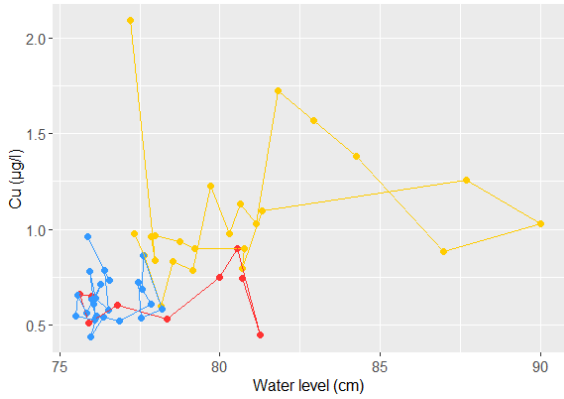

continues

Zinc

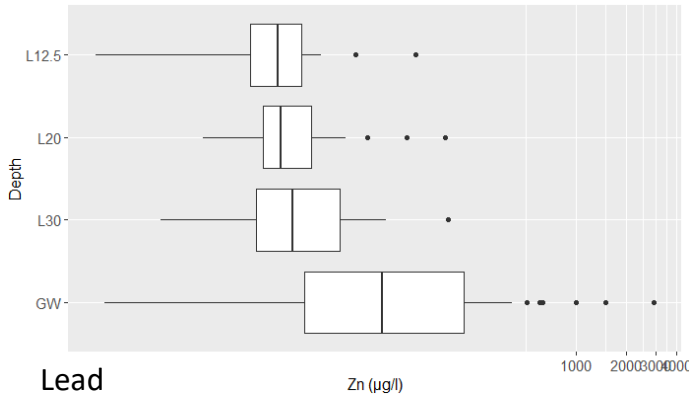

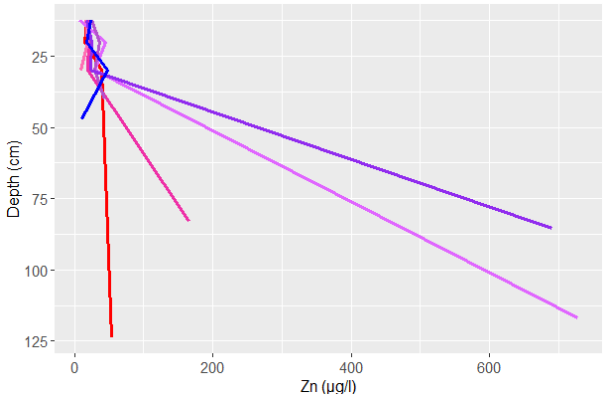

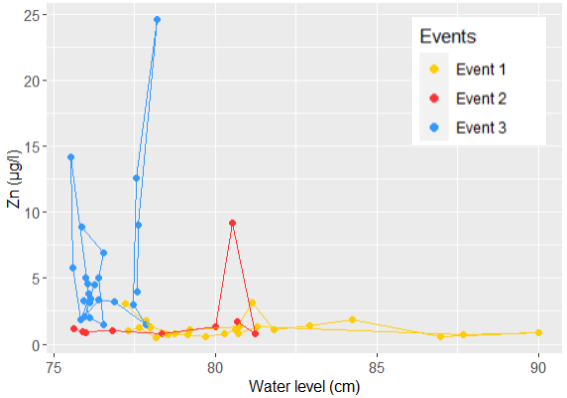

Lead

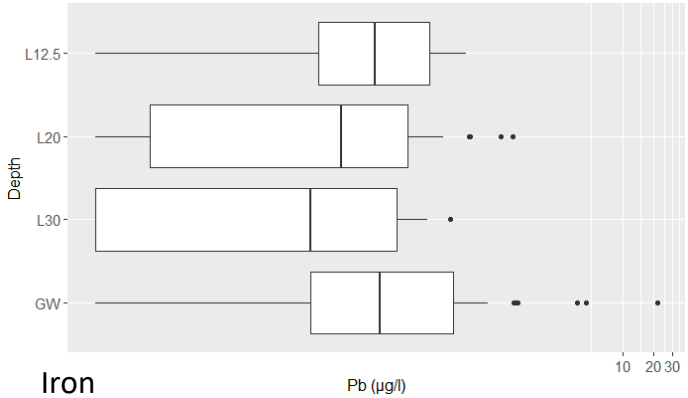

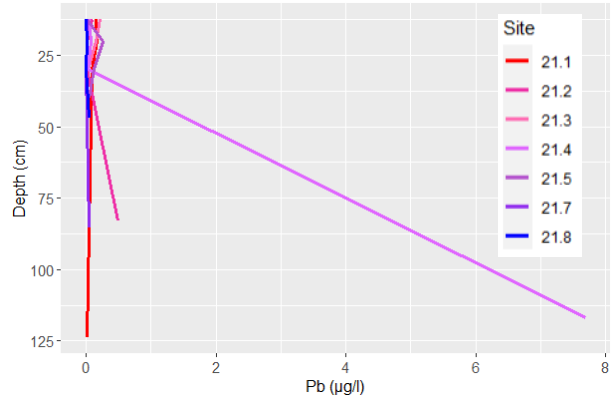

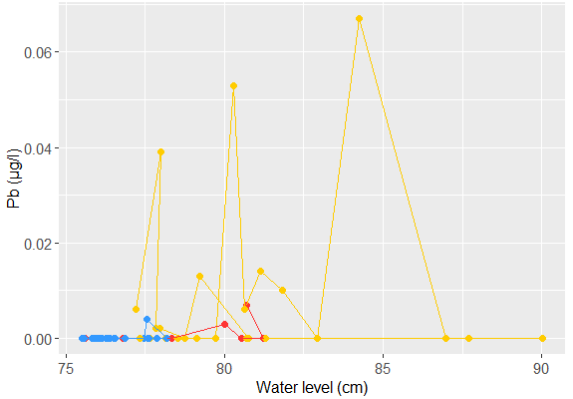

Iron

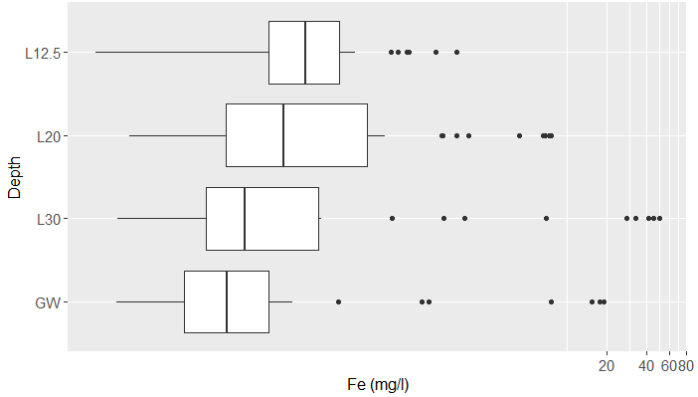

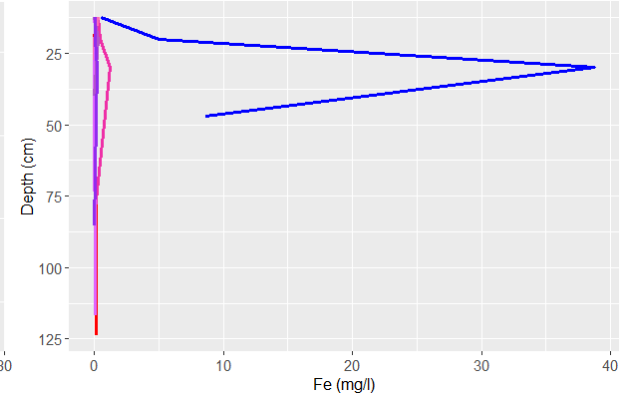

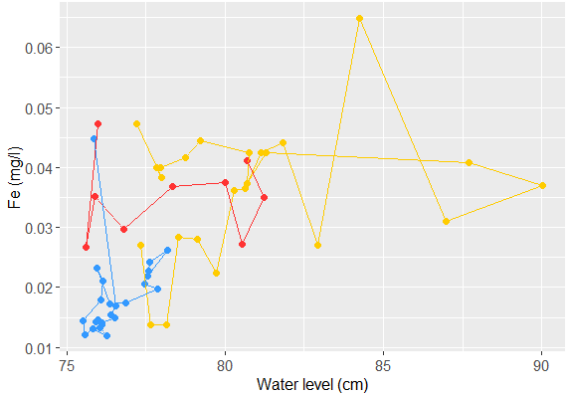

continues

Manganese

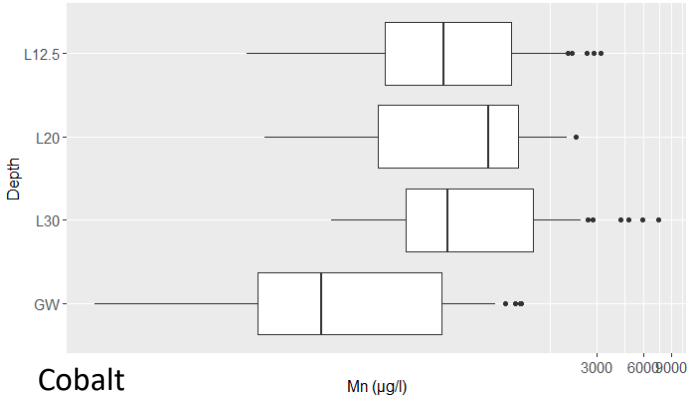

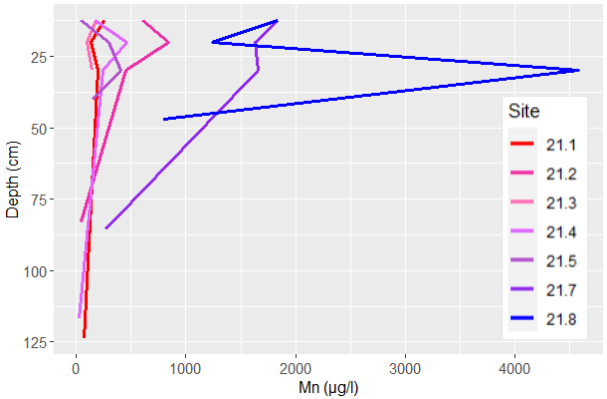

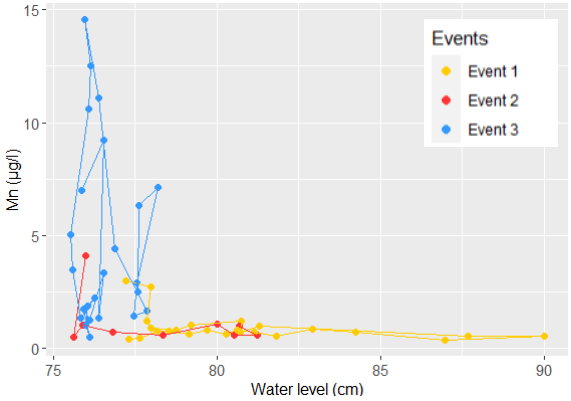

Cobalt

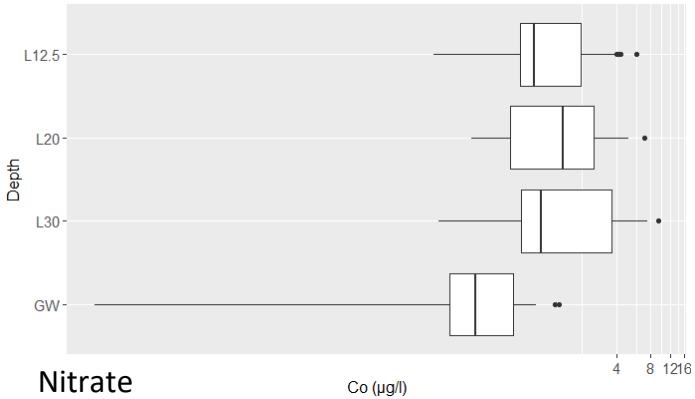

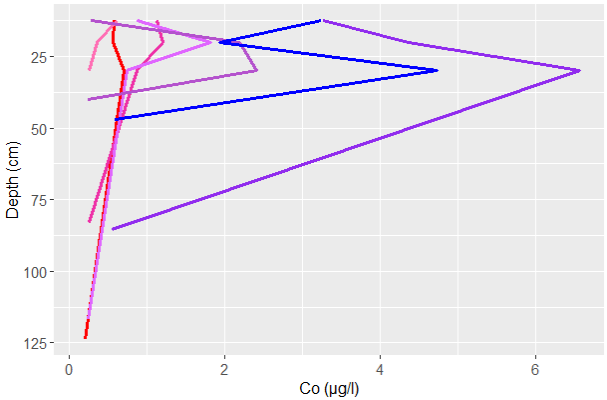

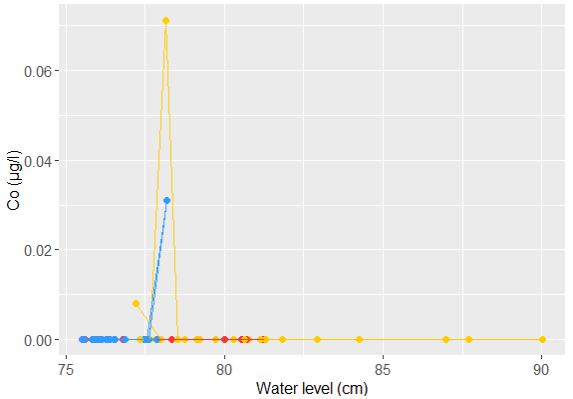

Nitrate

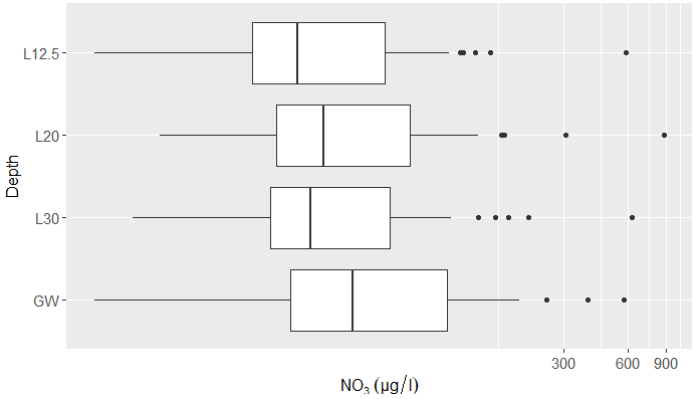

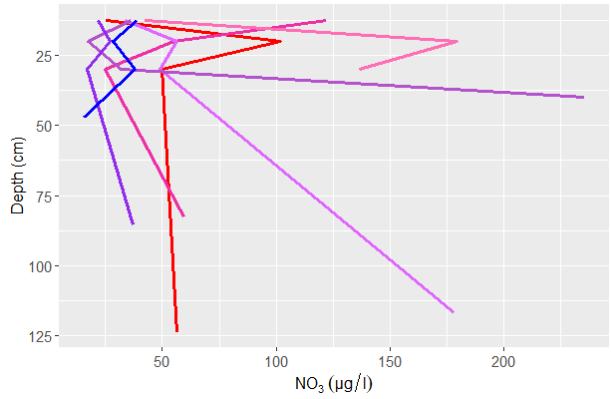

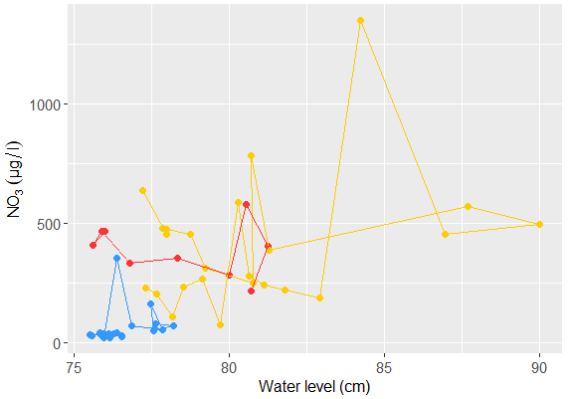

continues

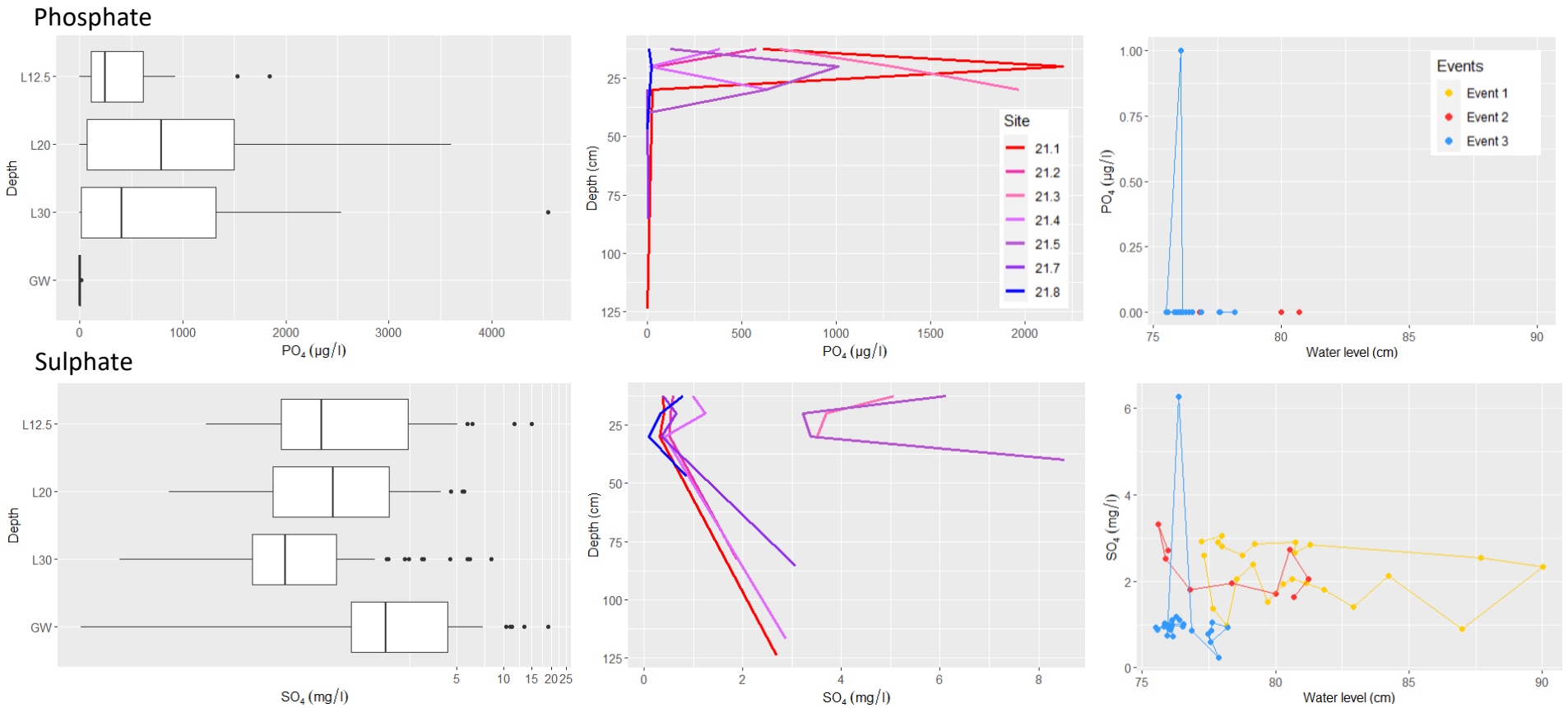

Figure 9.1: Concentration changes for all studied isotopes and solutes: change with soil depth as boxplots on the left, mean change across space in the middle (color-coded based on TWI) and mean change in the stream during rainfall event on the right. Note the log-scale in the boxplots and the different units in µg/l and mg/l.

Table 9.2: All soil characteristics per soil depth

Site	Depth (cm)	Lab-Nr	Wet soil (g)	Dry soil (g)	Stones (g)	Roots (g)	Biomass (g)	Skeleton (%)	Fine earth <2mm (g)	Soil moisture (%)	pH mean	LOI (%)
21.1	0 - 12.5	265H21AB01	145	62	0.0	0.2	1.8	3	60	57	6.1	25
21.1	12.5 - 20	265H21AB02	139	71	0.0	0.2	0.5	1	71	49	6.2	17
21.1	20 - 30	265H21AB03	159	90	3.2	-0.1	0.2	4	87	43	6.1	13
21.2	0 - 12.5	265H21AB04	107	39	0.4	0.2	0.6	3	38	64	7.0	32
21.2	12.5 - 20	265H21AB05	76	32	0.9	-0.1	0.6	4	31	58	6.7	17
21.2	20 - 30	265H21AB06	115	62	0.5	0.1	1.6	3	61	46	6.4	13
21.3	0 - 12.5	265H21AB07	139	62	0.2	0.5	1.1	2	61	55	5.6	26
21.3	12.5 - 20	265H21AB08	116	61	1.0	0.1	0.1	2	60	47	5.7	15
21.3	20 - 30	265H21AB09	177	112	1.4	0.1	0.2	2	110	37	7.5	10
21.4	0 - 12.5	265H21AB10	175	77	1.1	0.2	1.1	3	75	56	6.4	23
21.4	12.5 - 20	265H21AB11	133	70	0.6	0.1	0.2	1	69	47	6.2	16
21.4	20 - 30	265H21AB12	109	59	0.1	0	0.1	0	59	46	6.4	14
21.5	0 - 12.5	265H21AB13	113	53	0.1	0.4	1.9	5	50	53	5.5	29
21.5	12.5 - 20	265H21AB14	116	64	0.6	0	0.5	2	63	45	7.9	16
21.5	20 - 30	265H21AB15	110	61	0.1	0	2.1	4	58	45	7.9	14
21.7	0 - 12.5	265H21AB16	157	60	0.0	0.6	2.8	6	56	62	7.2	27
21.7	12.5 - 20	265H21AB17	86	26	0.0	0.1	2.2	9	24	70	6.1	35
21.7	20 - 30	265H21AB18	119	38	0.0	0	1.3	4	37	68	5.7	32
21.8	0 - 12.5	265H21AB19	140	30	0.1	0.3	0.6	5	29	78	6.4	38
21.8	12.5 - 20	265H21AB20	144	25	0.3	0.1	0.5	4	24	83	5.3	53
21.8	20 - 30	265H21AB21	119	30	0.0	0	0.5	2	29	75	5.4	38

Soil characteristics and elemental contents

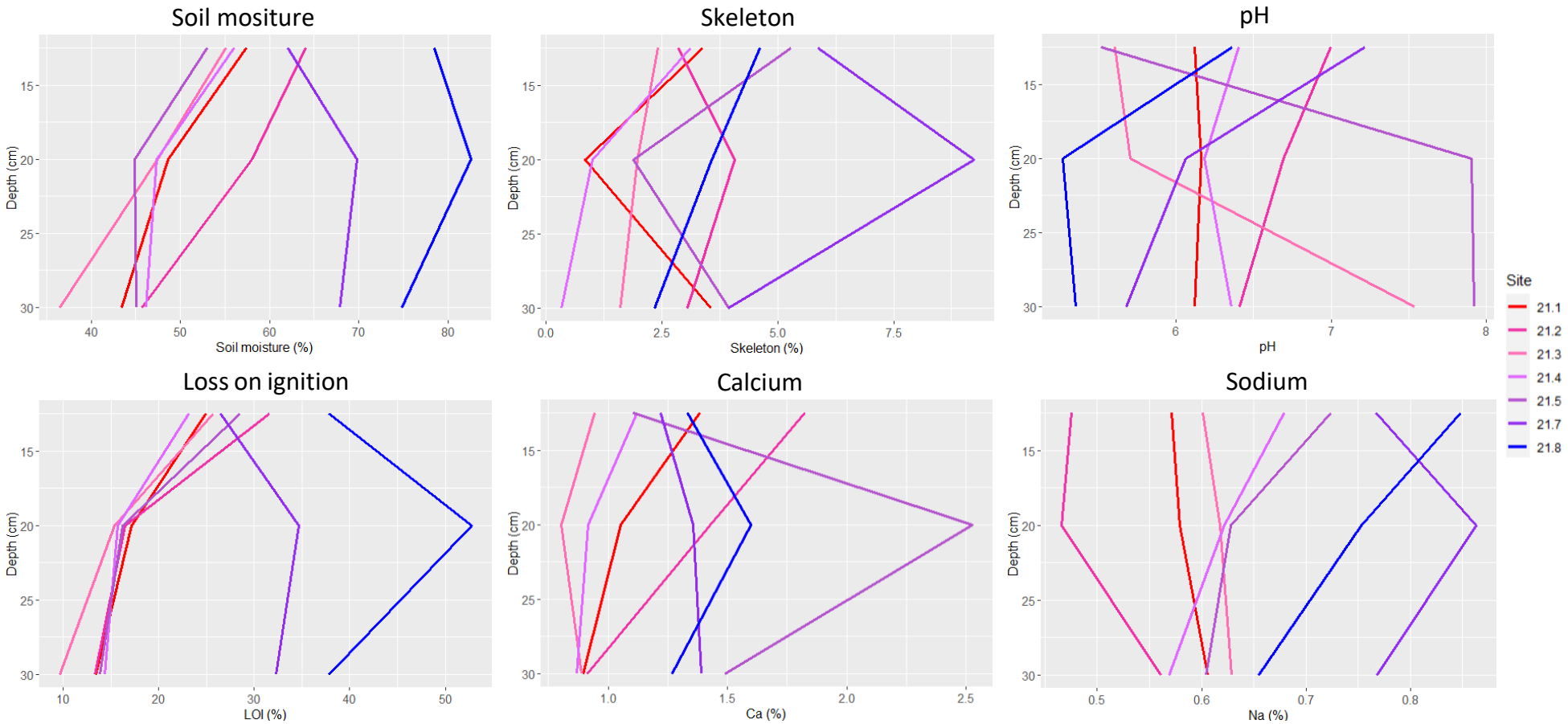

continues

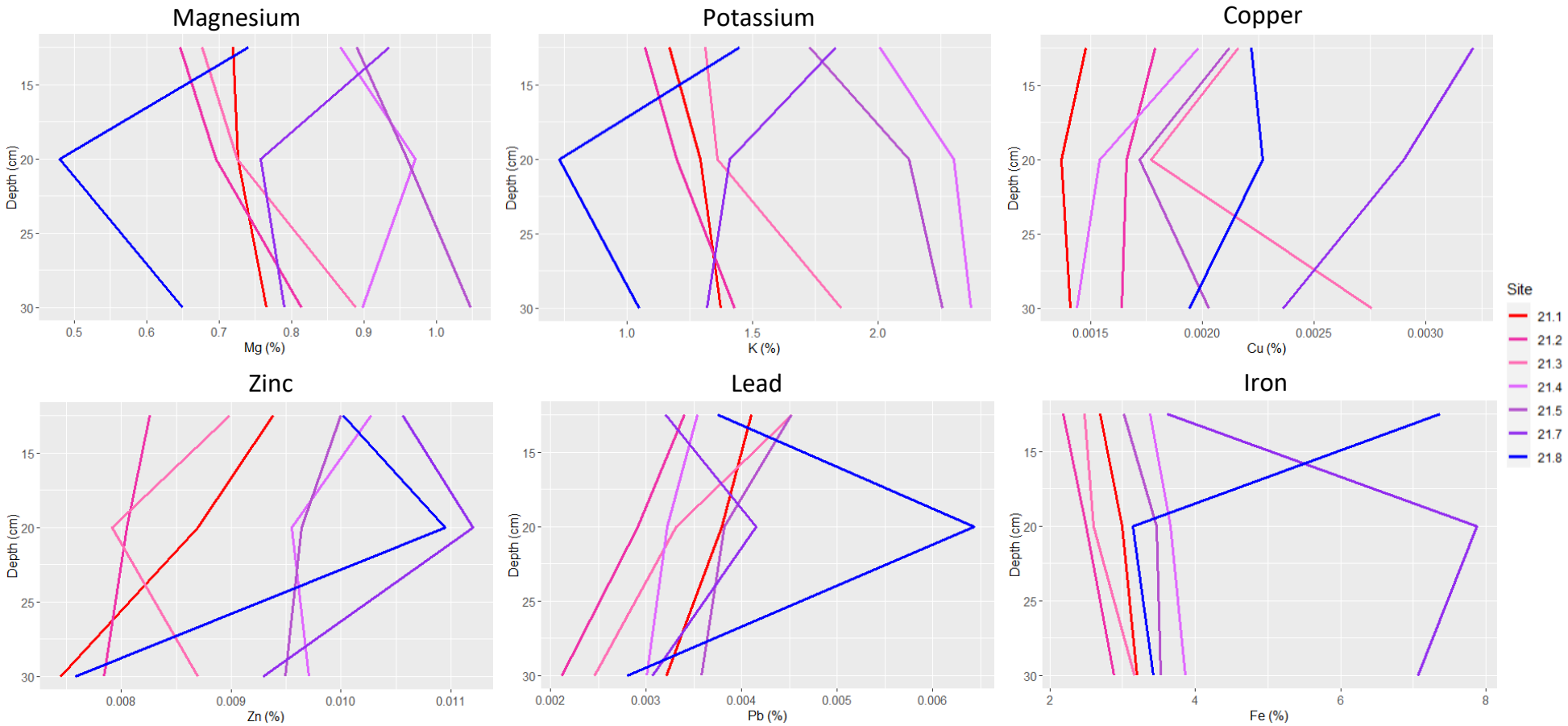
Magnesium
Potassium
Copper
Zinc
Lead
Iron
Depth (cm)
Mg (%)
K (%)
Cu (%)
Zn (%)
Pb (%)
Fe (%)
Site
21.1
21.2
21.3
21.4
21.5
21.7
21.8

continues

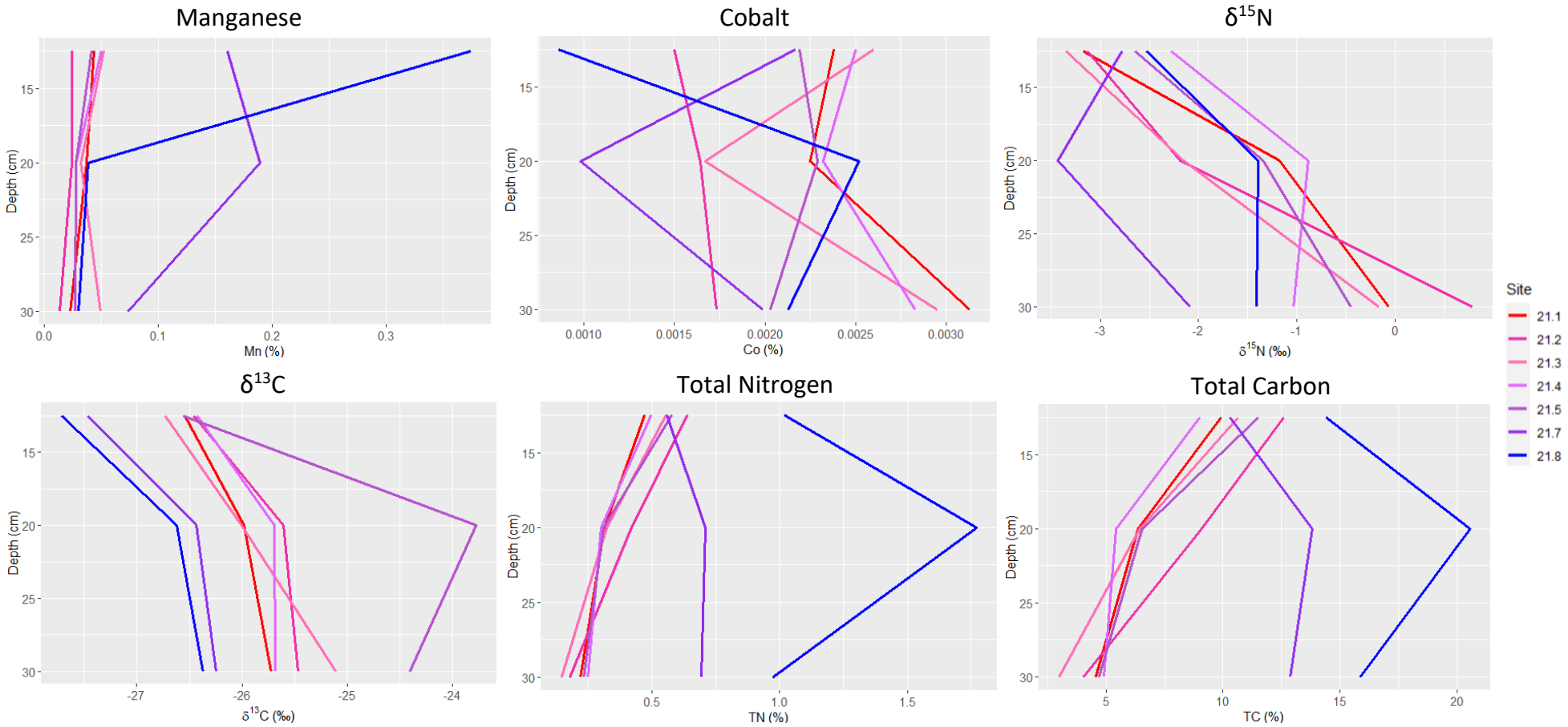

Figure 9.2: Pedological characteristics and soil concentrations as a function of depth for each site (color-coded based on topographic wetness index). The sample taken from 0-12.5 cm, 12.5-20 cm, and 20-30 cm are plotted at 12.5 cm, 20 cm and 30 cm depth, respectively.

Table 9.3: Statistical results of the temporal analysis for all solute concentrations by site and depth (using one sample t-test)

Site	Depth	$\delta^{18}O$	$\delta^{2}H$	B	Ca	Mg	Na	Cu	Zn	Pb	Fe	Mn	Co	K	NO_3	PO_4	SO_4
21.1	L12.5	0	0	0	0	0	0	0	0	0	0	0	0	0	0	0	0
21.1	L20	NA	NA	0	0	0	0	0	0	0	0	0	0	0	0	718	0
21.1	L30	0	0	0	0	0	0	0	0	0	0	0	0	0	46	0	0
21.1	GW	0	0	0	0	0	0	0	0	0	0	0	0	0	0	NA	0
21.2	L12.5	NED	NED	0	0	0	0	0	0	0	0	0	0	0	NED	NED	NED
21.2	L20	0	0	0	0	0	0	0	0	0	0	0	0	0	0	NED	0
21.2	L30	NED	NED	0	0	0	0	0	0	0	0	0	0	0	0	NA	0
21.2	GW	-0.5	0	0	0	0	0	0	112	0	0	0	0	0	0	NA	0
21.3	L12.5	0	0	0	5524	0	0	0	0	0	0	0	0	0	0	604	0
21.3	L20	NA	NA	0	0	0	0	0	0	0	0	0	0	0	0	1154	0
21.3	L30	NED	NED	0	0	0	0	0	0	0	0	0	0	0	0	0	0
21.3	GW	0	0	0	0	0	0	0	0	0	0	0	0	0	0	NA	7457
21.4	L12.5	NA	NA	NED	NED	NED	NED	NED	NED	NED	NED	NED	NED	NED	NED	NED	NED
21.4	L20	0	0	0	0	0	0	0	0	0	0	0	0	0	0	NA	725
21.4	L30	0	0	0	0	0	0	0	0	0	0	109	0.5	0	0	0	0
21.4	GW	NA	NA	0	0	0	0	0	0	0	0	0	0	0	0	NA	0
21.5	L12.5	NED	NED	0	0	0	0	0	0	-0.02	0	0	0	0	0	NED	0
21.5	L20	NED	NED	0	0	0	0	0	0	0	0	0	0	0	0	NED	0
21.5	L30	0	0	0	0	0	0	0	0	0	0	0	0	0	0	NED	0
21.5	GW	NED	NED	NED	NED	NED	NED	NED	NED	NED	NED	NED	NED	NED	NED	NA	NED
21.7	L12.5	NED	NED	0	0	0	0	0	0	0	0	607	0	0	0	0	0
21.7	L20	NA	NA	0	0	0	0	0	11	0	0	0	0	0	0	NA	0
21.7	L30	0	0	0	9574	0	0	-0.08	0	0	0	0	0	0	0	NA	0
21.7	GW	0	0	0	0	0	0	0	0	0	0	0	0	0	0	NA	0
21.8	L12.5	NA	NA	0	0	0	0	0	0	0	0	0	0	0	0	NA	0
21.8	L20	0	0	0	0	0	0	0	0	0	0	0	0	0	0	NA	0
21.8	L30	0	0	0	0	0	0	0	0	0	0	1695	0	0	0	NA	0
21.8	GW	0	0	0	0	0	0	0	0	0	0	0	-0.3	0	0	0	0

One-sample-t-test	
0	equal to 0
NA	no values
NED	not enough data, just one positive value
NED	not enough data, just one negative value
	statistically different from 0 (positive mean)
	statistically different from 0 (negative mean)

*Table 9.4 (left): Slope of logarithmic resp. linear regression of solute concentration with soil depth but only for soil water without groundwater (where * = linear regression, bold = statistically significant, grey = R^2 < 0.4). The column Expect indicated if the decrease (red) or increase (blue) in concentrations matched the expectations (as described in chapter 2.1).*
Table 9.4 (right): Spearman rank correlation between the change in solute concentration over soil depth but only for soil water without groundwater, as indicated by α (Equation 4.1) and topographic wetness index, slope, and groundwater level (where grey = R2 < 0.4, none are statistically significant)

Solute	21.1	21.2	21.3	21.4	21.5	21.7	21.8	Expect.
$d^{18}O$	-0.6	-1.4	0.9	0.3	**0.5**	-0.9	-1.3	(✓)
$d^{2}H$	-5.6	-11.9	6.7	1.4	**4.1**	-8.9	-11.0	(✓)
B	-0.3	-48	-123	224	76	-43	46	×
Ca	4'389	36'635	32'142	27'512	12'740	19'875	**41'618**	✓
Na	-186	220	27	**360**	209	133	1'221	✓
Mg	-8'789	13'664	2'950	-5'480	-20'763	-1'800	-479	(✓)
K	-427	-344	-2'606	-583	-1'305	**-258**	-993	✓
Cu*	-0.002	-0.030	-0.028	**-0.114**	-0.024	-0.052	-0.026	✓
Zn*	1.3	-0.1	-0.5	1.1	0.2	0.3	1.4	✓
Pb*	-0.003	-0.004	-0.010	-0.001	0.004	-0.001	-0.0002	✓
Fe	-96	1'058	-317	-8	163	202	42'659	×
Mn	-64	-152	-40	94	424	-210	3'010	(✓)
Co	0.1	-0.3	-0.4	-0.1	2.5	3.7	1.6	×
NO_3	31	-112	112	18	-6	-5	-1	×
PO_4	-567	-1'114	**1'446**	261	612	-101	4	×
SO_4	-74	-89	-1'801	-626	-3'225	-34	-788	×

Solute	α vs. TWI	α vs. slope	α vs. GW level
$\delta^{18}O$	-0.11	0.05	0.20
$\delta^{2}H$	-0.11	0.05	0.20
B	0.36	0.43	0.09
Ca	0.32	0.29	-0.31
Na	0.57	0.20	-0.26
Mg	-0.07	-0.29	-0.14
K	-0.11	0.29	0.37
Cu	-0.36	-0.45	-0.31
Zn	0.43	-0.09	-0.03
Pb	0.68	0.20	-0.54
Fe	0.57	-0.04	-0.71
Mn	0.43	-0.18	-0.43
Co	0.64	0.00	-0.60
NO_3	-0.25	-0.45	0.43
PO_4	0.32	-0.09	-0.26
SO_4	-0.21	0.07	0.43

10 Personal declaration

Personal declaration: I hereby declare that the submitted Thesis is the result of my own, independent work. All external sources are explicitly acknowledged in the Thesis.

Location, Date: Zurich, 26.08.2022 Signature: A. Bruppacher